Charles University in Prague
Faculty of Mathematics and Physics

# DOCTORAL THESIS

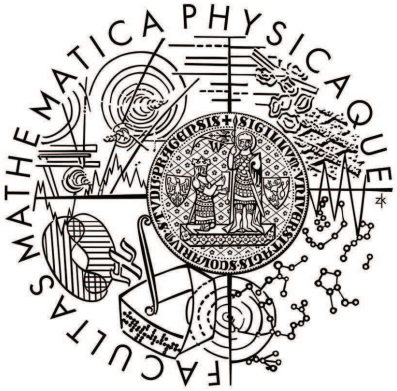


Irena Picková

## Study of the Chemical Oxygen-iodine Laser with the production of atomic iodine from gaseous compounds

Department of Surface and Plasma Science

Supervisor of the doctoral thesis: Prof. RNDr. Milan Tichý, DrSc.

Study programme: Physics
Specialization: f-2 – Physics of Plasmas and Ionized Media

Prague 2014

I would like to thank to my supervisor professor Milan Tichý and my consultant Vít Jirásek of Institute of Physics, as well as to the group of High Power Systems at the Institute of Physics of Academy of Sciences, namely Jarmila Kodymová, Josef Schmiedberger, Otomar Špalek and Miroslav Čenský and also to Pavel Kudrna from the Charles University, Faculty of Mathematics and Physicas, Department of Surface and Plasma Science. I also wish to thank to my family for their great support and I would also like to dedicate this work to the memory of my mother.

I declare that I carried out this doctoral thesis independently and only with the cited sources, literature and other professional sources.

I understand that my work relates to the rights and obligations under the Act No. 121/2000 Coll., the Copyright Act, as amended, in particular the fact that the Charles University in Prague has the right to conclude a licence agreement on the use of this work as a school work pursuant to Section 60 paragraph 1 of the Copyright Act.

In ..... date ..... signature

Název práce: Studium chemického kyslík- jodového laseru s produkcí atomárního jodu z plynných sloučenin

Autor: Irena Picková

Katedra: Katedra fyziky povrchů a plazmatu

Vedoucí doktorské práce: prof. RNDr. Milan Tichý, DrSc., Univerzita Karlova v Praze, Matematicko-fyzikální fakulta, Katedra fyziky povrchů a plazmatu,

Abstrakt: Tato práce se zabývá studiem disociace jodových molekul v souvislosti s vývojem chemického a výbojového kyslík-jodového laseru. Byla zkoumána chemická disociace molekuly HI a výbojová disociace molekul $CH_3I$ a $CF_3I$. Hlavní diagnostickou metodou je absorpční spektroskopie. Součástí práce je modelování systému chemických rovnic. Na základní část práce navazuje zkoumání plazmatu buzeného radiofrekvenčním zdrojem v plazmatické trysce s dutou katodou v argonu a ve směsi argonu s jodem metodou Langmuirovy sondy.

Klíčová slova: Chemický laser, jod, plazma, radiofrekvence, elektronegativní

Title: Study of Chemical Oxygen-Iodine laser with the production of atomic iodine from gaseous compounds

Author: Irena Picková

Department: Department of Surface and Plasma Science

Supervisor of the doctoral thesis: prof. RNDr. Milan Tichý, DrSc., Charles University in Prague, Faculty of Mathematics and Physics, Department of Surface and Plasma Science

Abstract: This work deals with the study of dissociation of iodine molecule for Chemical and Discharge Oxygen-Iodine laser. Chemical way of HI dissociation and discharge way of dissociation of $CH_3I$ and $CF_3I$ molecules is examined. Main diagnostics method is absorption spectroscopy. Part of the work is also modeling of system of chemical reactions. Last part of this work is dealing with the study of plasma generated by a radiofrequency generator in the hollow cathode plasma jet system using argon or mixture of argon with iodine. Diagnostic method used is Langmuir probe.

Keywords: Chemical laser, iodine, plasma, radiofrequency, electronegative

# Contents

# List of Figures

# Nomenclature

| | |
|---|---|
| $\alpha_{3-4}$ | Small-signal gain on the laser transition |
| $\Delta E$ | Energy gap between two electron energy levels of atoms or molecule |
| $\Delta\lambda_d$ | FWHM of Gaussian line profile |
| $\dot{n}$ | Total gas flow of all gases in system |
| $\dot{N}_I$ | Flow rate of iodine atoms |
| $\dot{n}_I$ | Molar flow rate of atomic iodine |
| $\dot{n}_{tot}$ | Total molar flow rate of all components in the COIL medium |
| $\epsilon$ | Extinction coefficient of light in matter |
| $\eta_{diss}$ | Dissociation fraction |
| $\lambda_D$ | Debye length |
| $\lambda_e$ | Mean free path of electrons colliding with neutrals |
| $\lambda_m$ | Wavelength of line center |
| $\nu$ | Frequency of collisions |
| $\nu$ | Frequency of radiation |
| $\omega$ | Driving frequency |
| $\omega_{pe}$ | Plasma frequency for electrons |
| $\omega_{pi}$ | Plasma frequency for ions |
| $\pi$ | Ludolf number $\pi = 3.141592$ |
| $\sigma_e$ | Collision cross section for electrons |
| $\sigma_{3-4}$ | Cross-section of laser transition of iodine atoms |
| $\varepsilon_0$ | Permittivity of vacuum |
| $c$ | Speed of light |

$c(O_2(\Delta))$ Concentration of singlet oxygen

$c(O_2(tot))$ Total concentration of oxygen

$c_I$ Concentration of atomic iodine evaluated from absorption spectroscopy

$c_I(\mathrm{y})$ Atomic iodine number density

$c_{pm}$ Heat capacity of reacting substance in J/mol.K

$d$ Diameter of cylindrical probe

$E$ Energy of particle

$e$ Charge of electron

$E_{bond}$ Dissociation energy of C-I bond in the $CH_3I$ or $CF_3I$ molecule

$fP_{diss}$ Fraction of power absorbed in plasma used for dissociation of iodine donor

$h$ Planck constant h = 6.63 $\times 10^{-34}$ Js

$H_i$ Enthalpy of i-th reacting substance in reaction system in kJ/mol

$I_2$ Iodine molecule

$I_e$ Electron current

$I_{es}$ Electron saturation current

$J$ Measured intensity of light

$J_0$ Initial intensity of light

$k$ Rate constant for chemical reactions

$k_B$ Boltzmann constant k = 1.38 $\times 10^{-23}$ J/K

$K_{eq}$ Equilibrium rate constant for pumping of COIL

$L$ Length which light travels in matter

$l$ Length of cylindrical probe

$m_e$ Mass of electron

$m_i$ Mass of ion

$N_A$ Avogadro constant $N_A = 6.022 \times 10^{23}$ mol$^{-1}$

$n_e$ Concentration of electrons

$n_i$ Concentration of positive ions

$n_n$ Concentration of negative ions

$p$ Pressure

$P_abs$ Power absorbed in discharge

$p_I$ Partial pressure of atomic iodine

$p_{cav}$ Pressure measured in the detection cavity

$R$ Molar gas constant R = 8.314 J mol$^{-1}$ K$^{-1}$

$R_p$ Probe size

$S$ Probe surface

$T$ Temperature

$T(y)$ Atomic iodine temperature

$T_e$ Electron temperature

$T_{e,eff}$ Effective temperature of electrons

$V$ Probe bias

$v_e$ Velocity of electron

$V_f$ Floating potential

$V_p$ Plasma potential

$V_{flow}$ Volumetric flow rate of gas mixture

$Y_\Delta$ $O_2(^1\Delta)$ yield

$Y_{th}$ Threshold yield of $O_2(^1\Delta)$ sufficient for laser operation

COIL Abbreviation for Chemical Oxygen-Iodine Laser

DOIL Abbreviation for Discharge Oxygen-Iodine Laser

EEDF Electron energy distribution function, also denoted $f(E)$

I($^2P_{1/2}$) Excited iodine atom, higher lasing level of COIL, can be written also as I($5^2P_{1/2}$)

I($^2P_{3/2}$) Ground state of iodine atom, lower lasing level of COIL, can be written also as I($5^2P_{3/2}$)

$O_2(^1\Delta)$ Singlet delta state of oxygen molecule – source of energy for COIL

$O_2(^3\Sigma)$ Ground state of oxygen molecule

RF Radiofrequency

# Introduction

Many everyday objects in our lives are connected with laser or plasma technology, which spread widely during the second half of the 20th century.

Lasers are nowadays widely used in industry (laser cutting, drilling etc.), in diagnostics (e.g. absorption spectroscopy) as well as in medicine (eye and skin treatment) and also in everyday objects like computer optical disc drives, CD and DVD players, barcode scanners, laser pointers and many more.

Plasma is nowadays used in many areas of industry – e.g. for thin layer deposition [1], plasma etching, plasma chemistry, which are important for the fabrication of microelectronics. Plasma is also used in electric thrusters and is also present in some types of lasers [2]. Also some conventional light sources use plasma. Very important area of plasma research is the thermonuclear fusion – possibly the source of energy in the future. Study of plasma is also connected with astrophysics, as the most matter in universe is in the plasma state (stars, nebulas) and many plasma diagnostics methods were first used in the astrophysics (spectroscopy).

Plasma can be created by various types of discharges: DC (direct current), RF (radiofrequency), microwave driven discharges or there are also plasmas sustained by particle beams. Discharges can be formed in various gases, even in vapors of metals.

In this work I will deal with RF discharges. There are many types of devices using RF generator as a source of energy for plasma. Among such devices are magnetrons [3], hollow cathodes [4, 5], helicons [6] and some more. Here we will deal with RF hollow cathode plasma jet system as is described e.g. in [7].

Thin layer deposition using RF driven plasma is advantageous in the case of non-conducting layers, which could in DC plasmas be charged to high voltage, which may lead to sparking, arcing and thin layer destruction.

Many diagnostic methods have been developed for investigation of plasma which are also helpful in investigation of lasers, such as emission and absorption spectroscopy. Many lasers also have electric discharge as a source of energy for laser operation. One of the most important methods in plasma diagnostics is Langmuir probe, sometimes called also electrostatic probe.

The current research in lasers is often concerned with improvement of already existing lasers, one of the examples may be Chemical Oxygen-iodine laser (abbreviated COIL) which is the object of research aiming to increase

laser power and to optimize its operation.

In this work I will deal with Chemical Oxygen-Iodine Laser (COIL) and Discharge Oxygen-Iodine Laser (DOIL). In these lasers, excited oxygen molecule is the source of energy of laser and iodine atoms are the source of radiation. Energy is transferred from oxygen molecule to iodine atom in collision accompanied by nearly resonant energy transfer. Both production of excited oxygen molecules and of iodine atoms present main tasks of COIL and DOIL research.

Both COIL and DOIL are candidates for high power lasers which could be used in industry as well as for military application (e.g. project of Airborne laser [8]).

This work describes laser systems of COIL and DOIL which were developed in the High Power Systems laboratory at the Institute of Physics.

In classical COIL system excited oxygen molecule serves for iodine atoms excitation, but also for dissociation of $I_2$ molecule which is the source of iodine atoms. Alternative schemes are developed to save energy consumed by dissociation process by producing iodine atoms in different way. Alternative ways can use chemical methods as will be seen in the chapter 2 or discharge methods as will be described in the chapter 3. This work is mainly concerned with dissociation of different molecules containing iodine, chemical way of dissociation of HI and discharge way of dissociation of $CH_3I$ and $CF_3I$ molecules are described.

Part of my work was also modeling of chemical reactions by the method of 1-D chemical kinetics. Reaction system contained three source molecules: $F_2$, NO and HI and several product molecules. This will be described in the section 2.4.4 in the chapter describing the COIL system.

As the continuation of the research of COIL and DOIL systems this work also contains third object – a study of the plasma created by the hollow cathode plasma jet system in argon and in mixture of argon with iodine $I_2$ which will be described in the chapter 4. Hollow cathodes are devices which serve for efficient thin layer deposition and plasma etching.

Diagnostic method for the hollow cathode plasma jet system is Langmuir probe, from I-V characteristics of which we can obtain basic plasma parameters like plasma potential, electron temperature, concentration of electrons and ions and also distribution function of electrons.

Hollow cathode plasma jets are used for efficient thin layer deposition. In this work the effect of both the presence of radiofrequency signal and deposition of the material sputtered from the cathode on the probe surface are examined. Also the presence of electronegative iodine changes the discharge characteristics, comparison of Langmuir probe I-V characteristics measured in argon and in argon with iodine admixture will be presented.

# Chapter 1

# Theory

In this chapter I will introduce some basic theory concerning the main studied phenomena – laser operation, plasma theory and diagnostic methods such as optical spectroscopy and Langmuir probe method.

## 1.1 Laser

### 1.1.1 Basic laser properties

Laser is a device producing coherent radiation. Its name is the abbreviation of "Light amplification by stimulated emission of radiation". Many types of lasers exist nowadays which are able to produce radiation of various energy, on different wavelengths and of different beam quality.

Very extensive laser theories can be found e.g. in textbooks written by Silvfast [9], Siegman [10] and Svelto [11] and history of laser development together with leading ideas of interaction of radiation with matter can be found e.g in article by Hecht [12].

In the laser theory, the very fundamental process is the stimulated emission of radiation. First theories involving stimulated emission were formulated by Albert Einstein in 1916. Three types of interactions of light and matter were described: absorption, spontaneous emission and stimulated emission.

When matter absorbs light, its energy is increased and excitation or ionization can occur. Spontaneous emission occurs when electron in excited atom or molecule undergoes transition to lower energy level and quantum of light (photon) is emitted.

Stimulated emission is the process, in which the electron also undergoes the transition to the lower energy level, but this time the transition is not spontaneous, but is stimulated (i.e. cased) by incident photon with the same energy as is the gap between higher and lower energy level of excited particle. Emitted photon is then coherent with the incident photon (has the same wavelength and the same phase).

Excited states of atoms and molecules are characterized by radiative lifetime, which describes how long can the excited particle last before tran-

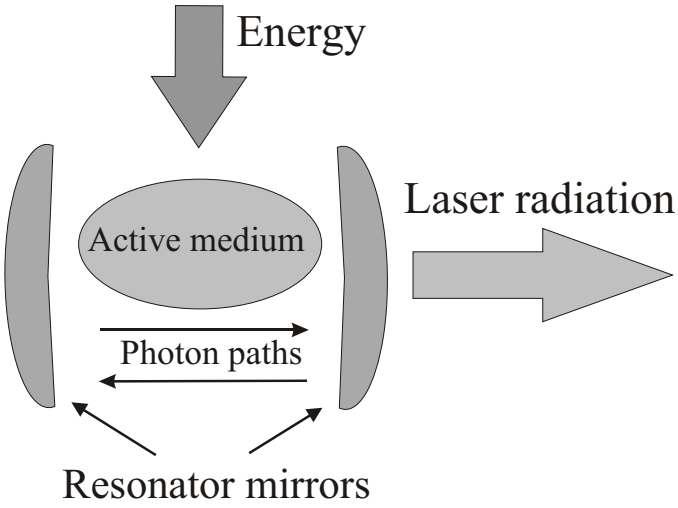


Figure 1.1: Scheme of classical laser device showing main parts of laser system, notably source of energy for laser, active medium which is the source of radiation and resonator which is most often formed by two mirrors with reflectivity over 99%.

sition to lower state occurs. There are two types of energy levels of atoms or molecules – resonant states with very short radiative lifetime (typically nanoseconds) and metastable states with quite long radiative lifetime (millisecond and longer). Metastable states can last for long times because transitions to the lower state are forbidden by selection rules.

From another point of view radiation by spontaneous emission can be described as originating from electric dipole transition. Radiation accompanying forbidden transition is usually originating from electric quadrupole or magnetic dipole transitions. Forbidden transitions are much slower than the allowed ones and radiation from them is usually much weaker.

Lifetime of excited particles can be shorter than radiative lifetime if there are collisions with another particles. Collisions can also lead to non-radiative decay of excited states.

### 1.1.2 Parts of laser

Classical lasers consist of three main parts: active medium, source of energy and resonator or amplifier (optical feedback element) as is shown in figure 1.1. Most of the lasers contain all three parts, there are only few exceptions like free-electron laser (FEL), but we will not deal with them.

Particles present in active medium of laser (atoms or molecules) are excited by delivered energy from some energy source. If the concentration of excited particles is high enough, then the population inversion is attained. Population inversion occurs when there are more particles in the excited state than in ground state and the medium is no longer in thermodynamic equilibrium.

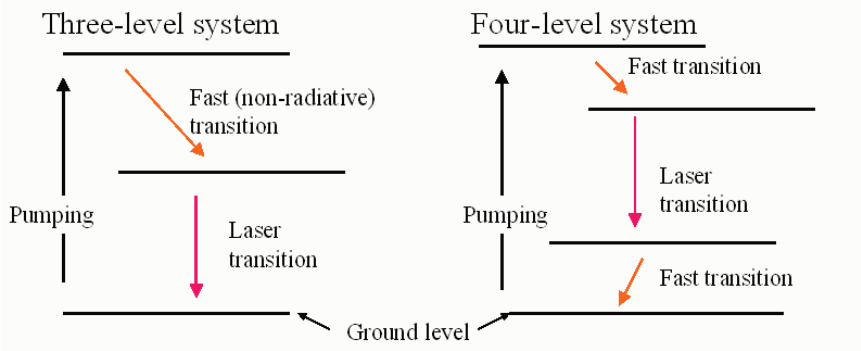


Figure 1.2: Three-level system (on the left) and four-level system (right) showing two main lasing schemes present in active medium. Four-level systems are capable to work in continuous regime, three-level systems can work in pulsed regime only.

Active medium in laser is the mixture of particles in different energy levels, while most important are three or four levels (which sometimes may consist of more sublevels).

Lower energy level often corresponds with ground level of particle. From the point of view of energy levels involved in pumping and laser action we distinguish three level laser system and four level laser system (see figure 1.2). In three level system the lower level of the laser corresponds to ground level of the atom or molecule and it is also the level from which pumping occurs.

In the four-level laser system the lower pumping level is different from the lower lasing level. Four level laser systems often have nearly empty lower lasing level, so the population inversion is easier to obtain. Three-level lasers can work only in pulsed regime. Four-level lasers can work in continuous regime, but can be also operated in pulsed regime.

Energy sources of laser are of very wide range. Mostly used is electric current, light produced by either lamp or another laser, chemical reaction etc. Energy must be supplied to the medium to create and sustain population inversion.

Active medium of laser is sometimes called gain medium, because when radiation on the same wavelength as is the laser transition going through through this medium shows not absorption, but gain which means that the light traveling through the medium is amplified.

Similar term is small-signal gain, which is gain in the medium measured when the signal traveling through the medium is far from the saturation intensity for the laser medium. Before reaching saturation, signal increases exponentially with distance, after that the increase is slower. Small-signal gain is therefore theoretical gain when saturation is not taken into account [10].

As a laser optical feedback usually serves resonator formed by two highly

reflective mirrors between which the light is traveling many times. One of the mirrors is less reflective than the other allowing part of the light to leave the system (so called output coupling).

### 1.1.3 Laser types

Lasers can be divided into many categories, e.g. according to their power, the state of active medium, wavelength, the source of energy, or if they are pulsed or work in continuous regime.

Lasers can radiate in very wide range of wavelengths from millimeters to nanometers and also in very wide range of powers from milliwatts to megawatts and even to higher energies in pulsed lasers.

Very important is division according to the state of active medium. We have solid state, liquid state and gas lasers.

Solid state lasers have solid state material as active medium. Examples of such lasers is ruby laser (one of the first lasers), titanium sapphire, yttrium-garnet (YAG), neodymium doped crystals or glass (e.g. Nd:YAG laser), fiber lasers or huge group of semiconductor lasers. Such lasers are used in many areas of industry, medicine and science. Some of these lasers can reach very high power.

In the category of liquid state lasers there are dye lasers, which have some organic dye as active medium which is dissolved in water, ethanol, or some other dissolving agent. Examples of such dyes are rhodamine, coumarine, stilbene. These lasers are tunable over a wide range of wavelengths and are capable to reach high energies usually in pulsed mode. The disadvantage is the degradation of organic materials with time. They are used in medicine, spectroscopy and another areas.

Gas lasers have gaseous active medium which has quite low density compared with solid or liquid state lasers. Optical pumping (i.e. by radiation) is usually ineffective, so such laser are often pumped by electric current or chemical reactions, sometimes also by the light of another laser [11] (chapter 10). Examples of gas lasers are helium-neon laser, argon ion laser, $CO_2$ laser or group of excimer lasers [13]. Also these lasers are used in industry, medicine and science, e.g. $CO_2$ laser can reach high powers and is used in industry for cutting and drilling.

Chemical lasers present a special group of gas lasers pumped by chemical reaction. There can be various mechanisms of energy transfer from chemical reaction to active medium excitation. Basically can excited particles created in the chemical reaction be used either directly as lasing species or they can transfer their energy to another particle in collisions [14].

Extraction of energy from chemical reaction proves to be highly efficient in laser pumping and quite high energies can be achieved. Chemical lasers therefore belong to the group of high energy lasers and most of them are scalable i.e. can reach higher energy (or power) of laser when using bigger device.

Most of the chemical lasers operate on the transition between vibrational or rotational states, but some of them (e.g. Chemical Oxygen-Iodine laser – abbreviated COIL) works on transition between electronic energy levels. COIL has shorter wavelength than the lasers working on vibrational or rotational transitions. Most chemical lasers operate in infrared part of spectra.

Example of chemical laser is HF (hydrogen fluoride) laser and DF (deuterium fluoride) laser operating on wavelengths between 2.7 and 2.9 $\mu$m (HF) and between 3.6 and 4.2 $\mu$m (DF) respectively, and COIL (chemical oxygen-iodine laser) operating on a wavelength 1315 nm.

## 1.2 Plasma

### 1.2.1 Basic plasma theory

Plasma can be simply described as an ionized gas, in which the concentration of charged particles (ions and electrons) is high enough to influence the behavior of the medium especially in the presence of electric or magnetic field. Most plasmas studied in laboratories contain positive ions, electrons and neutrals. In this work we deal with plasma containing besides neutrals and electrons only singly charged ions, although in some plasmas multiply charged ions can also play important role, especially in higher temperature plasmas.

Textbooks dealing with plasmas and their properties are written e.g. by Raizer [15], Chen [16, 17] or Lieberman [18] and they describe the behavior of plasma in different situations.

Charged particles are created in plasma in a process called ionization – electron leaves neutral atom or molecule and the result is the pair of positive ion and electron. In formula (1.1) ionization by electron impact is shown. In some types of plasmas negative ions are also present. They are created by a process called attachment, in which the free electron is caught by neutral particle and they form negative ion. Process of attachment is shown in (1.2).

$$A + e \rightarrow A^+ + 2e \tag{1.1}$$

$$A + e \rightarrow A^- \tag{1.2}$$

Plasmas are quasineutral – number of negatively charged particles (electrons and negative ions) is approximately the same as the number of positively charged particles. Near the walls the quasineutrality is violated by the wall bias and sheath is created to shield the bulk plasma from the electric field in the vicinity of the wall. The size of sheath is usually calculated as approximately the screening length called Debye length defined in (1.3) which depends on the temperature and the density of particles. Here $\varepsilon_0$ is the permittivity of vacuum, e is the charge of electron, $T_e$ is electron temperature and $k_B$ is Boltzmann constant.

$$\lambda_D = \sqrt{\frac{\varepsilon_0 k_B T_e}{n_e e^2}} \tag{1.3}$$

Neutral particles as well as ions can be in excited state. Deexcitation is accompanied by radiation characteristic for that particular atom or molecule. Radiation coming from plasma is examined by emission spectroscopy method.

Particles in plasma interact by electric forces or in collisions. Collisions of particles can be elastic (state of particles is not changed) or inelastic such as collisions leading to excitation or ionization. Frequency of collisions is very important parameter of plasma.

As electrons are the fastest species, their collisions with ions and neutrals are of the importance. In some types of plasma, electron collisions with neutrals are of the most importance, while in another types (higher density plasma), collisions of electrons with ions are of importance [17]. In plasmas described in this work the collisions of electrons with neutral particles are occurring more often than the collisions of electrons with ions. Collisions of two electrons can be usually neglected.

Often used quantity is mean free path as defined by (1.4) which presents the length the electron with velocity $v_e$ can travel without collision.

$$\lambda_e = \frac{1}{n_e \sigma_e(v)} = \frac{v}{n \nu_e(v)} \tag{1.4}$$

here v is velocity of electron, n is the density of particle with which electron is colliding (electrons, ions, neutrals etc.) and $\sigma_e$ is the cross section of momentum transfer and $\nu_e$ is frequency of collisions. The shortest mean free path should be for collision of ions with electron as there is attracting force between them.

Movement of one kind of particles can be described by distribution function [19]. Plasma in equilibrium would contain particles having the same energy corresponding with the temperature of the medium. In real plasmas light electrons and heavier ions and neutral do not exchange much energy, so there are usually several groups of different particles, each set having its own distribution of energies.

In equilibrium, Maxwell distribution shown in equation (1.5) takes place. We can then define the temperature of the particles.

$$f(E) = \left(\frac{m_e}{2\pi k_B T_e}\right)^{3/2} exp\left(-\frac{E}{k_B T_e}\right) \tag{1.5}$$

In cold laboratory plasmas there is usually not equilibrium between ions and electrons, as they do not exchange much energy in collisions due to their very different mass. So electrons can be described as having temperature $T_e$ and ions having temperature $T_i$ and usually $T_i \ll T_e$.

Another important plasma parameter is plasma frequency defined in (1.6) for electrons ($\omega_{pe}$). For plasma frequency of ions $\omega_{pi}$ similar relation holds, but electron density and mass ($n_e$ and $m_e$) are replaced by that of ion ($n_i$ and $m_i$).

$$\omega_{pe} = \sqrt{\frac{n_e e^2}{\varepsilon_0 m_e}} \tag{1.6}$$

Concentrations of electrons and ions are comparable in quasineutral plasmas, but masses of particles differ usually by four orders of magnitude.

### 1.2.2 Electronegative plasma

Part of the experiments was performed in plasma containing some iodine molecules like $CH_3I$, $CF_3I$ or $I_2$. Iodine is electronegative element and tends to form negative ions.

Electronegative plasma is a plasma in which the negative ions play important role. In some types of plasma, density of negative ions can be even greater than the density of electrons [20]. Because of plasma quasineutrality, concentration of singly charged negative ions plus concentration of electrons is equal to the concentration of singly charged positive ions in bulk plasma.

Negative ions are created by attachment (1.2) of electron to neutral particle, electron can leave neutral ion in a process called detachment or by recombination in collision with positive ion. Attachment to molecules is often dissociative i.e. leads to the dissociation of molecule. In iodine, negative ions are usually formed by dissociative attachment as is shown in (1.7).

$$I_2 + e \rightarrow I^- + I \tag{1.7}$$

Electronegative plasmas are created in electronegative substances whose atoms have high electron affinity. Such substances are e.g. hydrogen, oxygen or halogens (fluorine, chlorine, iodine).

Behavior of particles in electronegative plasmas was measured and modeled [21, 22]. Models of such plasmas show, that very often the bulk plasma far away from walls is electronegative with negative ions as an important species [18]. Nearer to the walls there is the layer, which is electropositive i.e. contains only positive ions and electrons and then there is normal sheath at the wall [23].

When negative ions are formed from neutral particles, free electrons are consumed in this process and can no longer serve for ionization of neutral particles. This leads to lower stability of electronegative plasmas, especially at ignition stage [24, 21].

### 1.2.3 Radiofrequency discharges

Radiofrequency is generally defined as a rate of oscillations with frequency from few kHz to hundreds of GHz. Most often plasma sources (RF generators) work on frequency 13.56 MHz or 27.12 MHz. For special purposes, e.g. when driving the atmospheric pressure dielectric barrier discharge (abbreviated DBD), the generator frequency can be however only a few kHz.

Frequency $\omega$ of RF generator working as a plasma source is such, that plasma frequency of electrons $\omega_{pe}$ as defined in formula (1.6) is higher than the driving frequency and this is higher than the plasma frequency of ions $\omega_{pi}$.

$$\omega_{pe} > \omega > \omega_{pi} \tag{1.8}$$

This means, that while electrons can follow the changes of electric field, ions cannot do this and they follow only slower changes. This effect is most pronounced in sheaths.

Radiofrequency discharges are of two types – capacitively coupled and inductively coupled. Capacitively coupled discharges are usually created between two plates or by hollow cathode nozzle, while inductively coupled discharges are created by coil usually positioned around the discharge chamber.

Particles in RF discharges are not in equilibrium, so the distribution function usually substantially differs from Maxwellian distribution. Review article by Goedheer [25] describes the basic parameters and behavior of capacitively coupled radiofrequency plasma.

Radiofrequency discharges are usually connected with RF generator through the impedance matching circuit. It is because the impedance of the generator (usually around 50 Ω) is different from the impedance of discharge. To deliver as much power as possible to the discharge and to prevent reflection back to the generator which can cause overheating, impedance matching circuit is employed [26, 27].

## 1.3 Diagnostics

Here the spectroscopy and Langmuir probe diagnostics will be described. Both these methods were used for diagnostics in our experiments.

### 1.3.1 Optical spectroscopy

Spectroscopy is diagnostic tool which uses radiation as a source of information about concentrations and temperatures of particles in gaseous media [28]. It can be divided into absorption and emission spectroscopy.

Absorption spectroscopy is an active method which uses light passing through the plasma as a source of information. By this method, concen-

trations and temperatures of mostly ground-state but also excited state particles can be obtained.

When light passes through the material, its intensity is changed. When absorption occurs, then it is proportional to the concentration of absorbing species and also on the path which light travels in the measured medium. This is so called Beer-Lambert law:

$$\frac{J}{J_0} = exp(-\epsilon c_m L) \tag{1.9}$$

Here $J$ is the detected intensity and $J_0$ the initial intensity of the light traveling through the medium, $\epsilon$ is extinction coefficient in the medium, $c_m$ is the concentration of particles in medium and L is the length the light travels through medium.

Emission spectroscopy is a passive method dealing with radiation coming from plasma. By this method, concentrations and temperatures of particles in excited states can be obtained.

Different atoms and molecules have different energy levels and can be identified by their radiation whose energy is determined by the energy gap between two energy levels $\Delta E$ as can be seen in (1.10). Energy levels in molecules are of three types – electronic, vibrational and rotational [29]. Atoms have only electronic energy states [30].

$$\Delta E = h\nu = \frac{hc}{\lambda} \tag{1.10}$$

In the spectra we can usually find spectral lines belonging to certain transition in the atom or molecule. We can however find parts in which we can distinguish no single lines. These are so called continuous spectra. They can arise either from molecular spectra when the lines are too wide and overlap, or this can be effect of so called bound-free transitions such as ionization and recombination, and free-free transitions which denote the changing of the electron velocity and momentum in the vicinity of atoms or molecule (so called bremsstrahlung) [31].

Radiating particle in plasma is usually affected by another particles and its movement in the medium also plays important role. This leads to the broadening of spectral line.

Two most important effects which broaden the spectral line are Doppler broadening and pressure broadening. Doppler broadening is the result of movement of emitting particles in different directions (random movement in which the mean velocity of particles depends on temperature). This broadening is inhomogeneous and results in Gaussian line-shape of the spectral line.

Another source of broadening is the effect of another particles in medium affecting radiating particles due to the collision or electric force. This is collisional (or pressure) broadening which is homogeneous and is leading to Lorentzian profile of the spectral line.

Width of peak with Gaussian shape is a function of temperature and of Lorentzian shape is a function of pressure. Combined pressure and Doppler broadening form spectral line with Voigt profile. From Voigt profile Gaussian and Lorentzian profile can be calculated by deconvolution.

If the pressure broadening can be neglected, gas temperature can be calculated from the full width at half maximum (FWHM) of spectral line from the Gaussian profile:

$$\Delta\lambda_d = \sqrt{\frac{8k_B T\, ln2}{mc^2}}\,\lambda_m \tag{1.11}$$

In hot plasmas also the relativistic effects influencing the spectral line-shape need to be taken into account.

### 1.3.2 Langmuir probe

Langmuir probe (also called electrostatic probe) is a conducting object inserted into plasma and biased with respect to another electrode i.e. it is biased with respect to plasma. By changing probe bias and recording current through the probe circuit we can obtain Langmuir probe I-V characteristics [32, 33]. From the probe I-V characteristics we can obtain plasma potential, floating potential, electron temperature and electron and ion densities.

The typical shape of I-V characteristics in a plasma consisting of just electrons and one kind of positive ions (and also neutrals) is shown in figure 1.3. This shape is mainly determined by different masses and therefore different velocities of light electrons and heavy ions.

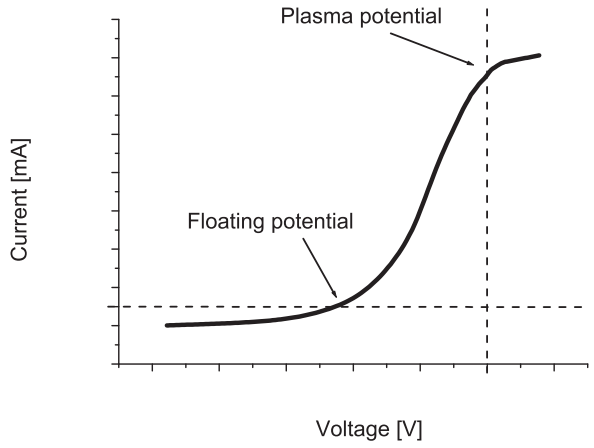


Figure 1.3: Typical shape of I–V characteristics of the Langmuir probe arising from different masses of electrons and ions. Ion saturation current (shown on the left) is exaggerated here.

We can distinguish three main parts of I-V characteristics. On the far left the bias of probe is negative and probe draws ion current. This part is called ion saturation current.

When rising bias, more electrons can reach the probe and when the currents of electrons and ions are equal, probe draws no net current. Bias of the probe when this condition is reached is called floating potential.

For higher bias of probe transition region is reached. Probe draws more electrons than ions, but is still repulsive to electrons. For Maxwellian plasma the dependence of electron current $I_e$ on probe bias is exponential in this part of I-V characteristics (equation (1.12)). From this part of characteristics, electron concentration and temperature can be obtained as well as electron distribution function.

$$I_e = I_{es}\, exp \frac{e(V - V_p)}{k_B T_e} \tag{1.12}$$

Plasma potential $V_p$ is reached when probe attracts neither ions nor electrons. Only random currents are then reaching the probe. In the case of Maxwellian distribution, plasma potential can be calculated also from the floating potential position according to equation (1.13).

$$V_f = V_p - \frac{k_B T_e}{2e}\, ln \left( \frac{2m_i}{\pi m_e} \right) \tag{1.13}$$

For bias higher than plasma potential electron saturation current is reached. In many experiments however electron current does not saturate, partly because of the sheath expansion around the probe. Higher probe voltage also means that plasma is more disturbed by the presence of the probe as it causes the drain of particles from plasma.

Typical shapes of Langmuir probe can be either spherical shape, cylindrical or planar. Most often used is cylindrical probe being just a wire inserted to plasma, so it is easier to construct.

Spatial resolution of a Langmuir probe is roughly determined by Debye length defined in (1.3) or by the dimension of Langmuir probe, whatever is greater. Temporal resolution is approximately determined by the reciprocal value of plasma frequency for ions as is defined in (1.6) [34].

Several theories describing particle collection for different conditions were created [35]. Main parameters are mean free path as defined in equation (1.4), Debye length as defined in equation (1.3) and size of the probe [36].

Classical Langmuir probe theory as well as orbital motion theory (OML) assume collisionless movement of particles, i.e. mean free path of particle is much larger than the probe dimension. These theories differs in assumed sheath thickness, classical Langmuir theory deals with thin sheath (smaller than the probe dimension $\lambda_{e,i} \gg R_p \gg \lambda_D$), orbital motion theory deals with thick sheath ($\lambda_{e,i} \gg \lambda_D \gg R_p$).

In OML regime, ion and electron currents in acceleration regime are proportional to the square root of probe bias V when the ion temperature is neglected [37].

Using Druyvesteyn method [38] we can calculate electron energy distribution function (EEDF) from second derivative of the electron current obtained from probe characteristics as is shown in (1.14). Here $S$ is the probe surface.

$$f(E) = \frac{2m_e}{e^2 S}\left(\frac{2e(V_p - V)}{m_e}\right)^{1/2}\frac{d^2 I_e}{dV^2} \tag{1.14}$$

Shape of EEDF is important parameter of plasma indicating presence of some processes which can take place in plasma as well as the non-equilibrium condition. For equilibrium conditions the distribution is Maxwellian, in some gases like argon we can encounter double-Maxwellian distribution with two groups of electrons having different temperatures [39]. Druyvesteyn distribution can be also often observed in many types of discharges.

From EEDF (here denoted $f(E)$, E being electron energy) we can obtain electron density and temperature as can be seen in (1.15) and (1.16).

$$n_e = \int_0^\infty f(E)\, dE \tag{1.15}$$

$$T_{e,eff} = \frac{2}{3}\int_0^\infty E\, f(E)\, dE = \frac{2}{3} < E > \tag{1.16}$$

Process of calculation of EEDF including smoothing of measured I-V characteristics is discussed e.g. in [40].

When measuring with Langmuir probe we must be aware of detrimental effects which can cause probe I-V characteristics distortion and to erroneous evaluation of plasma parameters.

As will be described in later parts of this work 4.3, Langmuir probe diagnostic data can be affected by noise [41] and because of the probe characteristics nonlinearity, this effect can cause changes in I-V characteristics which make obtaining plasma parameters complicated or even impossible.

Probe operation can also suffer from thin layer deposition on the probe tip or on the insulating probe holder. We will deal with this problem in the chapter 4 dedicated to hollow cathode.

In electronegative plasmas the situation is even more complicated as negative ions affect the plasma behavior [42, 43]. Some theoretical description of positive ions collection by the probe in electronegative plasmas can be found e.g. in [24].

# Chapter 2

# COIL – chemical oxygen-iodine laser

## 2.1 Introduction

Chemical oxygen-iodine laser (COIL) radiates on the wavelength 1315 nm (near infrared region). Radiation around this wavelength is not absorbed by atmosphere and can also easily propagate through optical fibers so it has this advantage over other chemical lasers which radiate on longer wavelengths and whose radiation is strongly absorbed by atmosphere. The reason of the shorter wavelength is that COIL works on the electronic transition while other chemical lasers use transitions between rotationally or vibrationally excited levels [44].

COIL is powered by energy from chemical reactions and can reach high power with the possibility of scalability i.e. reaching higher power with bigger devices.

COIL was originally operated in subsonic regime, but nowadays the important part of system is supersonic nozzle for gas cooling and for enhancement of population inversion as in gas-dynamic lasers [45]. Supersonic regime helped to decrease the size of laser system which is advantageous for practical COIL operation.

First chemical oxygen-iodine laser (COIL) operation was described in article of McDermott et al. [46]. Previous to this discovery, there were iodine lasers pumped by electric discharge [47] or iodine photodissociation laser [48].

Research activity in our group was aimed at improving COIL operation by using different chemicals as a source of iodine atoms and different ways from classical COIL system to obtain singlet oxygen and atomic iodine. This included modeling of chemical reactions and building new types of devices and also trying of electric discharge for dissociation of iodine molecules. The term "atomic iodine" here means iodine atoms as opposed to "molecular iodine" meaning iodine molecules.

In this chapter, many chemical reaction are described and shown with

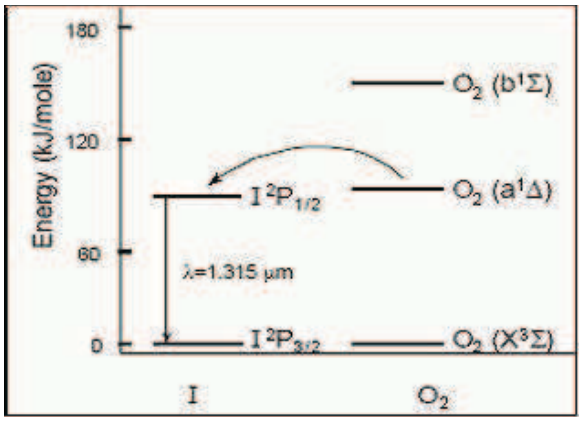


Figure 2.1: Energy levels of atomic iodine and molecular oxygen showing the vicinity of higher energy levels of (both metastable) of these particles [45, 49].

their rate coefficients. Units of rate coefficients are either $cm^3$ $molecule^{-1}$ $s^{-1}$ (often written only as $cm^3$ $s^{-1}$) in the case of reaction of two particles or $cm^6$ $molecule^{-2}$ $s^{-1}$ (often written as $cm^6$ $s^{-1}$) in the case of reaction of three particles. In the case of particles reacting (e.g. being quenched) on the wall, rate constant has unit $s^{-1}$. In later text the units of rate constants will be omitted.

## 2.2 COIL system

In COIL system, two particles are of importance [49]. First one is singlet oxygen molecule $O_2(^1\Delta)$ (more accurately denoted as $O_2(a^1\Delta_g)$) which is the first excited state of oxygen molecule and is metastable with extremely long radiative lifetime some tens of minutes [50]. $O_2(^1\Delta)$ is the source of energy for the laser. Second particle of interest is excited iodine atom $I(^2P_{1/2})$ which is the lasing particle of COIL i.e. is the source of laser radiation.

In figure 2.1 the energy levels of molecular oxygen and atomic iodine are shown. The similar size of energy gap between ground and first excited states of these particles enables nearly resonant energy transfer from $O_2(^1\Delta)$ to $I(^2P_{3/2})$ which is the ground state of iodine atom.

Radiation of the COIL comes from magnetic dipole transition between two electronic energy levels of iodine atom as is described in (2.1).

$$I(^2P_{1/2}) \rightarrow I(^2P_{3/2}) + h\nu \tag{2.1}$$

This transition actually involves six transition between hyperfine energy levels (see figure 2.2) [51]. Ground state $I(^2P_{3/2})$ has four hyperfine energy levels and $I(^2P_{1/2})$ has two hyperfine energy levels present without the magnetic field. The strongest of the six transitions is 3–4 transition in this

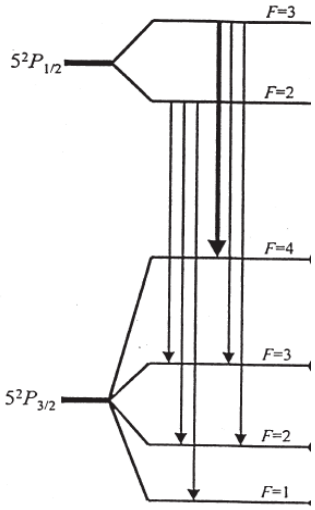


Figure 2.2: Manifold of energy levels of first excited and ground state of iodine atoms showing the six different transitions lines, the strongest (3–4) being the laser transition of COIL. With the presence of magnetic field even more energy levels are present due to the Zeeman effect and more transitions are then possible [51].

spin-orbit manifold of the $^2$P ground term of iodine atom. Magnetic dipole transition presents forbidden transition and I($^2P_{1/2}$) is metastable state [52].

Singlet oxygen $O_2(^1\Delta)$ state has energy 0.98 eV higher than the ground state and the difference between ground state of iodine I($^2P_{3/2}$) and excited state I($^2P_{1/2}$) is 0.95 eV. Principle of pumping of COIL is the near resonant transfer of energy between singlet oxygen molecule $O_2(^1\Delta)$ and iodine atom in ground state I($^2P_{3/2}$) as can be seen in reaction (2.2) and also in [53]. $O_2(^3\Sigma)$ is the ground state of oxygen molecule.

$$I(^2P_{3/2}) + O_2(^1\Delta) \leftrightarrow I(^2P_{1/2}) + O_2(^3\Sigma) \tag{2.2}$$

Reaction (2.2) has rate constant k = 7.8 × 10 $^{-11}$ at temperature 298 K. This rate coefficient actually contains two reaction rates for forward ($k_f$) and backward ($k_b$) direction [45].

$$k_f = 2.33 \times 10^{-8}/T$$
$$k_b = 3.1 \times 10^{-8}\, exp(-403/T)$$

Rate coefficients of the reaction (2.2) depend on the temperature. Lower temperatures are more advantageous for the laser operation, because the equilibrium of reaction (2.2) is shifted towards the excited iodine atoms ($k_b$

is smaller) and the lasing threshold is lower (i.e. lower amount of singlet oxygen is necessary to obtain laser radiation).

Coefficients $k_f$ and $k_b$ together can be written in the form of equilibrium rate constant (2.3) which describes the pumping of the iodine. Number 402 in exponent is the difference of energies of $O_2(^1\Delta)$ and $I(^2P_{1/2})$ in Kelvins.

$$K_{eq} = \frac{k_f}{k_b} = 0.75\ exp\left(\frac{402}{T}\right) \tag{2.3}$$

Production of singlet oxygen is very important process in COIL and is affecting the laser operation. Singlet oxygen yield $Y_\Delta$ is calculated as the part of oxygen molecules produced in $O_2(^1\Delta)$ state compared with the all produced oxygen molecules [54]. In following equation (2.4), $c(O_2(\Delta))$ is the concentration of singlet oxygen and $c(O_2(tot))$ is the overall concentration of oxygen molecules.

$$Y_\Delta = \frac{c(O_2(\Delta))}{c(O_2(tot))} \tag{2.4}$$

From $K_{eq}$ and $Y_\Delta$ a theoretical small-signal gain of active medium can be calculated using equation (2.5).

$$\alpha_{3-4} = \left(\frac{7}{24}\right)\sigma_{3-4}\frac{[(2K_{eq}+1)Y_\Delta - 1]}{[(K_{eq}-1)Y_\Delta + 1]}c_I \tag{2.5}$$

In this equation $\alpha_{3-4}$ is the gain which can be calculated from measured data, $\sigma_{3-4}$ is the cross section of laser transition of iodine atoms and $K_{eq}$ is equilibrium constant of energy pumping as defined in equation (2.3).

Comparison of measured and calculated small-signal gain can show discrepancies and can reveal some unpredicted and unnoticed but important reaction (or reactions), whose effect makes theoretical gain different from the measured one. Such reaction is often detrimental and the measured gain is then smaller then the theoretical one [55].

### 2.2.1 Iodine dissociation

In the classical COIL system iodine molecules $I_2$ are dissociated by the collisions with a several singlet oxygen molecules. One $O_2(^1\Delta)$ molecule does not carry enough energy to dissociate $I_2$, but it can excite it to higher state, which is then easily dissociated by another $O_2(^1\Delta)$ molecule [56, 57]. Overall process of dissociation can be described by reaction (2.6), but what particular processes it involves is yet uncertain, probably it involves higher excited states of both oxygen and iodine molecule [49]. At normal conditions usually between 4 and 6 oxygen molecules are used for dissociation of one iodine molecule.

$$I_2 + nO_2(^1\Delta) \rightarrow 2I + nO_2(^3\Sigma) \qquad n = 4 - 6 \tag{2.6}$$

The classical COIL system therefore contains singlet oxygen generator and the source of iodine vapors. Singlet oxygen and $I_2$ molecules are then mixed together and iodine dissociation as well as excitation of iodine atoms takes place. Mixing occurs usually in the vicinity of supersonic nozzle which cools down the gas and enhances population inversion in laser medium. Lower temperature means lower threshold for laser generation and higher extractable laser power.

Part of the energy carried by $O_2(^1\Delta)$ molecules is used for $I_2$ dissociation and cannot be used for laser pumping. To save the energy of $O_2(^1\Delta)$ molecules for laser pumping, the possibility of iodine production prior to its injection to the $O_2(^1\Delta)$ flow was examined.

Advantage of this proposition is not only the saving of $O_2(^1\Delta)$ energy for laser pumping, but also that other molecules containing iodine such as HI, $CH_3I$ etc. can be used.

Using predissociated iodine (iodine atoms) also improves the mixing, because of lighter particles present in the gas flow and it is beneficial to gain media homogeneity. $I_2$ molecule is actually most easily obtained and cheapest and by its dissociation two iodine atoms are obtained, but it has also many disadvantages.

Problems with $I_2$ are that it is solid at normal conditions and must be heated to obtain high enough gas flow, also substantial part of experimental device must be heated to temperatures about 80 – 100 °C to prevent iodine precipitation. Iodine is also highly corrosive and $I_2$ is also strong quencher of excited iodine atom $I(^2P_{1/2})$ as can be seen in reaction (2.7) [58].

$$I(^2P_{1/2}) + I_2 \rightarrow I(^2P_{3/2}) + I_2 \qquad k = 3.5 \times 10^{-11} \tag{2.7}$$

Even when we use another molecule than $I_2$, we must be aware that iodine atoms recombine to $I_2$ and the problem remains, though it is not so severe.

For efficient laser operation it is necessary to have partial pressure of oxygen and iodine high enough, so that there is high enough density of iodine atoms at least $10^{15}$ cm$^{-3}$.

In the course of the COIL research, different ways of producing both the singlet oxygen or the atomic iodine were investigated. Because this work deals predominantly with atomic iodine production, singlet oxygen generation will be mentioned only shortly.

Dissociation of different molecules containing iodine can be achieved by chemical way, by photolysis or by electric discharge. Here we will deal with dissociation by chemical way, in next part 3 of this work the discharge methods will be described.

Two possible ways of both species production are now most often used. Chemical methods will be described in this chapter and discharge methods in the next chapter.

## 2.3 Singlet oxygen

Singlet oxygen as a source of energy for COIL is very efficiently produced by chemical way in reaction of basic hydrogen peroxide (BHP) with chlorine $Cl_2$. Basic hydrogen peroxide is the solution of mixture of KOH (NaOH can also be used) and hydrogen peroxide $H_2O_2$ in the water. BHP is a liquid and chlorine $Cl_2$ is a gas, so efficient mixing presents one of the fundamental tasks of singlet oxygen generator construction.

Reaction (2.8) presents the overall reaction taking place in the mixture of chlorine and BHP in which singlet oxygen $O_2(^1\Delta)$ is produced

$$Cl_2 + H_2O_2 + 2KOH \rightarrow 2KCl + 2H_2O + O_2(^1\Delta) \tag{2.8}$$

Water produced in this reaction as well as KCl salt can complicate laser operation, because water is quite strong quencher of excited species and KCl is solid and tends to form layers inside the tubes which may lead to choking of the tube.

Actually reaction (2.8) involves $HO_2^-$ molecule created in the BHP, so the singlet oxygen generation can be described by the reaction (2.9).

$$Cl_2 + H_2O_2 + 2HO_2^- \rightarrow O_2(^1\Delta) + 2Cl^- + 2H_2O \tag{2.9}$$

Singlet oxygen has very long radiative lifetime, but can be quenched in collisions. With higher pressure loss reactions have greater effect. $O_2(^1\Delta)$ can be quenched in reactions with another $O_2(^1\Delta)$ (2.10) producing oxygen molecule in higher and lower energy level (so called pooling), also two singlet oxygen molecules can be quenched in the collision to the ground state (2.11) or singlet oxygen can collide with ground state oxygen molecule (2.12) or with water molecule (2.13) [54, 59].

$$O_2(^1\Delta) + O_2(^1\Delta) \rightarrow O_2(^3\Sigma) + O_2(^1\Sigma) \qquad k = 2.7 \times 10^{-17} \tag{2.10}$$

$$O_2(^1\Delta) + O_2(^1\Delta) \rightarrow 2O_2(^3\Sigma) \qquad k = 1.7 \times 10^{-17} \tag{2.11}$$

$$O_2(^1\Delta) + O_2(^3\Sigma) \rightarrow 2O_2(^3\Sigma) \qquad k = 4 \times 10^{-18} \tag{2.12}$$

$$O_2(^1\Delta) + H_2O \rightarrow O_2(^3\Sigma) + H_2O \qquad k = 4 \times 10^{-18} \tag{2.13}$$

Higher excited state of oxygen $O_2(^1\Sigma)$ can collide with water molecule as is shown in reaction (2.14) to partly repopulate singlet oxygen.

$$O_2(^1\Sigma) + H_2O \rightarrow O_2(^1\Delta) + H_2O \qquad k = 6.7 \times 10^{-12} \tag{2.14}$$

For successful COIL laser operation, yield of the singlet oxygen must have threshold value $Y_{th}$ greater than $(2K_{eq}+1)^{-1}$ [49]. Because equilibrium rate constant $K_{eq}$ depends on temperature, with lower temperature the threshold yield necessary for COIL operation is lower.

### 2.3.1 Singlet oxygen generators

Main aim of chemical singlet oxygen generator (SOG) construction is to have the maximum area of contact of liquid and gas phase and very thin layer of liquid so that $O_2(^1\Delta)$ can leave liquid phase without being quenched.

Several types of singlet oxygen generators were designed by different COIL groups to maximize oxygen yield and minimize the detrimental side-effects [45]. In article by Špalek et al. [59] we can find comparison of singlet oxygen generators of various types, such as wetted wall SOG, jet SOG, centrifugal bubble SOG etc.

The most recent are spray type generators [60]. They use nozzle which forms small droplets of BHP interacting with gaseous $Cl_2$. Such generator is capable to produce singlet oxygen with high partial pressure of tens of kPa. The disadvantage of this SOG is the high content of water vapor in the gas flow leaving generator. Very important part of some spray SOGs is separator, which separates water droplets from the flow of oxygen.

Diagnostics of singlet oxygen generator involves oxygen yield calculation from reaction (2.4), singlet oxygen $O_2(^1\Delta)$ concentration is measured by emission spectroscopy at the wavelength 1268 nm. Behind the singlet oxygen generator, concentration of residual $Cl_2$ is measured by absorption on the wavelength 345 nm. From measured data, chlorine utilization can be calculated, which is important parameter of singlet oxygen generator. In our laser experiments jet type SOG was used as described e.g. in [61], with singlet oxygen yield . New spray-type singlet oxygen generator was also built [62, 63, 64].

## 2.4 Chemical generation of atomic iodine

In classical COIL system part of singlet oxygen molecules is employed for $I_2$ dissociation and is therefore lost as a source of energy for the laser. The obvious idea of improvement of laser operation is to use atomic iodine produced before its injection into the flow containing $O_2(^1\Delta)$. Iodine pre-dissociation, according to calculations, can increase laser power by up to 25 % [65, 66].

The chemical way of producing atomic iodine was proposed in our group, this method consists of using hydrogen iodide HI as a donor molecule of iodine. HI molecules should react either with chlorine atoms Cl or fluorine atoms F to produce iodine atoms I [67, 68].

Chlorine or fluorine atoms are produced from $ClO_2$ or $F_2$ molecules respectively in reaction with nitrogen oxide NO [69].

COIL system with atomic iodine generation from HI is shown in figure 2.3. In the fist stages the experiments are performed without the presence of singlet oxygen, in that case flow containing $O_2(^1\Delta)$ is replaced by the flow of nitrogen $N_2$. With $N_2$ flow atomic iodine concentration is measured, while with the presence of $O_2(^1\Delta)$ either small-signal gain is measured or laser experiments are performed.

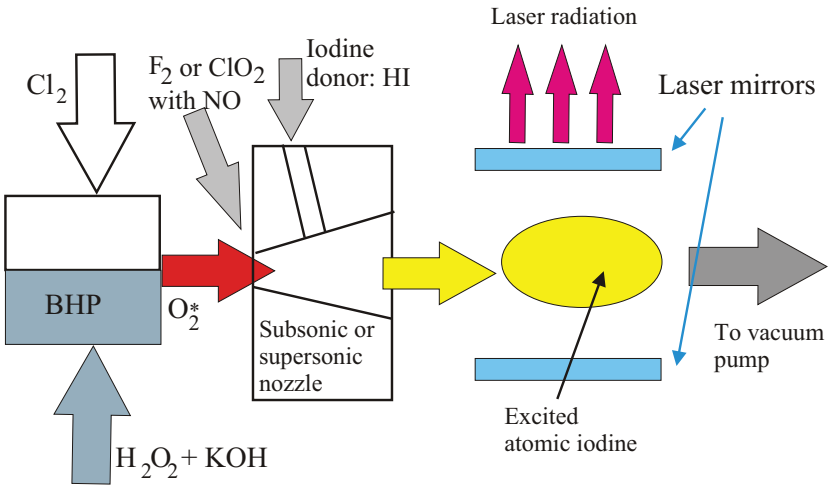


Figure 2.3: COIL scheme with chemically generated atomic iodine. On the left there is classical singlet oxygen generator, effluent from the generator flow to the supersonic nozzle. Then to the singlet oxygen flow molecules NO and $ClO_2$ or $F_2$ are introduced and also later iodine donor (HI in our case). Alternative scheme is possible in which the the iodine atoms are generated separately and then injected into the singlet oxygen flow.

For experiments involving $O_2(^1\Delta)$, classical jet type singlet oxygen generator is used, then to the primary flow containing singlet oxygen either NO, $ClO_2$ (or $F_2$) and HI are introduced or atomic iodine is generated separately and then introduced to the singlet oxygen flow. Mixing of the gas flows takes place in the vicinity of supersonic nozzle. Through this nozzle the gas is flowing to the diagnostic cell or to the laser resonator.

Before the experimental devices were built, the CFD (computational fluid dynamics) modeling was performed which aimed to find the characteristics of the gas flow and the optimal shape of device [70].

Important part of experimental device is a trap cooled by liquid nitrogen in which most of the compounds are separated from the gas flow going to the vacuum pump.

### 2.4.1 Diagnostics

Main diagnostics method to measure the concentration of produced iodine atoms is the absorption spectroscopy using narrow band tunable diode laser working on the narrow wavelength range in the vicinity of 1315 nm. From measured absorption profiles, iodine atoms concentration as well as temperature can be obtained. In the experiments with singlet oxygen $O_2(^1\Delta)$ it is then possible to measure small-signal gain using the same method. The diagnostics system is specially developed for COIL diagnostics and is denoted ISD – iodine scan diagnostics [71]. ISD was placed on movable holder which enabled diagnostics in different vertical and horizontal positions.

From measured absorption spectral line, usually Voigt profile is obtained, from which the Gaussian and Lorentzian profiles and their parameters are calculated by deconvolution. Temperature is calculated from the full width at half maximum (FWHM) of calculated Gaussian profile.

Molar flow rate of generated atomic iodine $\dot{n}_I$ was calculated using the equation (2.15), in which the $c_I$ is a local concentration (number density) of atomic iodine evaluated from ISD data.

$$\dot{n}_I = c_I \frac{V_{flow}}{N_A} \tag{2.15}$$

$N_A$ is the Avogadro constant and $V_{flow}$ is a volumetric flow rate of gas mixture through the detection cell calculated using the equation (2.16).

$$V_{flow} = \dot{n}_{tot} \frac{RT}{p} \tag{2.16}$$

Here $\dot{n}_{tot}$ is total molar flow rate representing the sum of molar flow rates of all gas components, $T$ is gas temperature, $p$ is pressure in detection cell and $R$ is molar gas constant (= 8.314 J/(mol.K)).

Besides atomic iodine also molecular iodine is detected by visible absorption spectroscopy at 488 nm using argon ion laser as a source of light. Detection is performed before the injection into the cavity. Molecular iodine is the result of reaction of two iodine atoms.

Temperature of the gas can be also measured independently by thermocouple. Gas flows are measured by flow-meters, measured flows are usually hundreds of $\mu$mol/s up to several mmol/s.

### 2.4.2 Generation of atomic iodine using chlorine

As is shown in reaction (2.17) iodine atoms in ground state are produced from hydrogen iodide reacting with chlorine atoms in fast and exothermic reaction.

$$Cl + HI \rightarrow HCl + I + 132\ kJmol^{-1} \qquad k = 1.64 \times 10^{-10} \tag{2.17}$$

Chlorine atoms are produced during experiments from chlorine dioxide $ClO_2$ with the help of NO molecule. This process is described by reaction (2.18), which however describes only the overall process.

$$ClO_2 + 2NO \rightarrow Cl + 2NO_2 \tag{2.18}$$

This is not the actual reaction which takes place in the reaction chamber, but it is a branched chain reaction consisting of the following steps of reactions (2.19),(2.20) and (2.21) [66].

$$ClO_2 + NO \rightarrow ClO + NO_2 \qquad k = 3.4 \times 10^{-13} \tag{2.19}$$

$$ClO + NO \rightarrow Cl + NO_2 \qquad k = 1.7 \times 10^{-11} e^{-120/T} \tag{2.20}$$

$$Cl + ClO_2 \rightarrow 2ClO \qquad k = 5.9 \times 10^{-11} \tag{2.21}$$

Reaction (2.19) initiates the chain, reaction (2.21) is the chain-branching step with Cl and ClO as chain carriers. ClO radical is important particle – more stable than Cl – which reacts with NO forming Cl atom. This fact lead to the proposition of injection of NO in two places – in the first place ClO is formed, in the second place Cl atoms are formed from ClO by reaction (2.20).

One serious disadvantage of the described method is that $ClO_2$ molecule cannot be prepared in advance, also cannot be stored under pressure (explosive gas) and is usually generated during experiment by reaction of solid $NaClO_2$ with gaseous chlorine $Cl_2$.

Atomic chlorine Cl is lost mainly in reactions involving three molecules (ternary reactions), fastest is the reaction (2.22) of Cl with nitrogen dioxide $NO_2$ originating from reactions (2.19) and (2.20) [72, 66], with third particle being buffer gas.

$$Cl + NO_2 + N_2 \rightarrow ClNO_2 + N_2 \qquad k = 1.5 \times 10^{-30} \tag{2.22}$$

The effect of this reaction is more pronounced at higher pressures. $NO_2$ molecule in the gas flow also plays role in recombination of iodine atoms as is shown in reaction (2.28).

Iodine atoms created in reaction (2.17) are lost in three-body reactions with carrier gas ($N_2$) and with molecular iodine (result of two iodine atoms recombination with third particle) and with some other molecules as can be seen from reaction (2.23) – (2.26).

$$I + I + N_2 \rightarrow I_2 + N_2 \tag{2.23}$$
$$k = 1.24 \times 10^{-32}\, exp(-7433/RT)\, (T/298)^{0.07}$$
$$I + I + I_2 \rightarrow I_2 + I_2 \tag{2.24}$$
$$k = 2.68 \times 10^{-31}\, exp(-6568/RT)\, (T/298)^{-3.06}$$
$$I + I + HI \rightarrow I_2 + HI \tag{2.25}$$
$$k = 8.13 \times 10^{-32} (T/298)^{-3.5}$$
$$I + NO + N_2 \rightarrow INO + N_2 \tag{2.26}$$
$$k = 1.8 \times 10^{-32}\, (T/298)^{-1}$$

INO molecule created in reaction (2.26) can also react with iodine atom in another loss reaction:

$$I + INO \rightarrow I_2 + NO \qquad k = 2.64 \times 10^{-10} \tag{2.27}$$

All reactions considered in this system can be found in articles by Jirásek et al. and Špalek et al. [58, 66]. Important are also reactions including $NO_2$, especially reactions (2.28) and (2.29).

$$I + NO_2 + N_2 \rightarrow INO_2 + N_2 \qquad k = 3.1 \times 10^{-31} \tag{2.28}$$

$$I + INO_2 \rightarrow I_2 + NO_2 \qquad k = 8.3 \times 10^{-11} \tag{2.29}$$

Very important process is also loss of iodine atoms on the wall.

$$I + I + \ wall \ \rightarrow I_2 + \ wall \qquad \gamma = 1 \tag{2.30}$$

Production of atomic iodine under COIL conditions (i.e. in the flow of oxygen $O_2$ diluted by helium) was at first investigated with the help of computer modeling. Numerical 1-D model was employed for investigation of behavior of chemical compounds in the gas flow. Assumptions are constant pressure, instantaneous mixing of reactants, negligible heat transfer to the walls and adiabatic conditions [58, 66].

The set of equations was solved by fourth order Runge-Kutta routine. Reaction path was calculated from the gas flow velocity and time which was parameter of the kinetic equations. For the chosen initial conditions modeling provided concentration profiles of all reaction components and also temperature profile along the reaction path.

It was found that more advantageous is the injection of HI downstream from the injection point of $ClO_2$ and NO. Also injection of part of NO molecules together with HI enhances the production of I atoms according to the models.

At first small scale atomic iodine generator was employed which consisted of three injectors for the mixing of $ClO_2$, HI and NO which were diluted by nitrogen $N_2$. Later the iodine generator was placed into the laser system and the effluent from iodine generator was introduced into the primary gas flow ($N_2$ and later also $O_2(^1\Delta)$). Injectors were made of stainless steel with one, two or three rows of small holes [66].

Optimal conditions were found for the situation when the NO flow was divided between first and second injector with HI injection very close to the second NO injector.

Laser experiments were performed in the reactor with supersonic nozzle (see figure 2.4). Primary gas flow contains singlet oxygen $O_2(^1\Delta)$ as well as residual $Cl_2$. Into the primary flow first $ClO_2$ and then HI is injected. Gas temperature was rising due to the exothermic reactions. Partial cooling was attained in supersonic nozzle.

The laser operation resulted in small-signal gain 0.3 – 0.35 % $cm^{-1}$ and the laser output power 430 W [51]. This was in the case of sequential admixing of the reacting gases into the primary flow of $O_2(^1\Delta)$ upstream from the supersonic nozzle. Chemical efficiency of the COIL was up to 13 % (best results for classical COIL are around 40 %) and was most probably limited by the quenching of $O_2(^1\Delta)$ by $HO_2^{\bullet}$ radical formed in reaction of

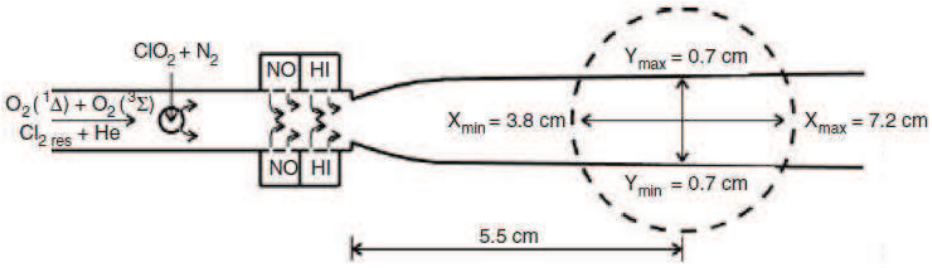


Figure 2.4: Scheme of the COIL system showing injection of $ClO_2$, NO and HI into the flow containing singlet oxygen. Behind injector supersonic nozzle is situated with laser cavity in which the ISD diagnostics (movable vertically and horizontally) takes place [66].

$O_2(^1\Delta)$ with HI. So even if the laser power is rather high, expected gain calculated from the formula (2.5) was 0.7 – 1 % $cm^{-1}$ which would enable us to reach even higher laser power.

### 2.4.3 Generation of atomic iodine using fluorine

In previous section we showed iodine predissociation by chemical reaction of hydrogen iodide with atomic chlorine. Alternative way is to use not chlorine, but fluorine for this purpose. System of reactions and also experiments are described in articles [72, 73, 74, 75, 76].

Atomic fluorine is formed in following reaction (2.31) of fluorine $F_2$ with NO.

$$F_2 + NO \rightarrow F + NOF \qquad k = 7 \times 10^{-13} e^{(-1150/T)} \tag{2.31}$$

Fluorine atoms then react with hydrogen iodide and iodine atoms together with hydrogen fluoride are generated as is shown in reaction (2.32). This reaction is very fast, so by instantaneous injection of $F_2$, NO, and HI fluorine atoms are quickly converted to iodine atoms.

$$F + HI \rightarrow HF + I \qquad k = 1.5 \times 10^{-10} e^{(-5057.8/RT)} \tag{2.32}$$

There is a problem that HF molecule created in reaction (2.32) is a strong quencher of excited iodine $I(^2P_{1/2})$, so there was an idea to replace hydrogen iodide HI with deuterium iodide DI. By comparing rate coefficients in reaction (2.33) and (2.34) we can see that DF is much weaker quencher of excited iodine atom.

$$HF + I(^2P_{1/2}) \rightarrow HF + I(^2P_{3/2}) \qquad k = 1.3 \times 10^{-11} \tag{2.33}$$

$$DF + I(^2P_{1/2}) \rightarrow DF + I(^2P_{3/2}) \qquad k = 1.05 \times 10^{-14} \tag{2.34}$$

F atoms are mostly lost in three-particle collisions with buffer gas, with NO, or by recombination on the wall [73].

$$F + NO + NO \rightarrow NOF + NO \qquad k = 1.8 \times 10^{-31}(T/298)^{-1} \tag{2.35}$$
$$F + NO + N_2 \rightarrow NOF + N_2 \qquad k = 1.1 \times 10^{-31}(T/298)^{-1} \tag{2.36}$$
$$F + F + N_2 \rightarrow F_2 + N_2 \qquad k = 6 \times 10^{-34} \tag{2.37}$$
$$F + F + wall \rightarrow F_2 + wall \qquad \gamma = 0.05 \tag{2.38}$$

There is however reaction (2.39), in which iodine atoms are created in reaction of fluorine atoms with $I_2$ (which is formed by reaction of two iodine atoms).

$$F + I_2 \rightarrow IF + I \qquad k = 4.3 \times 10^{-10} \tag{2.39}$$

Iodine atoms can be lost in ternary reactions which involve two iodine atoms and some other molecules like $N_2$, NO, $I_2$ or HI – reactions (2.23) – (2.26) and also important is loss on the wall as was shown in (2.30).

Some iodine atoms can be lost in reaction with fluorine molecule $F_2$ (2.40), but formed fluorine atoms can be another source of iodine by reaction (2.32).

$$I + F_2 \rightarrow IF + F \qquad k = 1.9 \times 10^{-14} \tag{2.40}$$

Iodine molecule can be also formed in the reaction of two iodine atoms on the wall as is shown in reaction (2.30). All these reactions are described in articles by Jirásek et al. [77] and Čenský et al. [78]. Most of these loss reactions are strongly exothermic, so they lead to the higher temperature of the medium.

We can observe, that the rate coefficient $\gamma$ is higher for iodine atoms than for fluorine atoms. Fluorine atoms are therefore not much affected by the wall as opposed to iodine atoms, whose loss on the wall is very important process.

As in the case of the chlorine, at first small scale reactors for iodine generation were employed [78, 77], later iodine atoms were injected into the flow containing $O_2(^1\Delta)$ and gain was measured. Iodine concentration and temperature of medium was measured by the ISD (Iodine Scan Diagnostics). Gas temperature was also measured by thermocouple.

Movable NO injector was employed to observe the effect of interval of NO and HI injection. Injectors are usually hollow tubes with closed end near which there are perpendicularly to the tube axis drilled small holes usually in several rows.

First experiments were performed in rather low pressure between 1.5 and 3 kPa (too low for COIL operation), with $F_2$, NO and HI gas flows some tens or hundreds of $\mu$mol/s and all gases diluted by $N_2$ (10 % of reacting gas in $N_2$).

To the main flow containing $F_2$, first NO and then HI were admixed [79]. Iodine atoms appeared to be quite stable in the gas flow and their concentration did not depend much on the interval between NO and HI injection, for rather longer times there was small decrease. Iodine atoms are mostly lost in three-particle reactions, and by reaction (2.40), which however presents new supply for fluorine atoms, which after reaction with HI (2.32) produced more iodine atoms. This was probably the reason of very small decrease of I atoms concentration along the flow path.

Best results were obtained at approximately the same amount of $F_2$, NO and HI. At some experiments the order of injection of NO and HI was changed, so first HI and then NO was injected. This resulted in increase of I atoms concentration. During experiments, temperature between 300 and 400 K was measured, increase in temperature is due to the exothermic reactions, but the presence of buffer gas lowers the temperature.

After first ascertaining of the system behavior, gas flows were increased which lead to the pressure increase in the range 4 – 9 kPa. Highest measured I atoms concentration was $5 - 8 \times 10^{15}$ cm$^{-3}$. Higher gas flows lead to higher temperature 400 – 700 K. Higher temperature increases rate constants of the main production reactions (2.31) and (2.32) and decreases rate constants of some loss reactions [78].

In later experiments, gas flows and pressure were further increased [77]. Gas flows reached 1.5 mmol/s and pressure was up to 20 kPa. Because of ternary loss effects and low yield of iodine atoms (relative to initial $F_2$), further experiments were performed with undiluted NO and HI and only $F_2$ was diluted by $N_2$ (20% of $F_2$). Iodine atoms concentration increased with increasing of gas flows of reacting gases, while higher pressure did not result in substantial decrease of iodine concentration. Concentration up to $4.2 \times 10^{16}$ cm$^{-3}$ was reached at pressure 12.5 kPa. Experiments showed that F atom is much more stable even at higher pressure than is Cl atom in chlorine reaction system. Because of higher reacting gas flows and less buffer gas, temperature increased up to 1500 K.

In the final stage, gain experiments were performed with primary gas containing $O_2(^1\Delta)$. Measured gain was however very low, under 0.22 % cm$^{-1}$ [73], although the small-signal gain estimated from equation (2.5) is approximately twice higher. Because measured iodine concentration was rather high (about $10^{15}$ cm$^{-3}$), low gain is probably caused by some detrimental reaction, probably quenching occurred by $DO_2^{\bullet}$ radical, which is similar problem that was encountered in chlorine system.

### 2.4.4 Chemical reactions modeling

The question have arisen about the reaction of $F_2$ with HI, whose possibility was mentioned in literature. The effect of this reaction was examined in experiment [77] and also with the help of modeling. From the experiment the value of rate coefficient about $3.7 \times 10^{-14}$ cm$^3$/s was estimated. This is quite high value so this reaction cannot be neglected.

My tasks during experiments with both chlorine and fluorine were only marginal, like helping the group to prepare experiments, to perform experiments and to finish clearing after experiments, as well as evaluation of measured ISD data (absorption or gain, depending on the type of experiment) with the help of program written in Origin environment by Miroslav Čenský. My own task was modeling of 1-D chemical kinetics of chemical reactions present in fluorine system as is described in the next section.

Modeling of chemical reactions system was performed to find optimal conditions (relative initial ratio of $HI/F_2$, time of injection of HI etc.) for experiments and also to ascertain the effect of reaction of $F_2$ with HI in the reaction medium. Chemical reactions taken into account can be found e.g. in [58, 73].

Numerical 1-D model was employed for investigation of behavior of chemical compounds in the gas flow. Assumptions are constant pressure and negligible heat transfer to the walls. The set of chemical equations was solved by fourth order Runge-Kutta routine. Reaction path was calculated from the gas flow velocity and time which was parameter of the kinetic equations. For the chosen initial conditions modeling provided concentration profiles of all reaction components and also temperature profile along the reaction path.

In the first stage of modeling with only $F_2$ and NO in reaction system, reactions (2.31) and set of loss reaction (2.35) – (2.38) were used. It was proposed that HI is injected downstream from the injection of $F_2$ and NO. Nitrogen $N_2$ is buffer gas, so it is not reacting, but plays the role in ternary loss reactions.

In second stage also reaction with iodine and its compounds were included, namely reactions (2.32) and loss reactions (2.40), (2.39), reactions (2.29) – (2.26) and also (2.27). Also reaction of three iodine atoms was taken into account:

$$I + I + I \rightarrow I_2 + I \qquad k = 5 \times 10^{-33}\, exp(-17626/RT) \tag{2.41}$$

The effect of mixing was also taken into account. In following reactions (2.42) and (2.43) N in brackets means that the compound is yet unmixed and cannot chemically react. Unmixed compounds are changing in time to mixed compounds and they can react with other compounds. Some rate constants are depending on temperature.

$$F_2(N) + NO(N) \rightarrow F_2 + NO \qquad k = 1 \times 10^{-14} \tag{2.42}$$

$$HI(N) + HI(N) \rightarrow HI + HI \qquad k = 1 \times 10^{-14} \tag{2.43}$$

It was observed, that reaction of $F_2$ with HI can take place, so the effect of this reaction was investigated [77]. In our model it was supposed, that this reaction has two steps (2.44) and (2.45). It is expected that the second reaction is much faster than the first reaction and is efficiently removing HI

and IF molecules from the gas flow. It is advantageous to remove unreacted HI (or DI) from the gas flow before the injection into the $O_2(^1\Delta)$ flow to prevent the formation of $HO_2^{\bullet}$ (or $DO_2^{\bullet}$) radical.

$$F_2 + HI \rightarrow IF + HF \tag{2.44}$$

$$IF + HI \rightarrow I_2 + HF \tag{2.45}$$

For these two reactions three possible sets of rate constant were proposed and modeled, later fourth set was added in which very small rate constants were proposed (both of the order $10^{-20}$ cm$^3$ s$^{-1}$), so that these reactions are not efficient in influencing the reaction system.

The model was built as a two stage process, first fluorine $F_2$ was mixed with NO and buffer gas, later HI was injected. The concentrations were depending on time, which in constant flow can be transformed into the x-coordinate (distance from point of the gas entry).

Three different times of injection of HI after the injection of $F_2$ and NO were proposed: $T_1 = 50$ $\mu$s (position 453 $\mu$m), $T_2 = 250$ $\mu$s (position 4.37 mm) and $T_3 = 800$ $\mu$s (position 22.3 mm).

Modeling was done for three different pressures: 3 kPa, 7.5 kPa and 15 kPa. Also different ratios of initial HI flow to initial $F_2$ flow were proposed: HI:$F_2$ = 0.5:1 or 1:1 or 1.5:1 or 2:1.

Temperature was changing with the time as the heat was produced in exothermic reactions. This lead to changing of rate constants in the case they were dependent on temperature, most often it is the case of ternary reactions (reactions involving three bodies on the left side). Initial temperature is 300 K. Changing of temperature was modeled using formula (2.46), in which $T$ is temperature, $p$ is pressure, $c_{pm}$ is the sum of molar heat capacities of reactants and $H_i$ is enthalpy of one reactant.

$$\frac{dT}{dt} = \frac{RT}{pc_{pm}} \sum H_i \frac{dc_i}{dt} \tag{2.46}$$

In the first stage of the modeling, reactions of $F_2$ and NO together with buffer gas took place as can be see in graph 2.5, later from the calculated concentrations at the time of injections, new modeling system was calculated containing now the HI.

By comparing results of modeling with experimental results we can deduce approximate values of rate constants of reactions (2.44) and (2.45) [73]. This is also important because IF molecule is strong quencher of excited iodine atom as is shown in reaction (2.47). Rate coefficient of this reaction is comparable with the quenching of $I(^2P_{1/2})$ by HF as shown in (2.33).

$$IF + I(^2P_{1/2}) \rightarrow IF + I(^2P_{3/2}) \qquad k = 1.3 \times 10^{-11} \tag{2.47}$$

So especially reaction (2.45) can be beneficial for COIL system, because it removes IF molecules and also removes excess of unreacted HI (or DI),

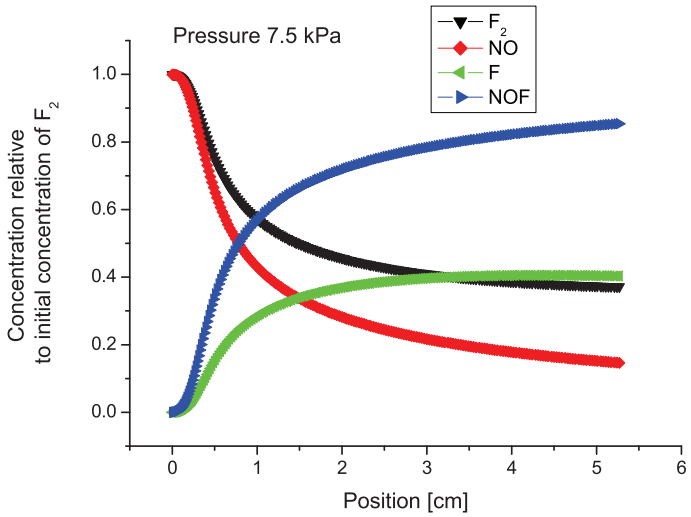


Figure 2.5: Concentrations of main components (without the buffer gas $N_2$) of reaction system with fluorine $F_2$ before the injection of HI.

which in presence of singlet oxygen form radical $HO_2^\bullet$ (or $DO_2^\bullet$) which is strong quencher of $O_2(^1\Delta)$.

In graph 2.6 four curves showing possible behavior of IF molecule concentration in case that rate constants of reactions (2.44) and (2.45) are $1\times10^{-20}$ and $1 \times 10^{-20}$ (curve 1, rate constants very small), $1 \times 10^{-15}$ and $1 \times 10^{-14}$ (curve 2), $1 \times 10^{-14}$ and $1 \times 10^{-13}$ (curve 3) and $1 \times 10^{-14}$ and $1 \times 10^{-12}$ (curve 4). Data obtained in simulation were then compared to measured data.

In fluorine system, instantaneous admixing of HI to the $F_2$ + NO flow is advantageous. This effect is more pronounced at higher pressure (15 kPa). Ratio of HI:$F_2$ is best near 1:1.

Concentration of iodine atoms is shown in graph 2.7. It shows that in this case more important for iodine concentration is the amount of HI admixed into the flow.

With higher gas flows and higher pressure the modeled temperature was higher. Calculated temperature is however higher than is expected to be measured, due to the cooling effect of the buffer gas and also due to the walls of the reaction chamber which remove part of heat from the system.

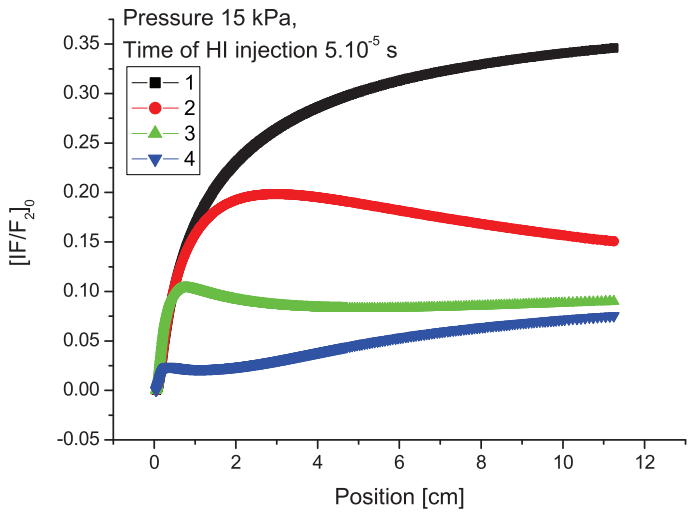


Figure 2.6: Calculated relative concentration of IF in dependence on the distance from HI injection, initial concentrations $F_2$:HI = 1:1. Curves 1–4: different rate constants for reactions (2.44) and (2.45), curve 1 shows the case of lowest rate constants (slow reactions) and curve 4 shows the case of highest rate constants (fastest reactions).

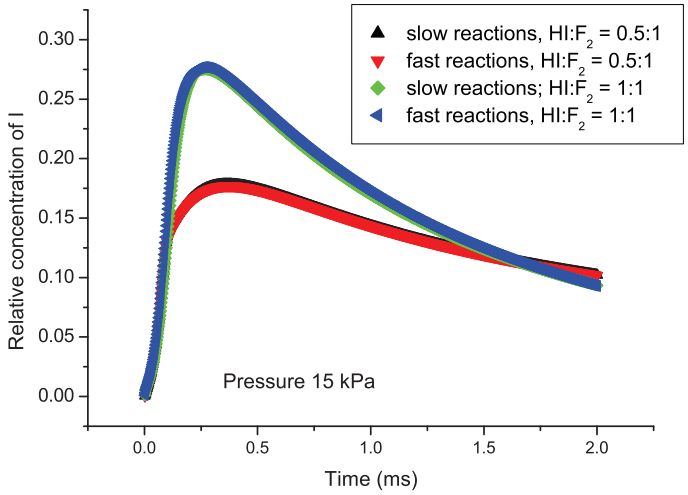


Figure 2.7: Calculated relative concentration of I atoms in dependence on the time passed from HI injection. Fast reactions means that rate constants for reactions (2.44) and (2.45) are $10^{-14}$ and $10^{-12}$ respectively, while for slow reactions both rate constants are $10^{-20}$. It is shown, that initial rate of concentrations HI:$F_2$ plays more important role than the rate constant of reactions (2.44) and (2.45).

## 2.5 Conclusion

Classical chemical oxygen-iodine laser is using singlet oxygen $O_2(^1\Delta)$ as a source of energy for laser and also for $I_2$ molecule dissociation. It was calculated, that by using different methods of iodine dissociation, about 25 % enhancement of laser power can be expected.

New method of atomic iodine generation by chemical way was examined, using atomic chlorine or fluorine reacting with HI. Its advantage is that HI from which I atoms are produced, is gas at normal conditions, so heating of the part of experimental device can be avoided.

Described chemical methods of atomic iodine generation by chemical way from hydrogen iodide HI (or DI) using either chlorine or fluorine atoms proved to be very efficient, but serious drawback is the formation of radical $HO_2^\bullet$ or $DO_2^\bullet$ respectively. It is therefore necessary to remove all HI (or DI) from the gas flow leaving atomic iodine generator. This can be done by reactions (2.44) and (2.45).

COIL operation with production of atomic iodine I in reaction of hydrogen iodide HI with $ClO_2$ was studied. After initial modeling of reactions gain measurements were performed and laser power of 430 W was achieved. It was found, that Cl atoms does not last long in gas flow, but ClO radical with longer lifetime can be used as Cl source before HI injection. The limitation of $ClO_2$ molecules is that it cannot be prepared in advance and cannot be pressurized.

In fluorine system, F atoms were obtained from $F_2$ molecule. Instead of HI, DI molecule was used because of the much smaller rate coefficient of quenching of excited iodine $I(^2P_{1/2})$ by DF (2.34) than by HF (2.33).

Concentration of iodine atoms was measured by iodine scan diagnostics (ISD) using absorption spectroscopy on the wavelength of 1315 nm. Other diagnostic methods involved pressure and temperature measurements and also gas flows before the injection of gases.

Chemical generation of atomic iodine proved to be efficient in that it is possible to produce iodine atoms in pressures and concentration sufficient for laser operation, these methods however suffer from the presence of chemical seriously quenching singlet oxygen (radicals $HO_2^\bullet$ or $DO_2^\bullet$) and also from very high reaction temperature. This lead to substantially lower small-signal gain than was calculated by theoretical formula. It was therefore possible to operate COIL with high power radiation over 400 W, but the efficiency was lower than expected.

# Chapter 3

# Oxygen-iodine laser with electric discharge

## 3.1 Introduction

Alternative system to the chemical oxygen-iodine laser (COIL) is discharge oxygen-iodine laser (DOIL) in which the singlet oxygen $O_2(^1\Delta)$ molecules are produced in the electric discharge. The theory and methods of singlet oxygen obtaining can be found e.g. in the review article by Ionin et al. [80].

Historically before the discharge oxygen-iodine laser was examined, laser with atomic iodine active medium which was produced and excited in discharge without the presence of singlet oxygen was studied [81, 47].

Singlet oxygen $O_2(^1\Delta)$, which is the source of energy for laser, can be used as in classical COIL system for $I_2$ dissociation and I atoms excitation (as was discussed in the previous chapter) or, with iodine atoms produced separately, it can be used for iodine atoms excitation only. Generation of iodine atoms prior to their injection into the singlet oxygen flow may lead to the higher laser power compared with the classical design and it also enables the use of different molecules containing iodine other than $I_2$.

Singlet oxygen $O_2(^1\Delta)$ can be produced by electric discharge [82, 83, 84] and it is possible to run electric discharge oxygen-iodine laser, but still with rather smaller power than chemical oxygen-iodine laser [85]. Such laser is usually denoted DOIL (discharge oxygen-iodine laser) or ElectriCOIL. Electrically driven oxygen-iodine laser was first demonstrated by Carroll et. al. [85] after series of calculations and experiments [86, 87, 88, 89]. Classical scheme was employed in which $I_2$ molecule was dissociated in the flow of $O_2(^1\Delta)$. Recently laser power reaching 538 W was announced [90].

In this work we will deal mostly with the atomic iodine generation in discharge. With separate iodine atoms generation, different iodine donors (i.e. molecules containing iodine) can be used, besides $I_2$ [91, 92] also HI, $CH_3I$, $CF_3I$ and some more [93, 94, 95, 96, 97, 98, 99] were studied. The advantage of HI and $CF_3I$ is that they are in gas state at normal conditions and $CH_3I$ is liquid at normal conditions so they have much higher vapor

pressure than $I_2$ and there is not necessary to use substantial heating to obtain high gas flow. Also by using different iodine donors than $I_2$ the effect of quenching of $I(^2P_{1/2})$ by $I_2$ in process (2.7) can be avoided or at least substantially diminished.

For iodine compounds predissociation, various types of discharges were used up to now, e.g. DC glow discharge [71, 101, 102], microwave discharge [65, 92] or radiofrequency discharge [103, 104] and also different iodine donors and different buffer gases were examined.

Dissociation of iodine donor by electric discharge is also one way to obtain pulsed COIL operation [100]. This method uses the mixture of singlet oxygen with iodine donor (not $I_2$) and when the discharge is switched on, the iodine donor is dissociated by discharge and then iodine atoms are excited by singlet oxygen.

Problem with electric discharge generation of either atomic iodine or singlet oxygen $O_2(^1\Delta)$ is lower pressure and higher temperature of laser medium even with cooling of the gas by the supersonic expansion. Higher temperature leads to the lower laser gain, lower pressure means that the concentration of active medium particles is low. It is therefore challenging to operate discharge oxygen-iodine laser and to reach high power.

Here we will deal with production of atomic iodine I in electric discharge using $CH_3I$ and $CF_3I$ molecules as iodine donors. The discharge singlet oxygen generator will not be described here and the principle of singlet oxygen generation will be only shortly mentioned.

## 3.2 Discharge generation of atomic iodine and singlet oxygen

### 3.2.1 Atomic iodine generation

$CH_3I$ and $CF_3I$ molecules were investigated as the iodine donors. Dissociation of $CH_3I$ and $CF_3I$ by electric discharge can be accomplished by several different processes present in plasma. For $CH_3I$ these processes were described by Mikheyev et al. [94].

Most important processes are dissociative attachment of electron to $CH_3I$ or $CF_3I$ molecule as is shown in equation (3.1), and also the excitation of $CH_3I$ or $CF_3I$ by electron impact (or possibly by radiation) to the antibound orbital by process (3.2). Because C-I bond is the weakest bond in the molecule, dissociation usually occurs along this bond. There are also processes involving positive ions $CH_3I^+$ or $CF_3I^+$, which can be dissociated by electron impact (3.3) or by impact of negative ion $I^-$ (3.4), both processes lead to the dissociative recombination. In the equation below only $CH_3I$ molecule is used, but similar processes occur for $CF_3I$ as well, only the rate constants of reaction are different.

$$CH_3I + e^- \rightarrow CH_3 + I^- \tag{3.1}$$
$$CH_3I + e^- \rightarrow CH_3I^* + e^- \rightarrow CH_3 + I + e^- \tag{3.2}$$
$$CH_3I^+ + e^- \rightarrow CH_3 + I \tag{3.3}$$
$$CH_3I^+ + I^- \rightarrow CH_3 + 2I \tag{3.4}$$

Inelastic collisions involving $CH_3I$ can usually involve many excited levels of molecules (mostly vibrational) [105]. More about formation of negative ions from $CH_3I$ by electron impact can be found e.g. in article by Nagesha et al. [106] and interactions of $CF_3I$ molecule with electrons is described in the article by Christophorou et al. [107].

Dissociative attachment has greatest cross section for low electron energies, while dissociative excitation has greater cross section for higher electron energies, so usually two main processes 3.1 and 3.2 take place together in the plasma.

For laser operation it is necessary to work at rather high pressure at least a few kPa. Three-particles loss reactions (3.5) and (3.6) (or (3.7) for $CF_3I$) are then important and limit the operation of laser. Here M is an arbitrary third particle present in gas medium (buffer gas, I, $I_2$ formed by recombination of two I atoms etc. ).

$$I + I + M \rightarrow I_2 + M \tag{3.5}$$
$$I + CH_3 + M \rightarrow CH_3I + M \tag{3.6}$$
$$I + CF_3 + M \rightarrow CF_3I + M \tag{3.7}$$

Also the recombination of iodine atoms on the wall as shown in (2.30) is important loss process, as the wall has strong catalytic effect especially for the iodine atoms [108].

The problem of many previous atomic iodine generators was the fast recombination of iodine atoms, either in the medium or on the walls before their injection into the singlet oxygen flow. The loss processes resulted in measurement of substantially lower concentration of iodine atoms than was predicted. It is therefore necessary to place the generator as near as possible to the point of injection of iodine atoms into the primary gas flow.

### 3.2.2 Singlet oxygen generation

Generation of singlet oxygen $O_2(^1\Delta)$ in electric discharge is an alternative to the chemical generation. Its advantage is that there are present no chemicals like $H_2O_2$, KOH or $Cl_2$. There is however usually lower $O_2(^1\Delta)$ yield (usually less than 20 % compared with over 60 % in chemical generator). Higher yield is usually attained at lower pressure which is insufficient for laser operation. Also substantial heating of medium occurs in discharge generators.

Singlet oxygen $O_2(^1\Delta)$ is produced by impact of electron with oxygen molecule. There is also possibility to enhance $O_2(^1\Delta)$ population by cascading from higher singlet states into which the oxygen molecule can also be excited. There are other possibilities such as impact with another molecule, ozone UV photolysis, oxygen atoms recombination or excitation by photons, but they have much lower efficiency.

The specialty of discharge oxygen generation is the presence of oxygen atoms in the primary flow consisting of singlet oxygen. Oxygen can enhance the dissociation of iodine $I_2$ in the reaction:

$$O + I_2 \rightarrow OI + I \qquad k = 1.25 \times 10^{10} \tag{3.8}$$

$$IO + O \rightarrow O_2 + I \tag{3.9}$$

Very important issue of generation of both atomic iodine and singlet oxygen is the discharge stability, because iodine and oxygen are electronegative elements and negative ions formed by attachment diminish the electron population in the discharge. As the electrons are usually main source of ionization, this leads to the lower stability of discharge, extinguishing of discharge or possibly sparking.

## 3.3 Experimental device

The aim of our work was to operate discharge oxygen-iodine laser (DOIL). It consists of singlet oxygen generator from which the primary gas flow is going around the iodine injector from which the iodine atoms are introduced into the flow of singlet oxygen. Mixed gases then flow through the supersonic nozzle to the laser cavity.

First part of this experimental device which was examined was atomic iodine generator using radiofrequency (RF) discharge for iodine donors dissociation. The scheme of the atomic iodine generator is shown in figure 3.1. Main part is iodine injector serving also as a discharge chamber and the shape of the injector is designed, so that it forms double-slit supersonic nozzle together with the walls of the cavity.

This configuration was proposed, to minimize the distance the iodine atoms must travel before their injection to the singlet oxygen flow. Iodine atoms undergo very fast recombination on the walls as is shown in reaction (2.30) as well as in the three-body loss reactions in the medium forming usually iodine molecules $I_2$ as is shown in reactions (3.5)and (3.6) or (3.7).

For successful DOIL operation, the atomic iodine generator should produce iodine atoms with high yield, low temperature and also high pressure for injection into the laser cavity, and the by-products should quench neither singlet oxygen nor excited iodine atoms.

Around the iodine injector primary gas is flowing. Iodine donor ($CH_3I$ or $CF_3I$) together with carrier gas (Ar or mixture of Ar with He) is introduced to the discharge chamber from the direction perpendicular to the primary

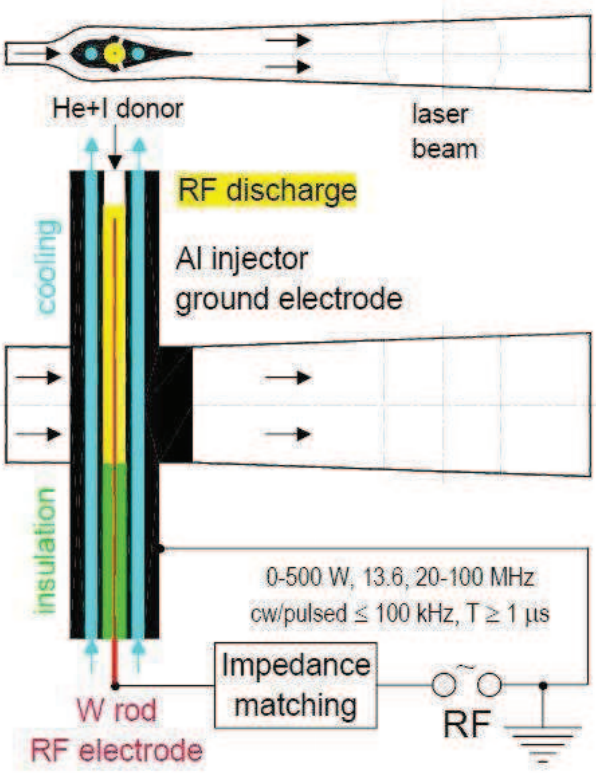


Figure 3.1: Discharge chamber for atomic iodine generation from side and top [109, 110].

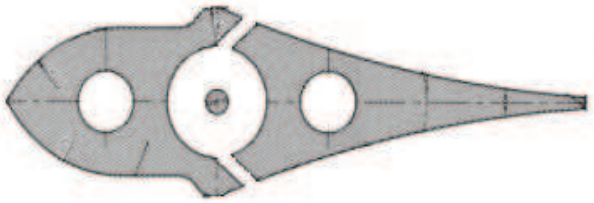

Figure 3.2: Shape of the iodine injector, which is serving as a part of double slit nozzle. Its shape was calculated by modeling of gas flow conditions. Drawing of injector modified according to [109].

gas flow. In the discharge chamber, the dissociation takes place and iodine atoms are injected into the primary flow. Behind the supersonic nozzle, the cavity is placed, in which either iodine concentration is measured (primary gas being only $N_2$) or small-signal gain can be measured (when primary gas flow contains singlet oxygen).

Depleted gas then flows through the cooled iodine trap to the vacuum pump. Description of experimental device together with experimental results can be found in article by Schmiedberger et al. [109].

The walls of the experimental device around and behind the iodine injector are made of plexiglass, which is optically transparent and allows observation of the discharge and the gas flowing through the supersonic nozzle and cavity. Spectroscopic diagnostics can then be used. Inner surfaces of plexiglass are covered with thin glass panes to prevent damages by heat or by fluorine and its compounds.

Supersonic expansion of the gas in the nozzle ensures cooling of the gas so that the equilibrium in process (2.2) will be in favor of excited atomic iodine and also the threshold yield will be smaller (i.e. for laser operation it will not be necessary to have so high yield as in the case of higher temperature of medium).

Iodine injector was designed by the computer modeling to the shape which would form double slit supersonic nozzle together with the device walls (see figure 3.2).

Iodine injector is made of aluminium, which is chemically resistant to corrosion caused by iodine. Aluminium has also good electric and thermal conductivity, reflects ultraviolet light (this helps enhancing iodine donor dissociation and production of iodine atoms in exited state) and also is quenching singlet oxygen only weakly.

In the middle of the injector there is cylindrical discharge chamber, parallel to the discharge chamber are two channels used for water cooling of the injector body. In the middle of the discharge chamber the tungsten cathode is placed.

Main discharge chamber is cylindrical cavity with diameter of 9 mm in which the tungsten electrode with diameter of 2 mm is inserted axially. There are two other channels parallel to the discharge chamber used for water cooling of the injector as it is heated by the RF power delivered to the discharge.

Injector has two rows of 15 output holes which are circular and have the diameter of 2.2 mm. It is quite large value and was chosen in order to prevent recombination of iodine atoms on the edges of the holes. This however caused pressure drop along the length of discharge chamber, higher pressure being near the inlet of iodine donor, lower pressure at the opposite side.

Used tunable RF generator can work on different frequencies from 20 to 100 MHz, with output power up to 500 W. It is also possible to use pulsed mode with pulse frequency from 100 Hz to 99 kHz and pulse duty ratio from 5 to 95%. Pulse regime may increase the stability of discharge in electronegative gases.

Between the RF generator and the discharge chamber the impedance matching circuit must be placed to minimize the reflection of radio waves back into the generator and to ensure the delivery of maximum power to the discharge. To ensure good impedance matching, after few initial experiments, frequency of 40 MHz was chosen.

## 3.4 Diagnostics

Concentrations of species, especially of atomic iodine were measured as in the COIL by iodine scan diagnostics ISD method which is absorption spectroscopy using tunable diode laser on the wavelength around 1315 nm monitoring the I($^2P_{1/2}$) – I($^2P_{3/2}$) transition. This diagnostics was installed on movable holder, so that iodine concentration was measured for different vertical and horizontal positions along the flow duct.

Single pass beam of diagnostic laser was employed (which differs from COIL at which double pass beam technique was used), because of the high losses on cavity walls (plexiglass and thin glass pane and especially on optical interface between them strongly affect the passing light). Laser beam was distorted on the walls and measured signal baseline was curved, so it was necessary to perform smoothing and averaging over several measured data sets. Single pass has unfortunately lower sensitivity than multiple pass.

From the measured absorption profiles, iodine I number density and temperature were obtained using deconvolution of measured Voigt profiles to Gaussian and Lorentzian profiles.

When only atomic iodine concentration was measured, it was possible to detect only ground state iodine atoms using absorption spectroscopy. Part of the iodine atoms was produced in excited state when could not be in this case detected, so the measured concentration was considered to be lower limit of the concentration of iodine.

Also the estimation of iodine atoms concentration downstream of the injector was lower due to the iodine atoms recombination.

Partial pressure of atomic iodine is evaluated from formula (3.10), in which $c_I(y)$ and T(y) are evaluated number density and temperature and y is the position in direction perpendicular to that of along the injector [110].

$$p_I = \frac{1}{y_2 - y_1} \int_{y_1}^{y_2} c_I(y) RT(y) dy \tag{3.10}$$

We can then calculate the dissociation fraction, which :

$$\eta_{diss} = \frac{p_I}{p_{cav}} \frac{\dot{n}}{\dot{n}_{CH3I}} \tag{3.11}$$

here $\dot{n} = \dot{n}_{Ar} + \dot{n}_{He} + \dot{n}_{N2} + \dot{n}_{CH3I}$ is total gas flow rate and $p_{cav}$ is the pressure in the detection cavity.

To measure the efficiency of the dissociation process, we can calculate the fraction of the absorbed RF power spent on the dissociation:

$$fP_{diss} = \frac{P_{diss}}{P_{abs}} = \frac{e\dot{N}_I E_{bond}}{P_{abs}} \tag{3.12}$$

$P_{diss}$ is the power used for dissociation of iodine donor, $P_{abs}$ is the absorbed power, e is the charge of electron, $\dot{N}_I$ is the evaluated flow rate of iodine atoms and $E_{bond}$ is the dissociation energy of C-I bond. Dissociation energy of C–I bond is 2.47 eV for $CH_3I$ and 2.34 eV for $CF_3I$.

To measure the concentration of excited particles, mainly of excited iodine atom I($^2P_{1/2}$), emission spectroscopy was employed. Spectral range of the spectroscope was between 600 and 1700 nm. Light coming from plasma was lead to the spectroscope by optical fibre. Light intensity was quite low, so better coupling using focusing element was necessary.

During experiments flows of gases, pressure and temperature were measured. Measured data were collected by the computer. In the flow duct behind the supersonic nozzle pressure was measured by the movable Pitot tube, from which the Mach number of the flow can be obtained.

## 3.5 Experimental results

Cold flow experiments i.e. experiments without discharge and without iodine donor were performed first to ensure the proper design of the supersonic nozzle and the cavity and of the gas flows control. At first only primary gas was used ($N_2$ or He or mixture of these two gases), later also secondary gas consisting of mixture of argon with helium was introduced into the iodine injector.

First experiments involved changing of primary gas flow and observing dependence of the Mach number on the flow of gases and on the position of

Pitot tube. It was found that with higher $N_2$ content the Mach number was higher.

Later experiments involved presence of iodine donor and of the discharge. Prior to introduction to discharge chamber iodine donor was mixed together with its carrier gas, which was usually mixture of argon and helium.

In first experiments iodine donors $CH_3I$ and $CF_3I$ were used [108]. $CH_3I$ is volatile liquid at normal condition (boiling point around 42.5 °C). It has fortunately high vapor pressure over the surface. $CF_3I$ on the other hand is gas at normal conditions (boiling point -22.5 °C).

Most of the experiments were performed for subsonic flow for which the pressure behind the nozzle is higher and higher absorption signal can be observed. Problem with many optical interfaces resulted in curved baseline detected in ISD measurements and in noisy data.

### 3.5.1 $CH_3I$

Flow containing $CH_3I$ molecules was introduced into the iodine injector together with carrier gas (mixture of Ar and He). Flow rate of $CH_3I$ changed between 0.1 and 0.77 mmol/s, argon flow between 1 and 3.1 mmol/s and helium between 0 and 6 mmol/s. Primary gas flow of nitrogen was between 10 and 37 mmol/s.

Cavity pressure was between 140 and 850 Pa, lower pressure was at supersonic flow, higher at subsonic flow. Pressure inside the injector varied between 2.0 and 3.2 kPa. Power delivered to discharge was between 50 and 250 W at frequency 40 MHz.

From ISD diagnostics the iodine concentration profiles were obtained, which for subsonic flow were homogeneous and parabolic as can be seen in graph 3.3. For supersonic flow similar profiles are sharper but less homogeneous (graph 3.4). With higher primary gas flow the profiles were rather flat even at supersonic regime. At supersonic conditions the temperature is also much lower (200 – 350 K) than for subsonic conditions (350 – 450 K). Lower temperature is advantageous for laser operation.

In some calculated data peaks were observed, which probably resulted from sparking in the discharge.

When vertical profiles of the temperature were measured, there was clearly visible the effect of output holes of the injector, behind which the gas had higher temperature.

Dissociation fraction calculated with use of equation (3.11) is shown in graph 3.5. Data were measured for different conditions, strong dependence on pressure was measured – with higher pressure the dissociation fraction was lower, reason is probably some three-particle reaction like e.g. (3.6). Graph of this dependence can be found in article by Schmiedberger et al. [109].

Dissociation fraction was over 17 % when the power delivered by RF generator was near to the 250 W which is the upper limit of measurements. The presence of helium in some cases had a slight negative effect on the dis-

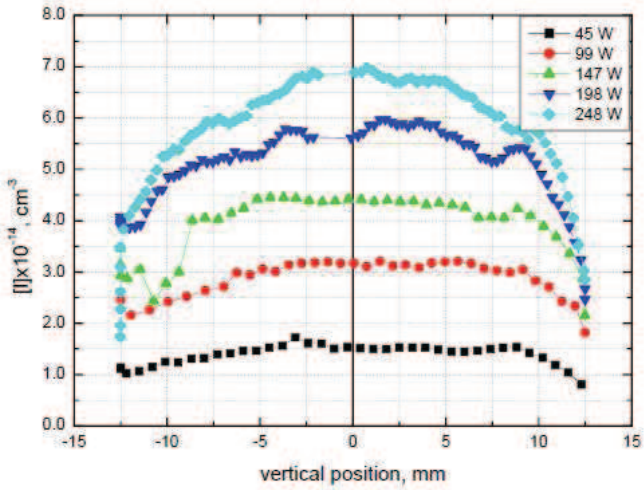


Figure 3.3: Vertical profiles of iodine number density depending on absorbed RF power, $p_{cav}$ = 780 Pa, flow rates (mmol/s): $CH_3I$ – 0.73, Ar – 1.96, He – 1.92, $N_2$ – 20.6.

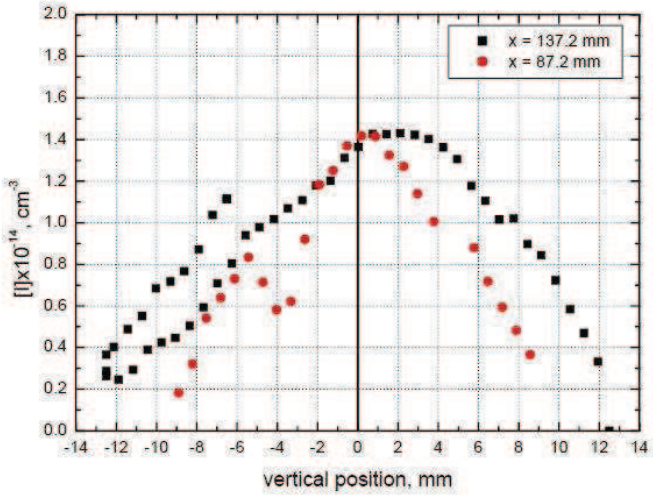


Figure 3.4: Vertical profile of I number density at two positions downstream the nozzle throat for the supersonic flow. Pressure in cavity was 139 Pa, discharge power 250 W. Flow rates were 0.76 mmol/s $CH_3I$, 1.95 mmol/s Ar, 1.92 mmol/s He and 37.7 mmol/s $N_2$ in primary gas flow.

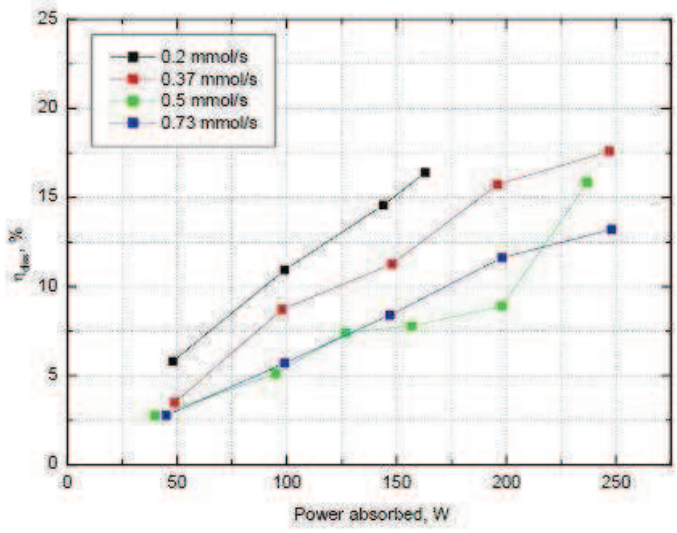


Figure 3.5: The dependence of dissociation fraction on the absorbed RF power and also on the $CH_3I$ flow rate. Data were measured 137 mm downstream the injector outlet. Pressure in cavity was between 560 and 780 Pa, argon gas flow 1.9 mmol/s, helium gas flow 1.9 mmol/s.

sociation degree. Number density of iodine atoms increased with power and also with the flow of $CH_3I$, but dissociation degree decreased with increasing flow of $CH_3I$.

### 3.5.2 $CF_3I$

$CF_3I$ gas flow in experiments was between 0.18 and 0.91 mmol/s, argon gas flow between 2 and 4.9 mmol/s, helium gas flow between 0 and 2 mmol/s and $N_2$ gas flow 20 mmol/s. Cavity pressure changed between 520 and 680 Pa and injector pressure was between 2.2 and 4.6 kPa.

$CF_3I$ is highly electronegative molecule because it contains also fluorine. The discharge stability was strongly affected by this molecule, at higher power levels sparking instabilities appeared destroying the plasma. It was necessary to work in pulsed mode of discharge, which increased the stability.

Dissociation fraction in figure 3.6 shows better results for the data measured without the presence of helium with only argon as a buffer gas.

When using helium together with argon as a buffer gas, instability of discharge for power over 150 W lead to sparking. Without helium it was possible to reach higher power [110] and dissociation fraction increased.

Dissociation fraction and the fraction of the power consumed for dissociation decrease strongly with pressure [110].

The shapes of density and temperature profiles were similar for both iodine donors. The dissociation fraction over 22 % was measured with $CF_3I$ flow 0.2 mmol/s and with only argon as a carrier gas. This is substantially higher than for $CH_3I$ with the same flow.

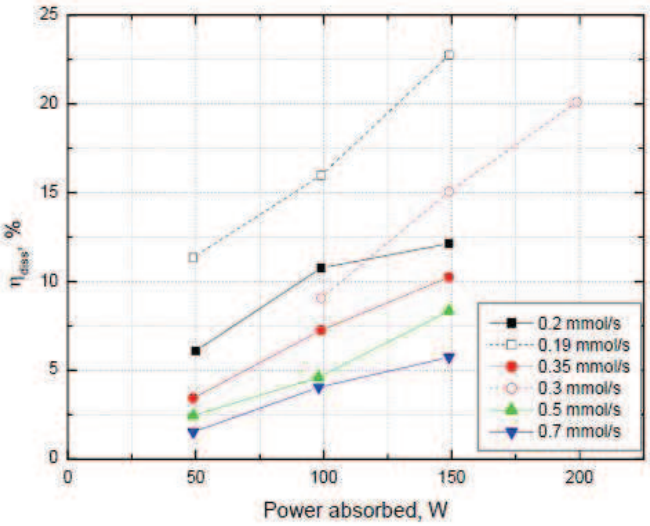


Figure 3.6: The dependence of dissociation fraction on the absorbed RF power and also on the $CF_3I$ flow rate. Data were measured 137 mm downstream the injector outlet. Pressure in cavity was between 480 and 540 Pa, argon gas flow either 1.9 mmol/s (solid lines) or 3.1 mmol/s (dashed lines), helium gas flow either 1.9 mmol/s (solid lines) or 0 mmol/s (dashed lines).

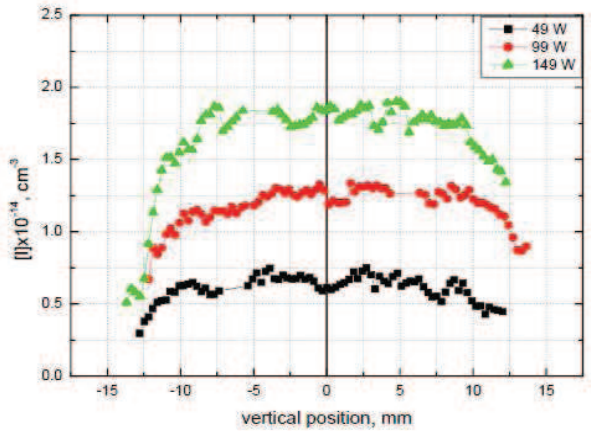


Figure 3.7: Vertical profile of I number density at three values of absorbed RF power. Pressure in cavity was 510 Pa, flow rates: 0.35 mmol/s $CF_3I$, 1.96 mmol/s Ar, 2.04 mmol/s He and 20.5 mmol/s $N_2$ (primary gas).

### 3.5.3 Emission spectroscopy diagnostics

Part of the iodine atoms produced in discharge is in the excited state and cannot be therefore properly detected by the absorption spectroscopy method (ISD diagnostics), so also the emission spectroscopy diagnostics was employed.

Emission spectra measured in the discharge cavity show very small signal near the wavelength of atomic iodine radiation around 1315 nm, the reason is that the excited state I($^2P_{1/2}$) is metastable and also that not many particles are in this excited state. Better results would be obtained with singlet oxygen as a primary gas, but singlet oxygen generator was not available at a time of these experiments. Transition between I($^2P_{1/2}$) and I($^2P_{3/2}$) involves actually six transitions from different sublevels, so instead of one line, six lines would be detected. Actually two quite thick emission lines were measured, each consisting of three emission lines.

During emission spectroscopy measurements, continuous spectra were detected between 600 and 900 nm approximately, whose origin is uncertain.

In figure 3.8 we can see emission spectrum of atomic iodine in the vicinity of 1315 nm. We can observe the presence of two main peaks, but as we can see from figure 2.2, there are actually six transitions, so each of the two peaks visible in the figure 3.8 consists of three peaks too near to each other to be distinguished in this resolution.

Also for $CF_3I$ emission spectra (see figure 3.9) were recorded with the similar results as in the case of $CH_3I$.

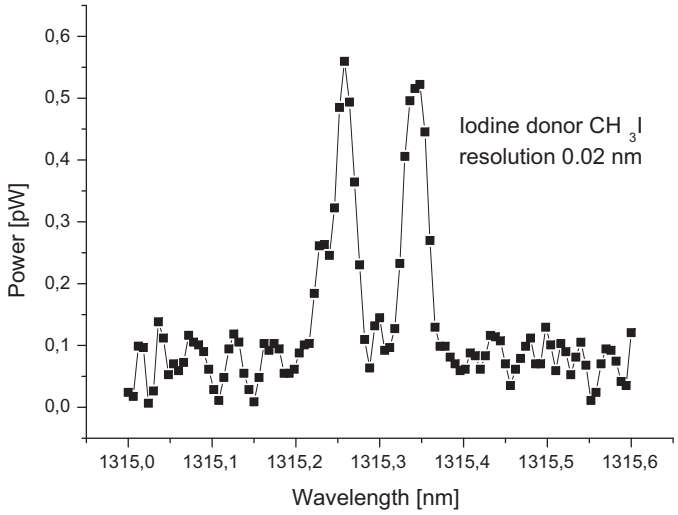


Figure 3.8: Recorded emission spectrum for iodine donor $CH_3I$. Four measured data sets are averaged to improve the signal to noise ratio. Spectral line belongs to atomic iodine and shows the transition in the vicinity of 1315 nm. Each of two visible peaks actually consists of three peaks.

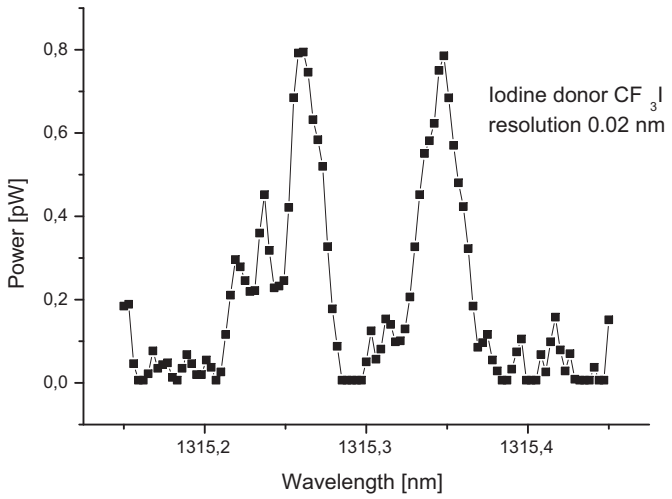


Figure 3.9: Recorded emission spectrum for iodine donor $CF_3I$. Two measured data sets are averaged to improve the signal to noise ratio. Spectral line belongs to atomic iodine and shows the transition in the vicinity of 1315 nm. Each of two visible peaks actually consists of three peaks.

## 3.6 Conclusion

Dissociation of $CH_3I$ and $CF_3I$ in radiofrequency driven discharge was studied in a part of future DOIL system which consisted of atomic iodine generator and gas flow tube. Employed discharge was radiofrequency (RF) driven on the frequency 40 MHz with power ranging from 50 to 250 W. Pressure in discharge chamber was 2–3 kPa.

Absorption spectroscopy diagnostics in the vicinity of 1315 nm was employed. Horizontal and vertical profiles of the gas flow were measured. Atomic iodine concentrations and temperatures were estimated from the absorption spectra. Most of the experiments were performed in subsonic conditions for better diagnostics signal. Measured atomic iodine concentration was of order of $10^{14}$ cm$^{-3}$.

Dissociation fraction $\eta_{diss}$ of $CF_3I$ was dependent on pressure and decreased with increasing pressure. It is probably due to the recombination reaction (3.7) in which third particle is argon or helium and which is quite fast [110]. $\eta_{diss}$ of $CH_3I$ on the other hand is not much dependent on pressure.

Dissociation fraction of $CH_3I$ was lower than for $CF_3I$ at similar conditions, the reason is probably that the integral cross section of dissociative attachment for $CH_3I$ is about four times lower than for $CF_3I$.

Temperature of iodine was higher than expected probably because of exothermic association reactions:

$$CH_3 + CH_3 \rightarrow C_2H_6 \tag{3.13}$$

$$CF_3 + CF_3 \rightarrow C_2F_6 \tag{3.14}$$

Also recombination of iodine atoms on the walls plays important role, because it is very fast process and substantially decreases the concentration of iodine atoms.

Iodine is electronegative element, so in the discharge negative ions are formed by dissociative attachment. This lead to decrease of electron concentration in discharge and especially in the case of $CF_3I$ to lower stability of discharge. By using the repetitively pulsed mode the stability was improved.

The problem with both these donors is the presence of carbon layers deposited on the inner surfaces of the discharge chamber.

Discharge efficiency for $CH_3I$ and $CF_3I$ dissociation was up to 11 %. Measured dissociation fraction was about 20% at the RF power 250 W with number density of iodine atoms being $2.5\times10^{14}$ cm$^{-3}$ in supersonic flow with flowrate of atomic iodine reaching 0.11 mmol/s. The results are therefore sufficient to obtain gain in case there is no detrimental process leading to quenching of either singlet oxygen molecules or excited iodine atoms.

# Chapter 4

# Hollow cathode plasma jet system

## 4.1 Description of the hollow cathode plasma jet system

In this chapter we will describe Langmuir probe measurements in the hollow cathode plasma jet system powered by radiofrequency (RF) generator. Discharge gas is either pure argon or argon with iodine admixture. Hollow cathode is the example of capacitively coupled radiofrequency discharge device.

Hollow cathodes are widely used for thin layer deposition and plasma etching, but can also be used e.g. as a source of electrons for neutralization of effluents from electric thrusters used e.g. for propulsion in space [111].

Principle of hollow cathode system thin layer deposition is that hollow cathode material is sputtered and either forms conducting layer on inner surfaces of a plasma device or sputtered material can react with some plasma compound (e.g. nitrogen or oxygen) to produce oxide or nitride layers [4].

Gas is flowing to the discharge chamber through the hollow metallic nozzle which is powered and serves as a cathode. Plasma jet is then formed at the exit from the nozzle. Cathode can be powered by DC [112], pulsed DC [113, 114] and also RF [115] power supply.

High density plasma plume is formed at the exit of the nozzle by the so called "hollow cathode effect". Its principle is prolongation of electron path in the plasma, so that more neutral particles can be ionized by electron impact. In hollow cathode, electrons are reflected by the sheath near the inner walls of the cathode back into the plasma [7].

Scheme of the plasma system with hollow cathode can be seen in figure 4.1, hollow cathode is positioned in the upper part of the device.

Hollow cathodes usually work at pressures from 10 Pa up to over 100 Pa. In lower pressures the hollow cathode effect is not triggered and we can sometimes observe only low density discharge between cathode and the conducting wall of discharge chamber. For ignition it is sometimes necessary to

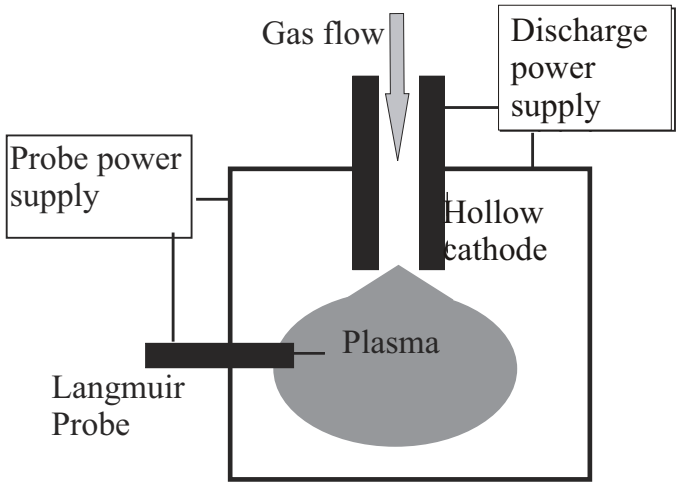


Figure 4.1: Scheme of the discharge chamber with hollow cathode, which serves also as a nozzle through which the gas is flowing to the discharge chamber. Langmuir probe shown on the left together with probe power supply.

have even higher pressure than for just discharge operation.

## 4.2 Experimental device

Our experimental device is the hollow cathode plasma jet system powered by RF generator working on frequency 13.56 MHz.

Discharge chamber has cubical shape, hollow cathode is made of aluminium and is positioned in the upper part of the discharge chamber. In the front and at one side the glass windows allow the observation of the discharge. At the back of the discharge chamber there is a gas outlet connected with the vacuum pump. Only primary vacuum pump is used – oil vane pump with minimum pressure in chamber around 3 Pa. Near to the gas outlet the Pirani manometer is placed, with which the pressure inside the chamber is measured.

Because hollow cathode is considerably heated by RF power, the cooling by the water is used.

Gas is delivered to the discharge chamber through the gas system containing two branches (figure 4.2). Three flow-controllers are used to control and measure the gas flows. First branch is to supply argon only, gas flows through the flow-controller with the range 200 sccm. Second branch should supply mixture of argon with iodine $I_2$ and contains two flow-controllers, one with the range of 100 sccm, other with the range of 20 sccm. Second branch is closed when only argon is used.

Because iodine $I_2$ is solid at normal conditions, iodine vapor generator (figure 4.3) is placed in one gas flow branch. Iodine crystals are placed on the porous silica surface, through which the argon is flowing. Iodine vapors

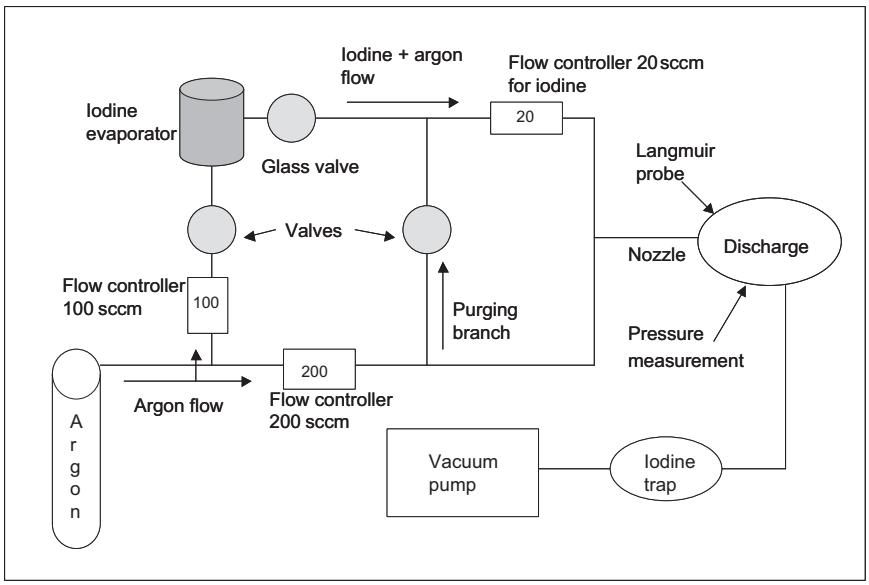


Figure 4.2: Scheme of gas flow showing two branches for the delivery of either pure argon or of argon with iodine admixture.

are then carried to the discharge chamber by the flow of argon.

With higher flow rates it may be possible to encounter iodine precipitation on the inside surfaces of the flow tubes. There is therefore possibility to heat the part of gas flow system from iodine vapor generator to the discharge chamber including special flow controller (range 20 sccm) whose electronic part is separated from main flow-controller body and is connected by the cable only. Temperature of the flow controller while heated is measured by USB thermometer.

Energy to the discharge is supplied by RF generator working on the frequency 13.56 MHz, with power up to 600 W. This generator is capable to provide continuous or pulsed regime.

To deliver energy from RF generator to plasma with maximum efficiency it is necessary to employ impedance matching. Impedance matching unit which was used in our experiments can be seen on the photo 4.4. Impedance matching circuit is usually kind of filter with tunable capacitors and inductors. When the matching circuit is properly tuned, reflection to generator is minimized [27].

There is always some loss of power in matching circuit, e.g. Scanlan et al. [116] expects, that about 50% of power coming from RF generator is lost.

Wires in the vicinity of radiofrequency system can also work as antennas, therefore they are either emitting or receiving radiofrequency waves. We can suppress this effect with proper shielding and grounding of the cables.

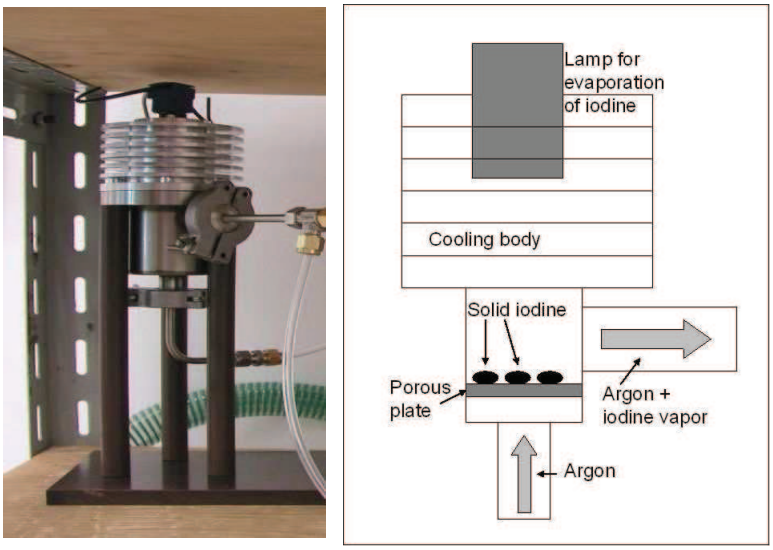


Figure 4.3: Photo and scheme of the iodine vapor generator.

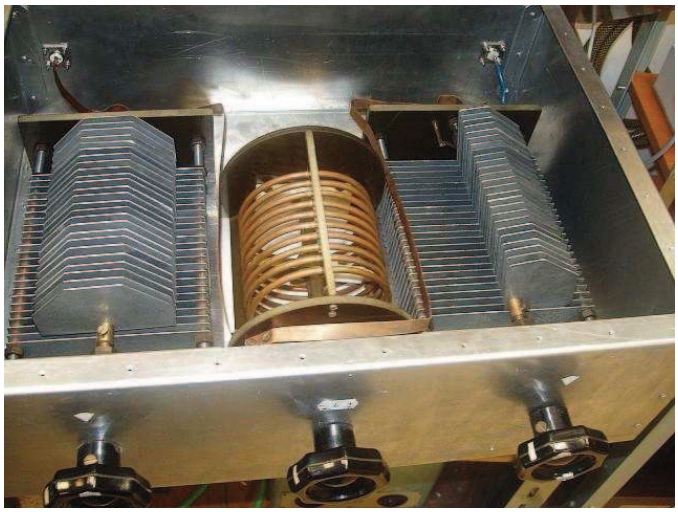

Figure 4.4: The impedance matching device showing one coil and two capacitors.

## 4.3 Langmuir probe operation

As a diagnostics tool, cylindrical Langmuir probe was used, actually tungsten wire with the diameter 0.1 mm and the length ranging from 3 to 9 mm. Position of the probe together with probe holder and probe circuit is shown in figure 4.1. Probe circuit contains also power supply for probe bias setting and multimeter to measure current flowing through the probe.

For power supplies control and data collection by multimeter by computer, special measuring program was created in the environment of Agilent VEE (see Attachment).

Probe tip was positioned 2 cm below the nozzle and was radially movable, so it was possible to measure at different distances from the center of the chamber and therefore in different distances from the nozzle.

Principle of Langmuir probe operation was theoretically described in section 1.3.2. Here we will mention some specific aspects of measurement with Langmuir probe, such as the behavior of Langmuir probe in radiofrequency driven plasma and the problem of contamination of the probe surface.

From measured I-V (current-voltage) characteristics of Langmuir probe we can obtain floating potential, then plasma potential and under the assumption of Maxwellian electron energy distribution function (EEDF) we can obtain electron temperature and electron concentration. We can also obtain from the second derivative of electron current the distribution function of electrons. In case the EEDF is not Maxwellian we can obtain the effective electron temperature $T_{e,eff}$ from formula 1.16 and electron density from 1.15.

Hollow cathode usually produces high density plasma which leads to efficient deposition of thin layers on the inner surfaces of discharge chamber. Such layers, and especially non-conducting layers, are detrimental for the probe operation and therefore probe was cleaned by the ion bombardment, when the probe was biased to high negative voltage around -48 V. Problem of thin layer deposition was more pronounced at higher pressures in discharge chamber (50, 80 and 100 Pa).

Because plasma devices often serve for thin layer deposition, probe measurements also suffer from contamination of probe surface by deposited layers [117]. Non-conducting layers present greatest problem, because they greatly distort measured probe characteristics and make it impossible to obtain reliable results [118]. Even the presence of conducting layers only can lead to distortion of characteristics caused by changing of the work function of the probe surface. Another problem is deposition on the probe holder, which can lead to bigger effective collecting area of the probe or to the problems with probe circuit.

There are several ways to clean the probe surface: possibilities are ion bombardment (probe strongly negative), electron bombardment (probe in the range of electron saturation current) and heating of the probe (heated or emissive probe).

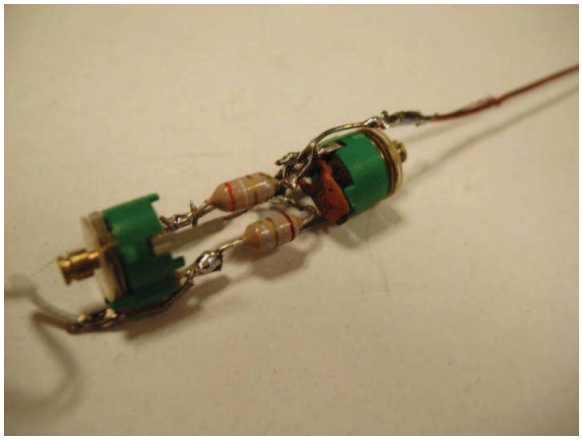

Figure 4.5: Photo of the RF compensation circuit which was placed inside the probe holder. Two inductances (coils) and two capacitances were used to filter the driving frequency and the first harmonic frequency.

### 4.3.1 Langmuir probe in RF plasma

Using Langmuir probe in RF plasma needs some consideration, because as is mentioned e.g. by Chen [32], measured I-V characteristics is averaged over many RF cycles and because of characteristics nonlinearity its transition part is not so steep as in DC plasma [119]. Also estimated floating potential is more negative and electron temperature is overestimated [120].

Reason of Langmuir probe I-V characteristics distortion is the oscillation of plasma potential [121, 25], which is due to the fact that driving frequency of plasma lies between electron plasma frequency and ion plasma frequency. Lighter electrons can therefore still follow the changes of electric field, but heavy ions react only to much slower changes. This effect occurs mostly in sheaths around the probe and at the walls, which also form part of the probe circuit.

To obtain undistorted I-V characteristics, it is necessary to employ RF compensation. There are two basic types of RF compensation — active and passive. Comparison of both compensation techniques can be found e.g. in article by Annaratone et al. [122]. Some plasma characteristics can be obtained with some care even without RF compensation [123, 124] or with incomplete RF compensation [125].

Active RF compensation [126, 127] employs the external source of RF signal with the same frequency as is the driving frequency of the RF generator. This signal with its phase shifted is delivered to the probe. There is a criterion, that floating potential should be as near to the plasma potential as possible to obtain good RF compensation. However the presence of higher harmonic frequencies in the plasma may be a problem.

Passive RF compensation uses filter circuit placed as near to the probe tip as possible. Usually it is placed inside the probe holder [128]. This circuit is band-stop or low pass filter for driving frequency and for some harmonic

frequencies, at least the fundamental one [129].

Circuit for RF compensation consists of capacitors and inductors which fulfill relation (4.1) also known as Thomson relation [130].

$$2\pi f = \frac{1}{\sqrt{LC}} \tag{4.1}$$

Besides the RF filter, auxiliary electrode can also be used, which is connected to the probe through the capacitor with high capacity. This electrode feeds collected RF signal to the probe. This is called hybrid RF compensation [131].

In our experiments, passive RF compensation was employed (photo is in the figure 4.5).

## 4.4 Experimental results

Experiments were performed in argon and later in argon with the small admixture of iodine $I_2$. Argon experiments were made first, for the reason that in the radiofrequency discharge many effects can be present which affect the measured data, and we must be able to distinguish the effect of electronegative substance (iodine) from the effects caused by plasma oscillations or by thin layer deposition on the probe surface or probe holder.

In the first experiments the Langmuir probe voltage supply reaching up to 50 V was used, plasma potential was however not detected (in the beginning, the detection of plasma potential was made by searching for the maximum of the first derivative of the probe characteristics). When adding second power supply capable to deliver additional 25 V (so that the probe voltage could reach 75 V), it was possible to find the plasma potential which in many cases was over 60 V.

Pulsed regime of RF generator was also examined, this however brings some disturbing effects to the probe circuit (such as switching on and off the power delivery), so that reasonable data cannot be obtained by the Langmuir probe method.

Data were evaluated with the help of Origin program and also with the help of special program START created by Pavel Kudrna [132]. Program START is capable to calculate floating and plasma potential and also electron temperature and electron and ion concentration under various assumptions from the measured I-V characteristics.

### 4.4.1 Argon

Argon experiments were performed using only one branch of gas delivery system (as is shown in figure 4.2). In first experiments, impedance matching was tuned, so that nearly zero power is reflected back to the RF generator.

In figure 4.6 there is a photo of the discharge in the chamber. Color of the discharge was changing slightly while changing pressure and discharge was brighter for higher power. It was also possible to observe sheath around

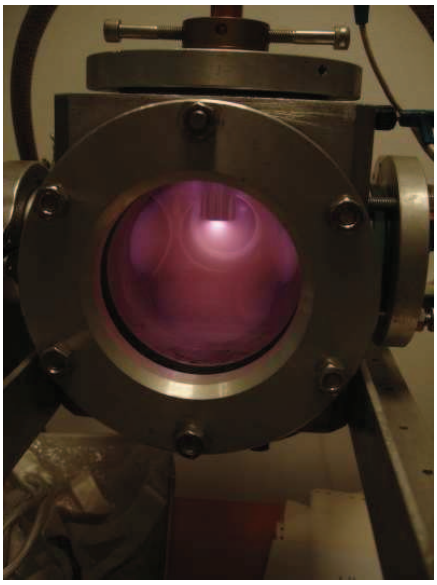

Figure 4.6: Photo of the discharge in argon at the pressure of 50 Pa.

the nozzle and around the walls because of its different color as compared with the bulk plasma.

Plasma jet was observed below the nozzle as a brighter plume. It is the plasma with higher density and higher electron energy, as was proved by the later experiments.

I-V characteristics measured in argon showed dependence on the probe position, on the power delivered to discharge, on the pressure in the discharge chamber and on the gas flow.

In following graphs we can see dependence of measured I-V characteristics on the probe position i.e. on the distance of the probe tip from the center of the discharge chamber (graph 4.7), dependence on pressure (in graph 4.8), on the power delivered to the plasma (in graph 4.9) and on the argon gas flow (graph 4.10).

Dependence on the power as seen in graph 4.9 is actually the dependence on the RF power coming from the RF generator and not on the power delivered to the discharge. It is obvious, that some of power coming from generator is lost in wires and in matching unit. Godyak [117] estimated, that power lost in matching unit can be over 50% and in some cases can reach 90%. That may be the reason, why the I-V characteristics measured for different values of power are very near one to each other.

From the I-V characteristics first the floating potential and the plasma potential were obtained. In graph 4.11 we can see changing of floating potential with probe position and in graph 4.12 we see the changing of plasma potential with the probe position. Plasma potential was calculated from the zero crossing of the second derivative of the I-V characteristics. When the probe position is zero, then the probe tip is just below the nozzle

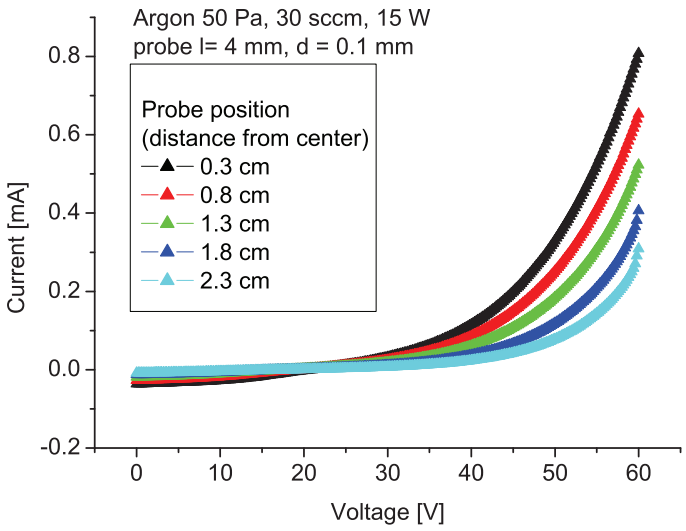


Figure 4.7: Measured I-V characteristics changing with the probe position. Further from the nozzle there is lower electron current and also lower ion current to the probe.

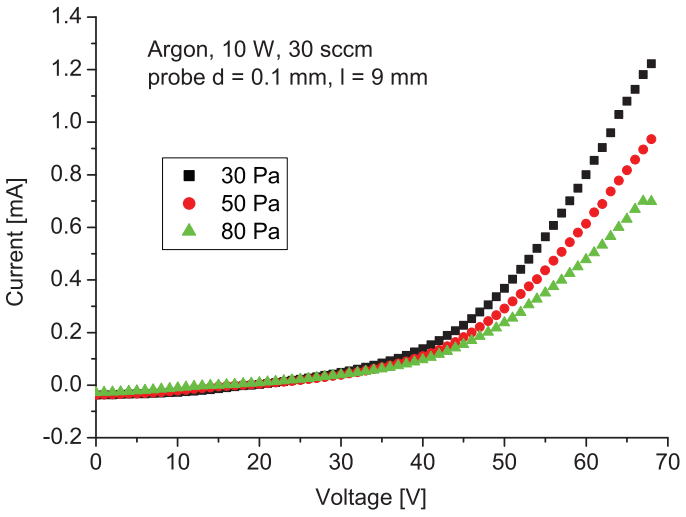


Figure 4.8: Dependence of measured I-V characteristics on pressure in the discharge chamber. Probe tip is positioned 0.5 cm from the center of the discharge chamber.

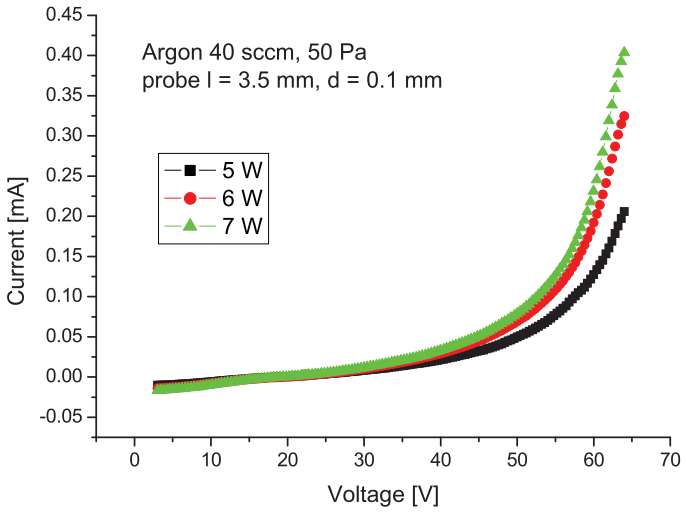


Figure 4.9: Dependence of I-V characteristics on the nominal power going from RF generator. Probe is positioned directly below the nozzle.

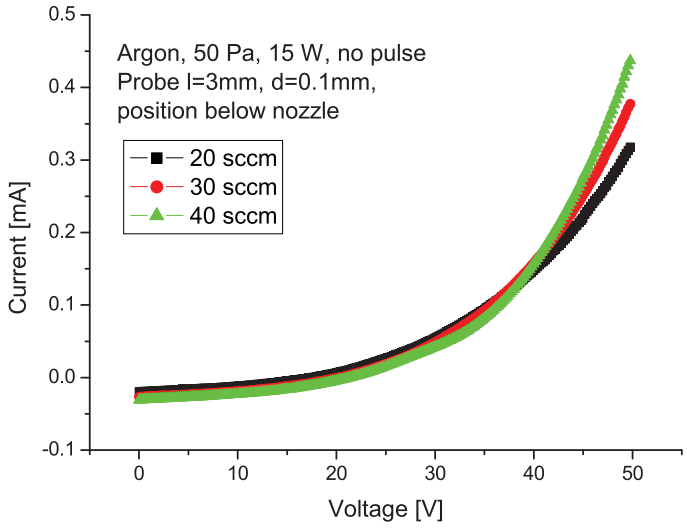


Figure 4.10: Dependence of I-V characteristics on the argon flow.

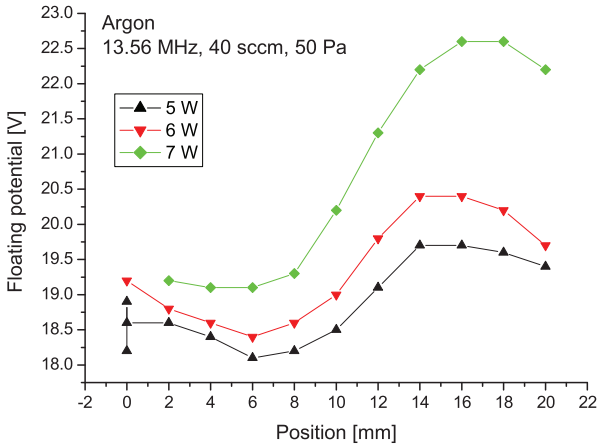


Figure 4.11: Dependence of the floating potential on the probe position i.e. on the distance of the probe tip from the center of the discharge chamber.

outlet and the vertical distance of the nozzle and probe tip is then about 2 cm.

Plasma potential is lower in the vicinity of the nozzle, which is to be expected, as the nozzle serves as a hollow cathode.

It was observed, that Langmuir probe is starting to emit visible radiation when reaching plasma potential. Current flowing to the probe is very high and probe is heated. This leads to the cleaning of the probe surface, so the probe I-V characteristics measured under the same conditions immediately after the first measurement is different from the first and hysteresis occurs.

In the graph 4.13 we can observe the effect of hysteresis in the behavior of the plasma potential. Each I-V characteristics was recorded first upwards from zero bias to 70 V and then immediately downward to zero again. Second measured characteristics was affected by saturation electron current which caused the probe tip heating. This lead to the lowering of the plasma potential, though the changing with position remained principally the same.

It was usually difficult to find the correct position of plasma potential, because saturation of electron current was not observed and also because many of the characteristics were noisy and very often also curvy. Curvy characteristics were found to result from the thin layer deposition on the probe surface. When bombardment of probe surface by ions was employed, this effect was suppressed, but regular bombardment had to be performed before each data set measurement.

In our experiments, measured plasma potential was usually very high, showing considerable difference from value obtained from floating potential using formula (1.13) which is valid for Maxwellian distribution of electrons and which was introduced in the section 1.3.2 in chapter Theory.

When calculating plasma parameters from electron current, it is usually

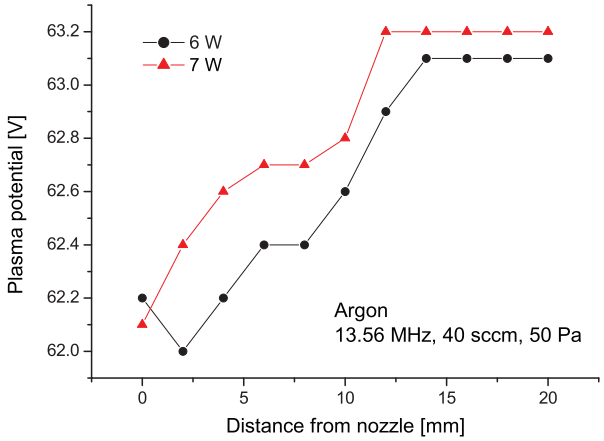


Figure 4.12: Plasma potential depending on the probe position. Estimated error is approximately 0.5 V.

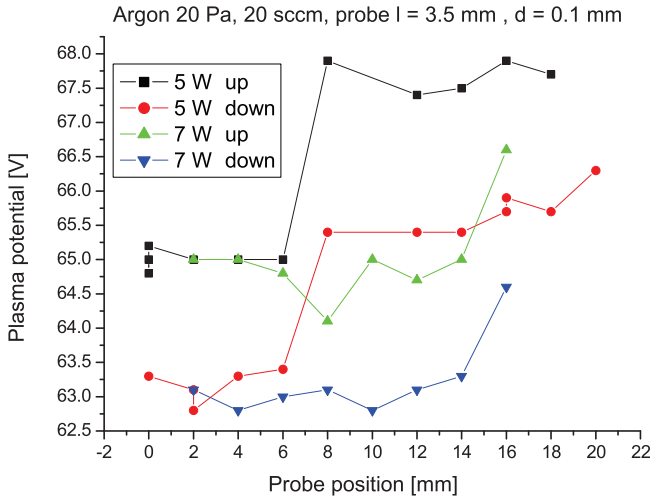


Figure 4.13: Plasma potential changing with the probe tip position. Two sets of data were measured, while I-V characteristics were recorded first with probe bias going upward and then downward. Downward characteristics were affected by the heating of the probe tip by electron current. This lowered the measured plasma potential of the probe by cleaning the probe surface.

necessary to subtract ion current. This can be done by either linear or parabolical approximation [39]. In many experiments ion current has very small effect and subtraction of ion current leads to bigger error than leaving it alone.

From the second derivative of the probe characteristics we can calculate EEDF (electron energy distribution function) using Druyvesteyn formula (1.14).

Differentiating process is very important for obtaining plasma parameters from I-V characteristics. There is however problem with the noise on the characteristics, whose effect increases with differentiation, especially when second derivative of the probe characteristics has to be calculated. It was therefore necessary to perform smoothing of data. In our calculations of EEDFs most often adjacent averaging or Savitzky-Golay smoothing were used as provided by the Origin program.

When evaluating plasma parameters, collisionless models were taken into account, since we expected that the mean free path of electrons (estimated to be approximately 1 m) is much larger than the size of the probe. The Debye length calculated from measured plasma parameters is some hundreds of $\mu$m (approximately 0.4 mm).The sheath size (several $\lambda_D$) is expected to be greater than the probe size and orbital motion limit (OML) model is expected to provide the most reliable data including the electron density estimation from $I^2$ vs V plot.

From second derivative of the I-V characteristics it was in some cases possible to obtain electron energy distribution function (EEDF). In figure 4.14 there is EEDF in logarithmic scale. From the shape of the EEDF we can deduce what distribution is present in the plasma. Calculated EEDF is here normalized to the electron concentration.

In graph 4.15 there is possible to see electron distribution function for different probe positions. Nearer to the nozzle the EEDF is more Druyvesteyn-like, while further from nozzle EEDF looks more like Maxwellian distribution.

In the graph 4.17 we can observe the shape of measured EEDF at the pressure 30 Pa. The shape is Druyvesteyn-like and because of the lower number of collisions than in higher pressure, there are more higher-energy electrons than is present in higher pressure plasma as can be seen in the graph 4.16. In the graph 4.17 the x axis is $E^2$, so the graph shows typical behavior of Druyvesteyn distribution which is linear in the $E^2$ vs log(EEDF) plot.

In figure (4.16) we can see the comparison of two EEDFs calculated from I-V characteristics measured in different pressures. It was observed, that at higher pressure there is higher concentration of low-energy electrons and the number of higher density electrons is lower and the EEDF is more steep for high-energy electrons.

EEDFs are generally lower at higher pressure for otherwise the same conditions. This effect is especially visible at higher energies. It is probably result of collisions. It was also observed, that power delivered to the dis-

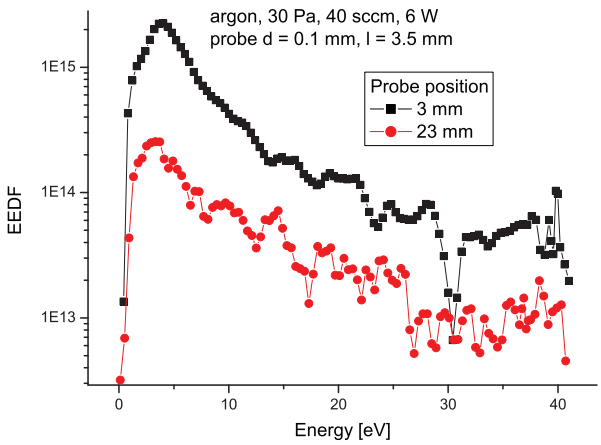


Figure 4.14: Two EEDF on logarithmic scale measured in argon, showing slight double-Maxwellian profile. EEDF is normalized to the electron concentration.

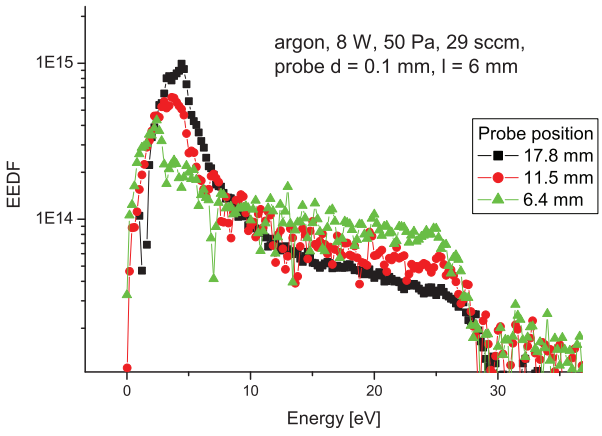


Figure 4.15: Electron energy distribution function changing with the probe position. Shape of EEDF shows double-Maxwellian profile.

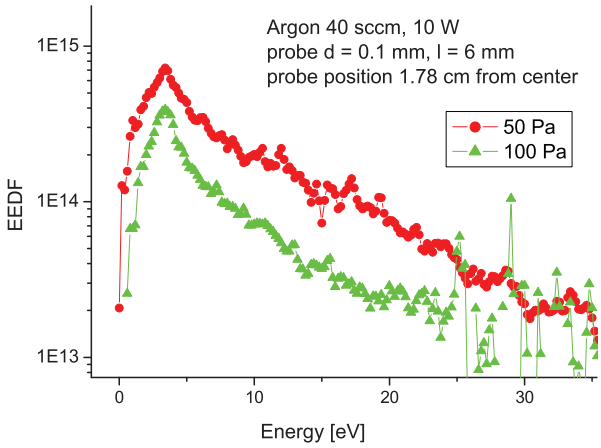


Figure 4.16: Two EEDFs on logarithmic scale measured in argon, showing different courses depending on pressure. There is probably effect of collisions which lowers the concentration of electrons.

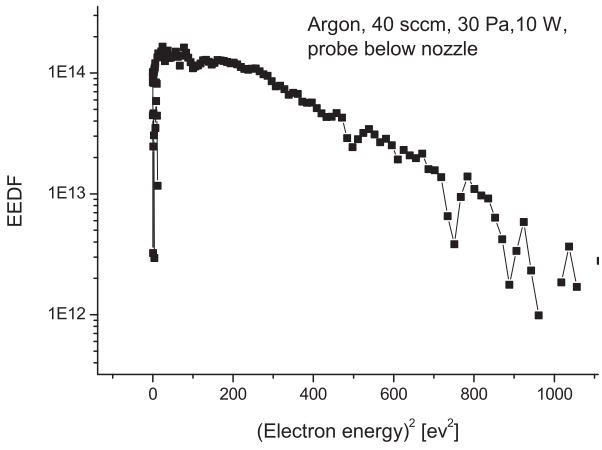


Figure 4.17: Electron energy distribution function measured at the pressure 30 Pa showing Druyvesteyn profile.

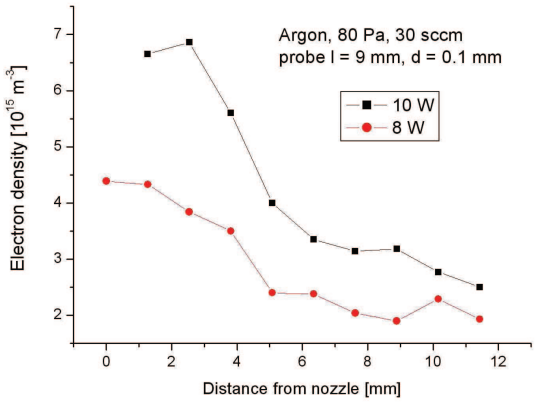


Figure 4.18: Dependence of electron density on the probe position.

charge has small effect, probably from the reason, that substantial part of the energy is lost in the impedance matching and in the wires [116] as was already mentioned in the section 4.2 describing the experimental device.

From I-V characteristics electron temperatures and concentrations can be calculated and dependence on the probe position can be observed. In graphs 4.18 and 4.19 the dependence of electron density on the probe position is shown.

In graph 4.20 we can see the position dependency of electron temperature calculated from the second derivative of the I-V characteristics. Usually the electron temperature is decreasing slightly when the probe tip is further from the nozzle.

As can be seen from figure 4.20, electron temperature is increasing when the probe is positioned nearer to the nozzle.

In some experiments we can observe changing of the shape of measured I-V characteristics. This is probably connected with the thin layer deposition on the probe tip surface and/or on the probe holder. In our first experiments we tried electron bombardment to clean the probe, which was biased to a high positive voltage and I-V characteristics was measured from zero up and then again down. Results can be seen in figure 4.21, see also graph 4.13 with plasma potential dependence.

Very often it was possible to observe, that I-V characteristics is more curvy and this effect was more visible at first derivative of the probe characteristics and even more at second derivative. In graph 4.22 we can see the shape of I-V characteristics and the shape of its first derivative. This shows that even if the I-V characteristics looks fine, there can be some effect visible in I-V characteristics derivatives.

Later we prevented thin layer deposition by applying negative probe voltage, so the probe was cleaned by ion bombardment. The question is however, how long treatment is necessary to clean the probe sufficiently.

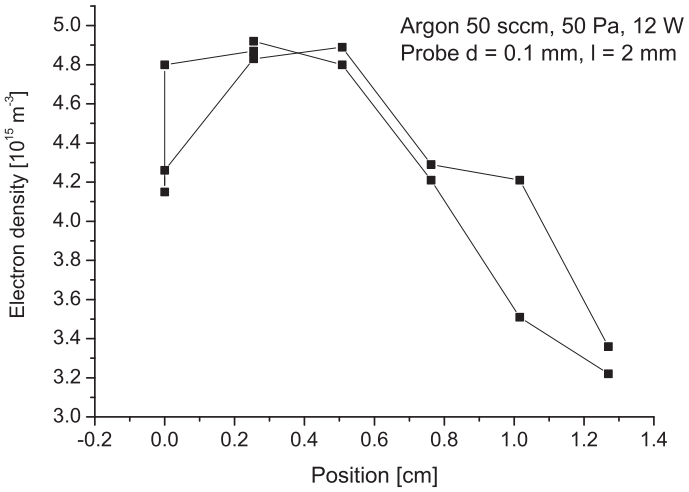


Figure 4.19: Dependence of electron density on the probe position.

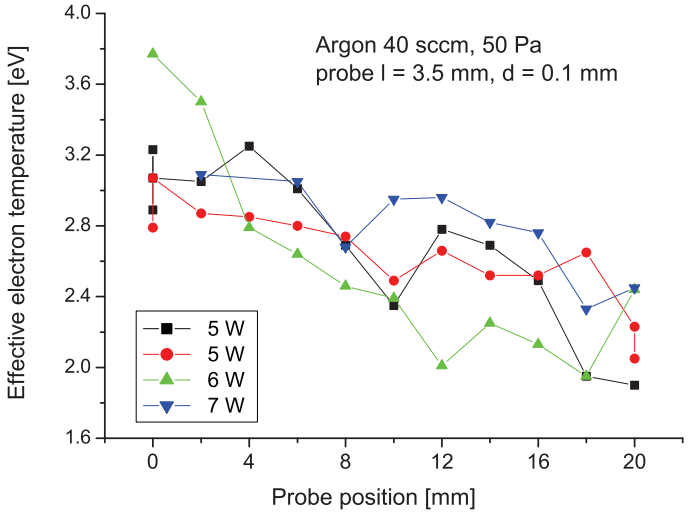


Figure 4.20: Dependence of calculated electron temperature on the probe position i.e. on the distance of the probe tip from the center of the chamber.

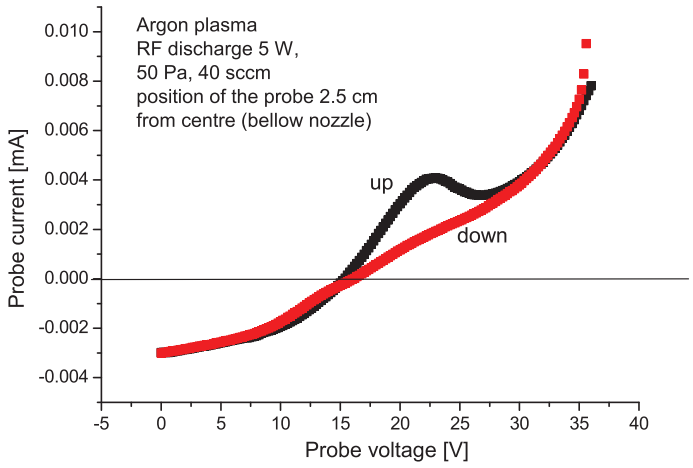


Figure 4.21: Hysteresis on the I-V characteristics.

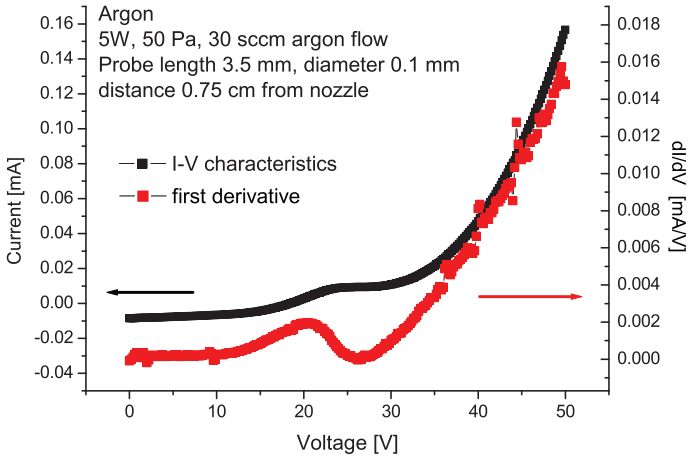


Figure 4.22: I-V characteristics and first derivative of the Langmuir probe showing the effect of layer deposition on the probe surface. Even if there is almost no effect visible on the I-V characteristics itself, first and second derivative are greatly distorted.

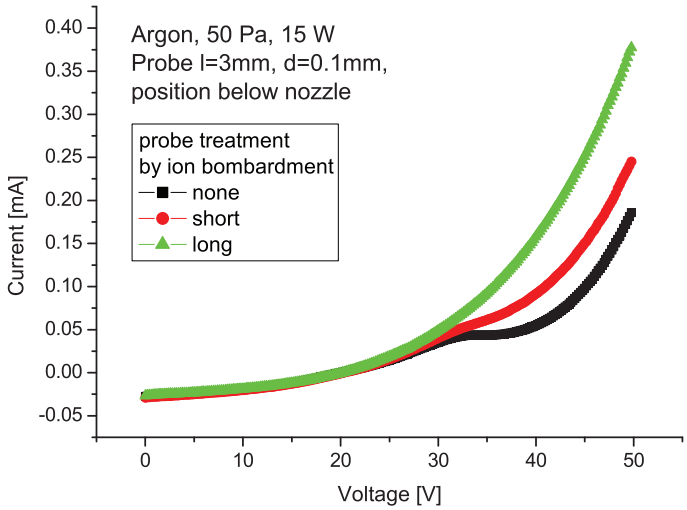


Figure 4.23: Three I-V characteristics are shown, in which only time of treatment of the probe surface by ions bombardment changes. Short treatment lasted about 120 s, long treatment 180 s. Negative voltage -48 V was applied to the probe.

Later evaluation of probe parameters leads to the acknowledgement, that our treatment was usually too short as is visible in measured EEDFs.

In fig. 4.24 we can see the example of EEDFs affected by thin layer deposition on the probe surface which leads to the negative value (this effect is described e.g. in [36] or [117]). The effect of thin layer deposition is more severe at higher pressure and also at higher power delivered to the discharge.

When the probe was new, ion bombardment caused bright flashes of light occurring on the probe tip surface. Those were probably the effect of organic materials contaminating the surface.

In some measurements we observe changing of the plasma state during the series of measurements — measured plasma parameters differ slightly in following measurement, even if the probe is at the same place. In the beginning the changing of the discharge color can be noticed. It is therefore necessary to wait at least few minutes (better tens of minutes) for discharge stabilization.

Measured concentration of $10^{15}$ in most measurements rises when the probe is nearer to the center of the discharge chamber i.e. nearer to the nozzle. Evaluated electron temperature is usually very noisy, but in some experiments we can see, that measured electron temperature is increasing slightly when the probe is nearer to the hollow cathode.

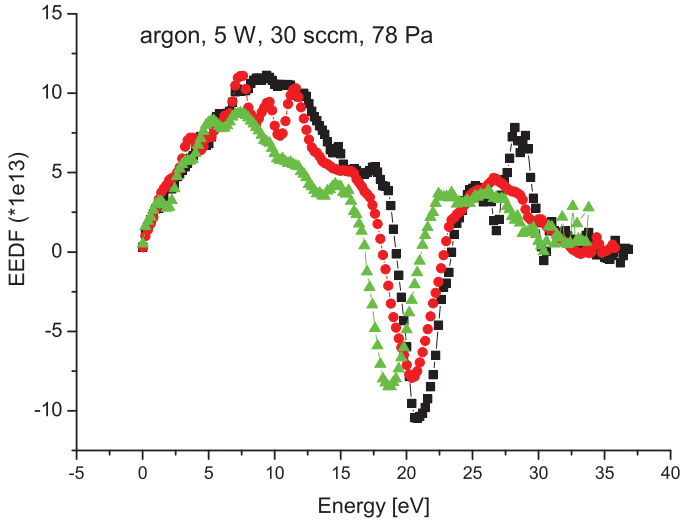


Figure 4.24: Two results of calculation of EEDF in the case of dirty probe showing negative part and distortion which leads to the impossibility to obtain data from I-V characteristics.

### 4.4.2 Argon with iodine

Iodine $I_2$ was admixed to the argon flow. It is electronegative element, so we expect formation of negative ions and effect connected with the lower concentration of electrons in the discharge such as the lower discharge stability and possibly the change of discharge color.

Because of presence of another charged particle the I-V characteristics cannot be evaluated as in previous section, but more complex models must be employed [24, 23, 21]. Also the effect of $I_2$ molecule dissociation must be taken to the account for proper interpretation of measured data.

In figure 4.25 we present I-V characteristics measured in the mixture of argon with iodine. We can observe, that when the probe tip is further from the nozzle, the electron current is increasing as opposed to the course observed in argon (as can be seen in graph 4.7) when the electron current is lower when the probe tip is further from nozzle. Direct comparison of I-V characteristics behavior in pure argon and in argon with iodine admixture can be seen in graph 4.26.

From the observed behavior we can deduce that negative ions are formed in hollow cathode, most often by dissociative attachment of low-energy electron to the iodine molecule, so that $I^-$ ions are formed together with neutral iodine atoms. Further from the nozzle the concentration of negative ions decreases possibly by the detachment of electrons (possibly caused by impact with another particle) or eventually by recombination with positive ions. When the detachment is caused by another iodine atom, the associative detachment can occur and $I_2$ molecule is formed.

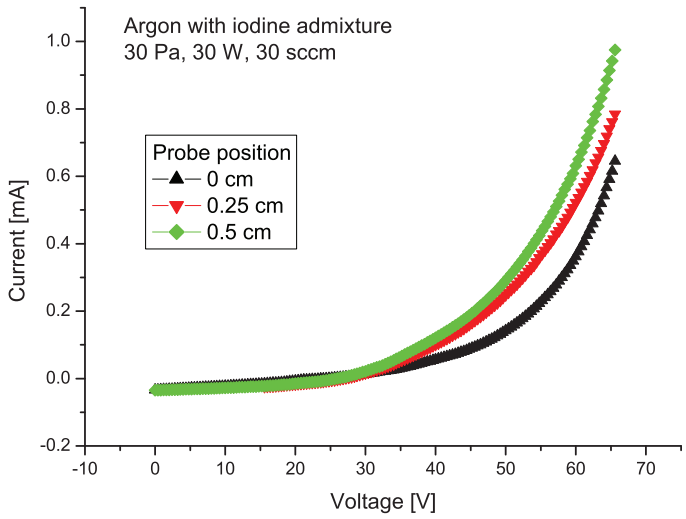


Figure 4.25: Three measured I-V characteristics in the mixture of argon with iodine showing interesting effect of electron current fall when going nearer to the center of discharge.

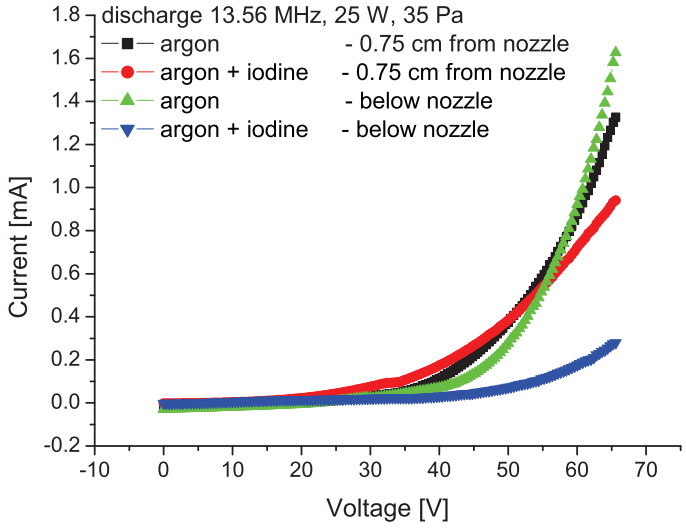


Figure 4.26: Four I-V characteristics are compared, two when probe was placed below nozzle and two when probe tip was placed 0.75 cm away. It is shown, that most pronounced effect of negative ions can be found below the nozzle while further from nozzle the characteristics are nearer one to each other.

## 4.5 Discussion of results and conclusion

Before the experiments it was necessary to build gas delivery system including the connection with vacuum pump. Next step was building the RF power delivery system. The last stage before experiments was building of Langmuir probe circuit.

In the beginning the measurement were made in pure argon, just to test the diagnostics and apparatus, and also for comparison of results. We met however many problems, which lead to quite longer time measuring in argon than was expected.

We measured several Langmuir probe current-voltage (I-V) characteristics. From measured data some plasma parameters were estimated, like floating potential, plasma potential, electron temperature and electron density.

To find a plasma potential from the I-V characteristic proved to be a difficult task. Saturation of electron current was not observed and due to the curved I-V characteristic (usually the result of thin layer deposition) there appeared to be false zero crossings in second derivative. Fortunately many of these zero crossings could be identified with the probe distortion, still this lead to the big uncertainty in obtaining the position of real plasma potential.

Highest plasma density was observed below nozzle, further from the nozzle there was lower concentration of charged particles. Also electron temperature decreased with increasing distance of the probe tip from the nozzle.

Theory of particle collection when mean free path for electrons is over 1 meter means that electrons are in collisionless regime, as $\lambda_D$ is of order of tens of microns and so comparable with the probe size, OML model should be employed for description of electron collection by the probe.

When the iodine was admixed, the different behavior of the probe was observed, especially there was dependence on the probe position which was different from the dependence measured in pure argon.

Deposition of the thin layers on the probe surface appeared to be most limiting problem and it was necessary to clean probe by ion bombardment for at least one minute to ensure undistorted characteristics. Deposited layers appeared to be insulating, this can be explained either by the fact that only primary vacuum pump was used and some part of atmospheric nitrogen and oxygen was still present in discharge forming compounds with aluminium cathode sputtered material. Another source of material forming insulating layers could be oxides on the hollow cathode surface.

To overcome this problem, we employed cleaning by ion bombardment, when the probe is negatively biased. This was done before all measurements, but the original time of treatment was too short to clean the probe properly, so at the end the necessary time for cleaning was about 1 minute with voltage -48 V (about -80 V compared with plasma potential).

Because we investigated only the plasma by the Langmuir probe and not the layers, we do not know which mechanism leads to the forming of the

insulating layers on the probe surface.

Measured I-V characteristics were processed in the program Origin, where the first and second derivative were calculated usually after smoothing. Obtaining plasma potential proved to be difficult due to the probe surface contamination with deposited thin layers.

It is very important to give proper credit to all difficulties which can be encountered while measuring in RF driven plasma and moreover in the device dedicated to thin layer deposition. We must therefore properly tackle the problem of plasma potential oscillations and also problem of thin layer deposition on the probe surface. When applying only low power, we can observe, that effect of thin layer deposition is the main problem in our experiments. It is also connected with the fact, that we use only one-stage vacuum pumping and therefore we measure at rather higher pressures some tens of Pa.

# Chapter 5

# Conclusion

In this work the three main subject were studied, the chemical oxygen-iodine laser (COIL), discharge oxygen-iodine laser (DOIL) and hollow cathode plasma jet system. The common object in these three studied areas is the iodine. Iodine atoms form active medium of laser (both COIL and DOIL) and they can be obtained by different ways. Classical way is dissociation of $I_2$ molecule by the collisions with singlet oxygen molecule $O_2(a^1\Delta_g)$. This method makes very simple laser system, because singlet oxygen also serves for iodine atoms excitation. It has however few drawbacks which lead to the alternative way of obtaining of iodine atoms.

Chemical way of obtaining iodine atoms from the HI (or DI) molecule reacting with either chlorine atoms or fluorine atoms was studied. The results are described in chapter 2. Concentration of produced atomic iodine was high, but the laser gain was diminished by the forming of radicals $HO_2^\bullet$ or $DO_2^\bullet$ which quenched the singlet oxygen molecules. However laser power exceeding 400 W was reached. Main diagnostic method was absorption spectroscopy in the vicinity of 1315 nm.

Part of my work was the writing of the program for 1-D chemical kinetic modeling of reaction system for the reaction of HI with F, including two reaction 2.44 and 2.45 whose rate constants were not known. The second reaction has beneficial effect on the overall system by removing both IF and unreacted HI from the gas flow. The program was written in the Fortran programming language which allowed creation of portable .exe files, listing of the program can be found in Attachment on the CD. Some of the results are shown in section 2.4.4.

There is also possibility to produce both singlet oxygen and atomic iodine (i.e. iodine atoms) in electric discharge as is described in chapter 3. New experimental device was built for the dissociation of different molecules containing iodine in capacitively coupled radiofrequency (RF) discharge. Discharge chamber was part of the iodine injector from which the iodine atoms were introduced into the primary gas flow. The injector also formed supersonic nozzle together with the walls of device. During the experiments, RF generator worked on the frequency 40 MHz, iodine donors were molecu-

les $CH_3I$ and $CF_3I$. Iodine as a halogen is electronegative, which effect quite strongly the behavior of electric discharge by lowering its stability. Main diagnostic method was again absorption spectroscopy in the vicinity of 1315 nm, but also emission spectroscopy was employed.

Part of the work was emission spectroscopy diagnostics of plasma in the discharge chamber, especially the radiation from excited iodine I($^2P_{1/2}$). It is however expected that only small part of iodine will be excited in discharge, partly by the ultraviolet radiation originating in the discharge and reflected by the wall and partly by collisions with other particles in discharge. The radiation arising from I($^2P_{1/2}$) was detected, signal was however very small, also from the reason that I($^2P_{1/2}$) is metastable state. Two peak were detected (with better resolution one another peak was distinguished), but actually six peaks are present in the vicinity of 1315 nm arising from the presence of sublevels. State I($^2P_{1/2}$) has two and stare I($^2P_{3/2}$) has four sublevels with different total atomic angular momentum F [51].

In hollow cathode plasma jet system the discharge in argon and in argon with small admixture of $I_2$ was studied. RF generator worked on the frequency 13.56 MHz. Diagnostic method was Langmuir probe equipped by passive RF compensation. From the current-voltage (I-V) characteristics of Langmuir probe, plasma parameters were obtained such as floating potential, plasma potential, also electron energy distribution function (EEDF) from which the electron density $n_e$ and effective electron temperature $T_{e,eff}$ were obtained. Several dependencies of plasma parameters were studied, especially on the probe position and pressure. The effect of deposition of the thin layer deposition on the probe surface was observed, as a method to prevent this the ion bombardment of probe prior to measuring I-V characteristics was used. Hollow cathode and performed experiments are described in chapter 4.

My previous study was concerned with the emissive probe which is the Langmuir probe heated to the temperature at which the electron emission from the probe surface occurs. This method is used for direct measurement of plasma potential and also to overcome the thin layer deposition on the probe surface. Several articles were written by A. Marek and one also by myself (see Publications).

In the course of my Ph.D. study I participated in the experiments performed at the Institute of Physics, from which following articles resulted written by V. Jirásek [73, 74, 76, 77, 110], J. Schmiedberger [109] and O. Špalek [62, 63, 75, 68]. I also participated in experiments performed at the Faculty of Mathematics and Physics which resulted in articles written by P. Kudrna [113], J. Klusoň [133] and S. Leshkov [134]. Some more articles were published in WDS (Week of doctoral students) proceedings in the years 2006 – 2009, 2011 and 2013 (see Attachments).

# Bibliography


[1] A. Anders, Plasma and ion sources in large area coating: A review, *Surface and Coatings Technology* 200, 1893–1906, 2005.

[2] H. Conrads, M. Schmidt, Plasma generation and plasma sources, *Plasma Sources Science and Technology* 9, 441–454, 2000.

[3] J.A. Thornton, Magnetron sputtering: basic physics and application to cylindrical magnetrons, *J. Vac. Sci. Technol.* 15 (2), 171–177, 1978.

[4] M. Tichý, Z. Hubička, P. Virostko, I. Picková, M. Šícha, M. Čada, J. Olejníček, O. Churpita, L. Jastrabík, P. Adámek, P. Kudrna, J. Klusoň, S. Leshkov, M. Chichina, Š. Kment, Langmuir probe measurements of spatial plasma profiles and temporal dependences in a DC-energized hollow-cathode plasma jet system, *J. Plasma Fusion Res. SERIES* 8, 1277–1282, 2009.

[5] L. Bárdoš, H. Baránková, S. Berg, Thin film processing by radio frequency hollow cathodes, *Surface and Coatings Technology* 97, 723–728, 1997.

[6] I.D. Sudit, F.F. Chen, RF compensated probes for high-density discharges, *Plasma sources Sci. Technol.* 3, 162–168, 1994.

[7] L. Bárdoš, V. Dušek, High rate jet plasma-assisted chemical vapour deposition, *Thin Solid Films* 158, 265–270, 1988.

[8] J. Kodymová, Laser pro budoucí náročné technologie, *CHEMagazín* 4 (XVI), 8–10, 2006.

[9] W.T. Silvfast, Laser fundamentals, Cambridge University Press, second edition, 2004.

[10] A.E. Siegman, Lasers, University Science Books, Mill Valley, California, 1986.

[11] O. Svelto, Principles of lasers, Springer Science + Business Media, New York, 1998.

[12] J. Hecht, Short history of laser development, *Optical Engineering* 49 (9), 091002, 2010.

[13] A.V. Eletskii, Excimer lasers, *Sov. Phys. Usp.* 21 (6), 502–521, 1978.

[14] I.W.M. Smith, Chemical lasers, *Optics and laser technology* 77–83, 1980.

[15] Yu. Raizer, Gas discharge physics, Springer Verlag, 1991.

[16] F.F. Chen, Úvod do fyziky plazmatu, Academia, Praha, 1984.

[17] F.F. Chen, J.P. Chang, Lecture notes on principles of plasma processing, Kluwer Academic/Plenum Publishers, New York, 2003.

[18] M.A. Lieberman, A.J. Lichtenberg, Principles of Plasma Discharges and Materials Processing, *New York: Wiley–Interscience*, 1994.

[19] V.A. Godyak, V.I. Demidov, Probe measurements of electron-energy distributions in plasmas: what can we measure and how we can achieve reliable results ?, *Journal of Physics D, Applied Physics* 44, 233001, 1–30, 2011.

[20] G.A. Woolsey, I.C. Plumb, D.B. Lewis, Langmuir probe characteristics in a postitive–ion/negative–ion plasma, *J. Phys. D: Appl. Phys.* 6, 1883–1890, 1973.

[21] R.N. Franklin, A critique of models of electronegative plasmas, *Plasma Sources Sci. Technol.* 10, 162–167, 2001.

[22] R.F. Fernsler, Modeling Langmuir probes in multi-component plasmas, *Plasma Sources Sci. Technol.* 18, 014012 (12pp), 2009.

[23] I.G. Kouznetsov, A.J. Lichtenberg, M.A. Lieberman, Modelling electronegative discharges at low pressure, *Plasma Sources Sci. Technol.* 5, 662–676, 1996.

[24] H. Amemiya, B. M. Annaratone, J. E. Allen, The collection of positive ions by spherical and cylindrical probes in an electronegative plasma, *Plasma Sources Sci. Technol.* 8, 179–190, 1999.

[25] W.J. Goedheer, Lecture notes on radio-frequency discharges, dc potentials, ion and electron energy distributions, *Plasma Sources Sci. Technol.* 9, 507–516, 2000.

[26] Advanced Energy Industries, Impedance matching, *White papers*, `http://www.advanced-energy/white_papers/`.

[27] H. Norström, Experimental and design information for calculating impedance matching networks for use in rf sputtering and plasma chemistry, *Vacuum* 29 (10), 341–350, 1979.

[28] S. Svanberg, Atomic and molecular spectroscopy, *Springer Verlag*, 1992.

[29] U. Fantz, Emission spectroscopy of molecular low pressure plasmas, *Contrib. Plasma Phys.* 44, No. 5–6, 508–515, 2004.

[30] U. Fantz, Basics of plasma spectroscopy, *Plasma Sources Sci. Technol.* 15, S137-S147, 2006.

[31] L.M. Biberman, G.É. Norman, Continuous spectra of atomic gases and plasma, *Soviet Physics Uspekhi* 10 (1), 1967.

[32] F.F. Chen, Lecture Notes on Langmuir Probe Diagnostics, Mini–Course on Plasma Diagnostics, IEEE–ICOPS meeting, Jeju, Korea, June 5, 2003.

[33] B.E. Cherrington, The use of electrostatic probes for plasma diagnostics – a review, *Plasma Chemistry and Plasma Processing* 2 (2), 113–140, 1982.

[34] S.Pfau, M. Tichý, Langmuir probe diagnostics of low-temperature plasmas, in *Low temperature plasmas, Fundamental, Technologies and Techniques* edited by R. Hippler, H. Kersten, M. Schmidt, K.H. Schoenbach, Wiley-VCH Verlag Berlin GmbH, 2007.

[35] Chung, Talbot, Touryan, Electrical probes in stationary and flowing plasma, Springer-Verlag, New York, 1975.

[36] V.I. Demidov, S.V. Ratynskaia, K. Rypdal, Electric probes for plasmas: The link between theory and instrument, *Rev. Sci. Instrum.* 73, 3409-3439, 2002.

[37] J.E. Allen, B.M. Annaratone, U. de Angelis, On the orbital motion limited theory for a small body at floating potential in a maxwellian plasma, *J. Plasma Physics* 63, 4, 299–309, 2000.

[38] M.J. Druyvesteyn, Der Niedervoltbogen, *Zeitschrift für Physik* 64, p. 781, 1930.

[39] V.A. Godyak, R.B. Piejak, B.M. Alexandrovich, Probe diagnostics of non-Maxwellian plasmas, *J. Appl. Phys.* 73 (8), 3657–3663, 1992.

[40] H. Andrei, V. Covlea, V.V. Covlea, E. Barna, The smoothing and the digital processing of Langmuir probe characteristics, *Romanian Reports in Physics* 55, 2, 51–56, 2003.

[41] A. Garscadden, K.G. Emeleus, Notes on the effect of noise on Langmuir probe characteristics, *Proc. Phys. Soc.* 79, 535–541, 1962.

[42] R.L.F. Boyd, J.B. Thompson, The operation of Langmuir probes in electro-negative plasmas, *Proceedings of the royal Society of London. Series A, Mathematical and Physical*, 252 (1268), 102–119, 1959.

[43] N.S.J. Braithwaite, J.E. Allen, Boundaries and probes in electronegative plasmas, *J. Phys. D: Appl. Phys.* 21, 1733-1737, 1988.

[44] J.F.Bott, R.W.F. Gross, Handbook of chemical lasers, *Wiley*, New York, 1976.

[45] P.V. Avizonis, G. Hasen, K.A. Truesdell, The chemically pumped oxygen-iodine laser, *High-Power Gas Lasers*, Proceedings of SPIE 1225, 448–476, 1990.

[46] W.E. McDermott, N.R. Pchelkin, D.J. Benard, R.R. Bousek, An electronic transition chemical laser, *Applied physics Letters* 33 (8), 469–470, 1978.

[47] V. Yu. Zalesskii and M. G. Ivanov, Possibility of the development of a $CF_3I$ glow-discharge laser, *Kvant. Elektron. (Mosc.)* 2, 277-280, 1975.

[48] J.V.V. Kasper, G.C. Pimentel, Atomic iodine photodissociation laser, *Applied Physics Letters* 5 (11), 231–233, 1964.

[49] N.N. Yuryshev, Chemically pumped oxygen-iodine laser, *Quantum Electronics* 26 (7), 567–584, 1996.

[50] J. Kodymová, O. Špalek, $O_2(^1\Delta_g)$ radiative lifetime: Contribution to discussion on the Einstein A-coefficient sed in COIL of $O_2(^1\Delta_g)$ determination from fundamental emission, *Proceedings of SPIE* 3612, 92–99, 1999.

[51] J. Kodymová, O. Špalek, V. Jirásek, M. Čenský, Advances in the development of chemical oxygen-iodine laser, *Czechoslovak Journal of Physics* 54 (5), 561–574 , 2004.

[52] R.G. Derwent, B.A. Thrush, The radiative lifetime of the metastable iodine atom $I(5^2P_{1/2})$, *Chemical Physics Letters* 9, 6, 591–592, 1971.

[53] R.G. Derwent, D.R. Kearns, B.A. Thrush, The excitation of iodine by singlet molecular oxygen, *Chemical Physics Letters* 6, 2, 115–116, 1970.

[54] V. Jirásek, J. Hrubý, O.Špalek, M. Čenský, J. Kodymová, Spray generator of singlet oxygen for a chemical oxygen-iodine laser, *Applied Physics B* 100, 779–791, 2010.

[55] O. Špalek, M. Čenský, V. Jirásek, J. Kodymová, I. Jakubec, G.D. Hager,Chemical oxygen-iodine laser using a new method of atomic iodine generation, *IEEE Journal of Quantum Electronics* 40 (4), 564–570, 2004.

[56] V. Rybalkin, A. Katz, K. Waichman, D. Vingurt, Z. Dahan, B.D. Barmashenko, S. Rosenwaks, How many $O_2(\Delta)$ molecules are consumed per dissociated $I_2$ in chemical oxygen-iodine lasers ?, *Applied Physics Letters* 89, 021115, 1–3, 2006.

[57] K. Waichman, V. Rybalkin, A. Katz, Z. Dahan, B.D. Barmashenko, S. Rosenwaks, Toward understanding the dissociation of $I_2$ in chemical oxygen-iodine lasers: Combined experimental and theoretical studies, *Journal of Applied physics* 102, 013108, 1–13, 2007.

[58] V. Jirásek, O. Špalek, J. Kodymová, M. Čenský, Chemical generation of atomic iodine for chemical oxygen-iodine laser. I. Modelling of reaction system, *Chemical Physics* 269, 167–178, 2001.

[59] O. Špalek, J. Hrubý, M. Čenský, V. Jirásek, J. Kodymová, Centrifugal spray generator of singlet oxygen for a chemical oxygen-iodine laser, *Appl. Phys. B* 100, 793–802, 2010.

[60] S. Yoshida, H. Saito, T. Fujioka, H. Yamakoshi, T. Uchiyama, New singlet oxygen generator for chemical oxygen-iodine lasers, *Appl. Phys. Lett.* 49 (18), 1143–1144, 1986.

[61] J. Kodymová, O. Špalek, Performance characteristics of jet-type generator of singlet oxygen for supersonic chemical oxygen-iodine laser, *Japanese Journal of Applied physics* 37 (1), 117–121, 1998.

[62] O. Špalek, J. Hrubý, V. Jirásek, M. Čenský, J. Kodymová, I. Picková, Advanced spray generator of singlet oxygen, *Proceedings of SPIE* 6346, 63460C, 2007.

[63] O. Špalek, V. Jirásek, M. Čenský, J. Kodymová, I. Picková, Spray generator of singlet oxygen with a centrifugal separation of liquid, *Proceedings of SPIE* 7131, 71310H, 2009.

[64] J. Kodymová, V. Jirásek, J. Schmiedberger, O. Špalek, M. Čenský, Research on chemical and discharge oxygen-iodine lasers, *Optics and Spectroscopy* 107 (5), 813–825, 2009.

[65] M. Endo, D. Sugimoto, H. Okamoto, K. Nanri, T. Uchiyama, S. Takeda, T. Fujioka, Output power enhancement of a chemical oxygen-iodine laser by predissociated iodine injection, *Jpn. J. Appl. Phys.* 39, 468–474, 2000.

[66] O. Špalek, V. Jirásek, M. Čenský, J. Kodymová, I. Jakubec, G.D. Hager, Chemical generation of atomic iodine for the chemical oxygen-iodine laser. II. Experimental results, *Chemical Physics* 282, 147–157, 2002.

[67] O. Špalek, V. Jirásek, M. Čenský, J. Kodymová, I. Jakubec, G. D. Hager, Chemical oxygen-iodine laser with atomic iodine generated via Cl or F atoms, *Proc. SPIE* 5777, 192–197, 2004.

[68] O. Špalek, V. Jirásek, M. Čenský, J. Kodymová, I. Picková, I. Jakubec, Chemical oxygen-iodine laser with atomic iodine generated in a separate reactor, *Proceedings of SPIE* 6261, 62611T, 2006.

[69] O. Špalek, V. Jirásek, J. Kodymová, I. Jakubec, M. Čenský, Preliminary experimental results on chemical generation of atomic iodine for a COIL, *Proceedings of SPIE* 4184, p. 111, 2000.

[70] V. Jirásek, CFD modeling of an instantaneous generation of atomic iodine in chemical oxygen-iodine laser, XV International Symposium on Gas Flow and Chemical Lasers and High-Power Laser Conference, 30.8.-3.9. 2004, Prague, Czech Republic, *Proc. SPIE* 5777, 192-197, 2004.

[71] S.J. Davis, W.T. Rawlins, W.J. Kessler, S. Lee, A.J.R. Hunter, M. Silva, Next generation diagnostics for COIL: New approaches for measuring critical parameters, presented at XV International Symposium on Gas Flow and Chemical Lasers and High Power Lasers Conference, *Proceedings of SPIE* 5448, 2004.

[72] J. Kodymová, O. Špalek, V. Jirásek, M. Čenský, G.D. Hager, Development of the Chemical Oxygen-Iodine Laser (COIL) with chemical generation of atomic iodine, *Appl. Phys. A* 77, 331–336, 2003.

[73] V. Jirásek, M. Čenský, O. Špalek, J. Kodymová, I. Picková, I. Jakubec, Chemical oxygen-iodine laser with atomic iodine generated via fluorine atoms, *Chemical Physics* 345, 14–22, 2008.

[74] V. Jirásek, O. Špalek, M. Čenský, J. Kodymová, I. Picková, I. Jakubec, Study of COIL active medium with atomic iodine generated via fluorine atoms, *Proceedings of SPIE* 7131, 71310M, 2009.

[75] O. Špalek, V. Jirásek, M. Čenský, J. Kodymová, I. Picková, I. Jakubec, Chemical oxygen-iodine laser with atomic iodine generated via fluorine atoms, *Proceedings of SPIE* 6735, 73506, 2007.

[76] V. Jirásek, O. Špalek, M. Čenský, J. Kodymová, I. Picková, I. Jakubec, COIL with supersonic injection of chemically produced atomic iodine, *Proceedings of SPIE* 6346, 63462J, 2007.

[77] V. Jirásek, O. Špalek, M. Čenský, I. Picková, J. Kodymová, I. Jakubec, Generation of atomic iodine via fluorine for chemical oxygen-iodine laser, *Chemical Physics* 334, 167–174, 2007.

[78] M. Čenský, O. Špalek, V. Jirásek, J. Kodymová, I. Jakubec, Atomic iodine generation via fluorine atoms for chemical oxygen-iodine laser, *Collect. Czech. Chem. Commun.* 71, 5, 739–755, 2006.

[79] M. Čenský, O. Špalek, V. Jirásek, J. Kodymová, I. Jakubec, Generation of atomic iodine for COIL via atomic fluorine at higher pressure, XV International Symposium on Gas Flow and Chemical Lasers and High-Power Laser Conference, 30.8.-3.9. 2004, Prague, Czech Republic, *Proc. SPIE* 5777, 192-197, 2004.

[80] A.A. Ionin, I.V. Kochetov, A.P. Napartovich, N.N. Yuryshev, Physics and engineering of singlet delta oxygen production in low-temperature plasma, *Journal of Physics D: Applied Physics* 40, R25–R61, 2007.

[81] L.D. Pleasance, L.A. Weaver, Laser emission at 1.32 $\mu$m from atomic iodine produced by electrical dissociation of $CF_3I$, *Applied Physics Letters* 27 (7), 407–409, 1975.

[82] D.L. Carroll, W.C. Solomon, ElectriCOIL: An advanced chemical iodine laser concept, *Proceedings of the XIII International Symposium on Gas Flow and Chemical Lasers and High Power Laser Conference*, 40–44, 2000.

[83] A.P. Napartovich, A.A. Deryugin, I.V. Kochetov, Discharge production of the singlet delta oxygen for an iodine laser, *J. Phys. D: Appl. Phys.* 34, 1827–1833, 2001.

[84] A. Hicks, S. Norberg, P. Shawcross, W.R. Lempert, J.W. Rich, I.V. Adamovich, Singlet oxygen generation in a high pressure non-self-sustained electric discharge, *J. Phys. D: Appl. Phys.* 38, 3812–3824, 2005.

[85] D.L. Carroll, J.T. Verdeyn, D.M. King, J.W. Zimmerman, J.K. Laystrom, B.S. Woodard, G.F. Benavides, K.W. Kittell, D.S. Stafford, J.J. Kushner, W.C. Solomon, Continuous-wave laser oscillation on the 1315 nm transition of atomic iodine pumped by $O_2(a^1\Delta_g)$ produced in an electric discharge, *Appl. Phys. Let.* 86 (111104), 2005.

[86] D.L. Carroll, J.T. Verdeyen, D.M. King, B. Woodard, L. Skorski, J. Zimmerman, W.C. Solomon, Recent work on the development of an electric discharge oxygen iodine laser, GCLHPL, 2002.

[87] D.L. Carroll, J.T. Verdeyen, D.M. King, J.W. Zimmerman, J.K. Laystrom, B.S. Woodard, N. Richardson, K. Kittell, M.J. Kushner, W.C. Solomon, Measurement of positive gain on the 1315 nm transition of atomic iodine pumped by $O_2(a^1\Delta)$ produced in an electric discharge, *Applied Physics Letters* 85 (8), 1320–1322, 2004.

[88] D.L. Carroll, J.T. Verdeyen, D.M. King, J.W. Zimmerman, J.K. Laystrom, Experimental effect of atomic oxygen on the development of an electric discharge oxygen iodien laser, GCLHPL, 2004.

[89] D.L. Carroll, J.T. Verdeyen, D.M. King, J.W. Zimmerman, J.K. Laystrom, B.S. Woodard, G.F. Benavides, K.W. Kittel, W.C. Solomon, Path to the measurement of positive gain on the 1315-nm transition of atomic iodine pumped by $O_2(a^1\Delta)$ produced in an electric discharge, *IEEE Journal of Quantum Electronics* 41 (2), 213–223, 2005.

[90] D.L. Carroll, B.S. Woodard, G.F. Benavides et. al., Super-linear enhancement of the Electric Oxygen-iodine laser, *Proceedings of SPIE* 8677, UNSP 867702, 2013.

[91] A. Katz, Z. Dahan, V. Rybalkin, K. Waichman, B. D. Barmashenko, S. Rosenwaks, Power enhancement in chemical oxygen-iodine lasers by iodine predissociation via corona/glow discharge, *Applied Physics Letters* 90 (161122), 1–3, 2007.

[92] H. Okamoto, T. Hirata, K. Shinoda, D. Sugimoto, M. Endo, T. Fujioka, S. Takeda, Supersonic chemical oxygen-iodine laser with microwave predissociation of iodine, *AIAA Pap.* 2000-2492, 1, 2000.

[93] P.A. Mikheyev, A.A. Shepelenko, A.I. Voronov, A.A. Shepelenko, Atomic iodine production in a gas flow by decomposing methyl iodide in a dc glow discharge, *Quantum Electronics* 32 (1), 1–4, 2002.

[94] P.A. Mikheyev, A.A. Shepelenko, Application of vortex-flow dc glow discharge for atomic iodine production for oxygen-iodine laser, *Proc. SPIE* 5479, 50, 2003.

[95] V.N. Azyazov, M.V. Vorobev, A.I. Vornov, N.V. Kupryaev, P.A. Mikheyev, N.I. Ufimtsev, Parameters of an electric–discharge generator of iodine atoms for a chemical oxygen–iodine laser, *Quantum Electronics* 39, 1, 84–88, 2009.

[96] T. Wakazono, K. Hashimoto, T. Takemoto, T. Uchiyama, M. Muro, Chemical oxygen-iodine laser using rf-discharge dissociation of $I_2$, *Proc. SPIE* 3574, 290, 1998.

[97] S. Ide, T. Wakazono, T. Takemoto, T. Uchiyama, Study of Chemical Oxygen Iodine Laser for high power utilizing RF discharge dissociation of $I_2$, XIII International Symposium on Gas Flow and Chemical Lasers and High-Power Laser Conference, 18.-22.9. 2000, Florence, Italy , *Proc. SPIE* 4184, 95–98, 2000.

[98] G.F. Benavides, J.W. Zimmerman, B.S. Woodard, D.L. Carroll, J.T. Verdeyen, T.H. Field, A.D. Palla, W.C. Solomon, Gain and continuous-wave laser power enhancement with a secondary discharge to predissociate molecular iodine in an electric oxygen–iodine laser, *Applied Physics Letters* 92, 041116, 1–3, 2008.

[99] N.P. Vagin, V.S. Pazyuk, N.N Yuryshev, Pulsed chemical oxygen-iodine laser with bulk formation of iodine atoms by an electric discharge, *Quantum Electronics* 25 (8), 746–748, 1995.

[100] N.V. Yuryshev, Pulsed COIL - schievements and problems, AIAA, conference of American Institute of Aeronautics and Astronautics, 1–9, 2003.

[101] P.A. Mikheyev, A.A. Shepelenko, A.I. Voronov, N.V. Kupryayev, Production of iodine atoms by dissociating $CH_3I$ and HI in a dc glow discharge in the flow of argon, *J. Phys. D: Appl. Phys.* 37, 3202–3206, 2004.

[102] P.A. Mikheyev, V.N. Azyazov, Properties of $O_2(^1\Delta)$–$I(^2P_{1/2})$ laser medium with a dc glow discharge iodine atom generator, *Journal of Applied Physics* 104 (123111), 1–6, 2008.

[103] J. Schmiedberger, S. Hirahara, Y. Ichinohe, M. Suzuki, W. Masuda, Y. Kihara, E. Yoshitani, H. Fujii, RF plasma jet generator of singlet delta oxygen for oxygen-iodine laser, *Proceedings of SPIE* 4184, 32–35, 2000.

[104] J. Schmiedberger, H. Fujii, RF plasma jet generator of singlet delta oxygen and RF discharge predissociation of iodine for oxygen-iodine laser at lowered temperature, *Proc. SPIE* 5777, 211–214, 2005.

[105] A. Schramm, I.I. Fabrikant, J.M. Weber, E. Leber, M.-W. Ruff, H. Hotop, Vibrational resonance and threshold effects in inelastic electron collisions with methyl iodide molecules, *J. Phys. B: At. Mol. Opt. Phys.* 32, 2153–2171, 1999.

[106] K. Nagesha, V.R. Marathe, E. Krishnakumar, Negative ion formation from $CH_3I$ by electron impact, *Internation Journal of Mass Spectrometry and Ion Processes* 145, 89–96, 1995.

[107] L.G. CHristophorou, J.K. Olthoff, Electron interactions with $CF_3I$, *J. Phys. Chem. Ref. Data* 29 (4), 2000.

[108] V. Jirásek, J. Schmiedberger, M. Čenský, J. Kodymová, Generation of I atoms for oxygen-iodine lasers using RF discharge dissociation of various I donors, 40th AIAA Plasmadynamics and Lasers Conference, San Antonio, Texas, June 2009, *AIAA paper*, 2009.

[109] J. Schmiedberger, V. Jirásek, M. Čenský, I. Picková, J. Kodymová, RF discharge generation of I atoms in $CH_3I$ and $CF_3I$ for COIL/DOIL, *Proceedings of SPIE* 7131, OF-1, 2009.

[110] V. Jirásek, J. Schmiedberger, M. Čenský, I. Picková, J. Kodymová, O. Špalek, Plasmachemical generation of atomic iodine for iodine lasers pumped by singlet oxygen, *Chem. Listy*, II Central European Symposium on Plasma Chemistry, 2008.

[111] N.J. Behlman, Electron energy distribution measurements in the plume region of a low current hollow cathode, Thesis, Worcester Polytechnic Institute, 2009.

[112] M. Tichý, Z. Hubička, M. Šícha, M. Čada, J. Olejníček, O. Churpita, L. Jastrabík, P. Virostko, P. Adámek, P. Kudrna, S. Leshkov, M.

Chichina, Š. Kment, Langmuir probe diagnostics of a plasma jet system, *Plasma Sources Sci. Technol.* 18, 014009, 1–11, 2009.

[113] P. Kudrna, J. Klusoň, S. Leshkov, M. Chichina, I. Picková, Z. Hubička, M. Tichý, A Study of Plasma Parameters in Hollow Cathode Plasma Jet in Pulse Regime, *Contrib. Plasma Phys.* 50 (9), 1–6, 2010.

[114] Z. Hubička, G. Pribil, R.J. Soukup, N.J. Ianno, Investigation of the rf and dc hollow cathode plasma-jet sputtering systems for the deposition of silicon thin films, *Surface and Coatings Technology* 160, 114–123, 2002.

[115] J. Touš, M. Šícha, Z. Hubička, L. Soukup, L. Jastrabík, M. Čada, M. Tichý, The radio frequency hollow cathode discharge induced by the RF discharge in the plasma-jet chemical reactor, *Contrib. Plasma Phys.* 42, vol. 1, 119–131, 2002.

[116] J.V. Scanlan, M.B. Hopkins, Langmuir probe measurements of the electron energy distribution function in radio-frequency plasmas, *J. Vac. Sci. Technol.* A 10(4), Jul/Aug 1992, 1207–1211, 1992.

[117] V.A. Godyak, R.B. Piejak, B.M. Alexandrovich, Measurements of electron energy distribution in low-pressure RF discharges, *Plasma Sources Science and Technology* 1, 36–58, 1992.

[118] E.P. Szuszczewicz, J.C. Holmes, Surface contamination of active electrodes in plasmas: Distortion of conventional Langmuir probe measurements, *Journal of Applied Physics* 46 (12), 5134–5139, 1975.

[119] R.R.J. Gagne, A. Cantin, Investigation of an rf plasma with symmetrical and asymmetrical electrostatic probes, *Journal Appl. Phys.* 43 (6), 2639–2647, 1972.

[120] A.P. Paranjpe, J.P. McVittie, S.A. Self, A tuned Langmuir probe for measurements in rf glow discharges, *J. Appl. Phys.* 67 (11), 6718–6727, 1990.

[121] F.F. Chen, Time–varying impedance of the sheath on a probe in an RF plasma, *Plasma Sources Sci. Technol.* 15, 773–782, 2006.

[122] B.M. Annaratone, N.S.J. Braithwaite, A comparison of a passive (filtered) and an active (driven) probe for RF plasma diagnostics, *Meas. Sci. Technol.* 2, 795–800, 1991.

[123] L. Oksuz, F. Soberón, A.R. Ellingboe, Analysis of uncompensated Langmuir probe characteristics in radio-frequency discharges revisited, *Journal of Applied Physics* 99, 013304, 2006.

[124] S. Linnane, M.B. Hopkins, Analysis of an uncompensated Langmuir probe in a radio frequency plasma, *Plasma Sources Sci. Technol.* 18, 045017, 1–8, 2009.

[125] M. Hannemann, F. Sigeneger, Langmuir probe measurements at incomplete rf-compensation, *Czechoslovak Journal of Physics* 56, Suppl. D, D1–D8, 2006.

[126] A. Dyson, P. Bryant, J.E. Allen, Multiple harmonic compensation of Langmuir probes in rf discharges, *Meas. Sci. Technol.* 11, 554–559, 2000.

[127] N.S.J. Braithwaite, N.M. Benjamin, J.E. Allen, An electrosctatic probe technique for RF plasma, *J. Phys. E: Sci. Instrum.* 20, 1046–1049, 1987.

[128] G. Dilecce, M. Capitelli, S. De Benedictis, Electron energy distribution function measurements in capacitively coupled rf discharges, *J. Appl. Phys.* 69, 1, 121–128, 1991.

[129] A.E. Wendt, Passive external radio frequency filter for Langmuir probe, *Review of Scientific Instruments* 72 (7), 2926–2930, 2001.

[130] "All about circuits" web page: `http://www.allaboutcircuits.com`.

[131] P.A. Chatterton, J.A. Rees, W.L. Wu, K. Al-Assadi, A self-compensating Langmuir probe for use in rf (13.56 MHz) plasma systems, *Vacuum* 42 (7), 489–493, 1991.

[132] P. Kudrna, Sondová diagnostika plazmatu v přechodovém režimu tlaků, Diploma work, Department of Electronics and Vacuum Physics, Faculty of Mathematics and Physics, Charles University, 1993.

[133] J. Klusoň, P. Kudrna, A. Kolpaková, I. Picková, Z. Hubička, M. Tichý, Experimental study of the discharge in the low pressure plasma jet sputtering system, *Contributions to Plasma Physics* 53 (1) Special Issue, 10–15, 2013.

[134] S. Leshkov, P. Kudrna, M. Chichina, J. Klusoň, I. Picková, P. Virostko, Z. Hubička, M. Tichý, Spatial Distribution of Plasma parameters in DC-energized hollow cathode plasma jet, *Contributions to Plasma Physics* 50 (9) Special Issue, 878–885, 2010.

# Publications

## Journals


1. V. Jirásek, M. Čenský, O. Špalek, J. Kodymová, I. Picková, I. Jakubec, Chemical oxygen-iodine laser with atomic iodine generated via fluorine atoms, *Chemical Physics* 345, 14–22, 2008.

2. V. Jirásek, O. Špalek, M. Čenský, I. Picková, J. Kodymová, I. Jakubec, Generation of atomic iodine via fluorine for chemical oxygen-iodine laser, *Chemical Physics* 334, 167–174, 2007.

3. V. Jirásek, J. Schmiedberger, M. Čenský, I. Picková, J. Kodymová, O. Špalek, Plasmachemical generation of atomic iodine for iodine lasers pumped by singlet oxygen, *Chem. Listy*, II Central European Symposium on Plasma Chemistry, 2008.

4. P. Kudrna, J. Klusoň, S. Leshkov, M. Chichina, I. Picková, Z. Hubička, M. Tichý, A Study of Plasma Parameters in Hollow Cathode Plasma Jet in Pulse Regime, *Contrib. Plasma Phys.* 50 (9), 1–6, 2010.

5. J. Klusoň, P. Kudrna, A. Kolpaková, I. Picková, Z. Hubička, M. Tichý, Experimental study of the discharge in the low pressure plasma jet sputtering system, *Contributions to Plasma Physics* 53 (1) Special Issue, 10–15, 2013.

6. S. Leshkov, P. Kudrna, M. Chichina, J. Klusoň, I. Picková, P. Virostko, Z. Hubička, M. Tichý, Spatial Distribution of Plasma parameters in DC-energized hollow cathode plasma jet, *Contributions to Plasma Physics* 50 (9) Special Issue, 878–885, 2010.

7. A. Marek, M. Jílek, I. Picková, P. Kudrna, M. Tichý, R. Schrittwiesser, C. Ionita, Emissive probe diagnostics in low temperature plasma – Effect of space charge and variations of electron saturation current, *Contributions to Plasma Physics* 48 (5–7), 491–196, 2008.

8. A. Marek, I. Picková, P. Kudrna, M. Tichý, R.P. Apetrei, S.B. Olenici, R. Gstrein, R. Schrittwieser, C. Ionita, Experimental investigation of the change of the electron saturation current of a dc-heated emissive probe, *Czechoslovak Journal of Physics* 56, B932–B937, Part 5, Supplement B, 2006.

9. I. Picková, A. Marek, M. Tichý, P. Kudrna, R.P. Apetrei, Measurements with the emissive probe in the cylindrical magnetron, *Czechoslovak Journal of Physics* 56, B1002–B1008, Part 5, Supplement B, 2006.

## Conference proceedings

1. V. Jirásek, O. Špalek, M. Čenský, J. Kodymová, I. Picková, I. Jakubec, Study of COIL active medium with atomic iodine generated via fluorine atoms, *Proceedings of SPIE* 7131, 71310M, 2009.

2. V. Jirásek, O. Špalek, M. Čenský, J. Kodymová, I. Picková, I. Jakubec, COIL with supersonic injection of chemically produced atomic iodine, *Proceedings of SPIE* 6346, 63462J, 2007.

3. J. Schmiedberger, V. Jirásek, M. Čenský, I. Picková, J. Kodymová, RF discharge generation of I atoms in $CH_3I$ and $CF_3I$ for COIL/DOIL, *Proceedings of SPIE* 7131, OF-1, 2009.

4. O. Špalek, J. Hrubý, V. Jirásek, M. Čenský, J. Kodymová, I. Picková, Advanced spray generator of singlet oxygen, *Proceedings of SPIE* 6346, 63460C, 2007.

5. O. Špalek, V. Jirásek, M. Čenský, J. Kodymová, I. Picková, Spray generator of singlet oxygen with a centrifugal separation of liquid, *Proceedings of SPIE* 7131, 71310H, 2009.

6. O. Špalek, V. Jirásek, M. Čenský, J. Kodymová, I. Picková, I. Jakubec, Chemical oxygen-iodine laser with atomic iodine generated via fluorine atoms, *Proceedings of SPIE* 6735, 73506, 2007.

7. O. Špalek, V. Jirásek, M. Čenský, J. Kodymová, I. Picková, I. Jakubec, Chemical oxygen-iodine laser with atomic iodine generated in a separate reactor, *Proceedings of SPIE* 6261, 62611T, 2006.

8. I. Picková, M. Tichý, V. Jirásek, O. Špalek, J. Kodymová, M. Čenský, COIL — chemical oxygen-iodine laser, *WDS'06 Proceedings of Contributed Papers: Part II - Physics of Plasmas and Ionized Media* (eds. J. Šafránková and J. Pavlů), Prague, Matfyzpress, 81–85, 2006.

9. I. Picková, V. Jirásek, J. Schmiedberger, Discharge generation of atomic iodine, *WDS'07 Proceedings of Contributed Papers: Part II - Physics of Plasmas and Ionized Media* (eds. J. Šafránková and J. Pavlů), Prague, Matfyzpress, 194–197, 2007.

10. I. Picková, J. Schmiedberger, V. Jirásek, M. Čenský, Generation of atomic iodine in RF discharge, *WDS'08 Proceedings of Contributed Papers: Part II - Physics of Plasmas and Ionized Media* (eds. J. Šafránková and J. Pavlů), Prague, Matfyzpress, 37–41, 2008.

11. I. Picková, P. Kudrna, M. Tichý, New experimental device for investigation of RF discharge plasma in Ar + $I_2$ mixture, *WDS'09 Proceedings of Contributed Papers: Part II - Physics of Plasmas and Ionized Media* (eds. J. Šafránková and J. Pavlů), Prague, Matfyzpress, 223–227, 2009.

12. I. Picková, P. Kudrna, M. Tichý, Langmuir probe measurements in the hollow cathode plasma jet system, *WDS'11 Proceedings of Contributed Papers: Part II - Physics of Plasmas and Ionized Media* (eds. J. Šafránková and J. Pavlů), Prague, Matfyzpress, 131–135, 2011.

13. I. Picková, M. Tichý, P. Kudrna, Langmuir probe measurements in electronegative RF plasma, *WDS'13 Proceedings of Contributed Papers: Part II - Physics of Plasmas and Ionized Media* (eds. J. Šafránková and J. Pavlů), Prague, Matfyzpress, 134–138, 2013.

14. A. Marek, M. Jílek, I. Picková, P. Kudrna, J. Klusoň, A. Kolpaková, M. Tichý, Emissive probe diagnostics in low temperature plasma effect of the space charge and variations of the electron saturation current, *Plasma 2007*, AIP conference proceedings, Volume 993, 231–234, 2008.

# Attachments

Following attachments are present on the CD.

- Fortran program listing
- VEE program scheme
- Articles:

  1. V. Jirásek, M. Čenský, O. Špalek, J. Kodymová, I. Picková, I. Jakubec, Chemical oxygen-iodine laser with atomic iodine generated via fluorine atoms, *Chemical Physics* 345, 14–22, 2008.
  2. V. Jirásek, O. Špalek, M. Čenský, I. Picková, J. Kodymová, I. Jakubec, Generation of atomic iodine via fluorine for chemical oxygen-iodine laser, *Chemical Physics* 334, 167–174, 2007.
  3. V. Jirásek, J. Schmiedberger, M. Čenský, I. Picková, J. Kodymová, O. Špalek, Plasmachemical generation of atomic iodine for iodine lasers pumped by singlet oxygen, *Chem. Listy*, II Central European Symposium on Plasma Chemistry, 2008.
  4. J. Schmiedberger, V. Jirásek, M. Čenský, I. Picková, J. Kodymová, RF discharge generation of I atoms in $CH_3I$ and $CF_3I$ for COIL/DOIL, *Proceedings of SPIE* 7131, OF-1, 2009.
  5. I. Picková, M. Tichý, V. Jirásek, O. Špalek, J. Kodymová, M. Čenský, COIL — chemical oxygen-iodine laser, *WDS'06 Proceedings of Contributed Papers: Part II - Physics of Plasmas and Ionized Media* (eds. J. Šafránková and J. Pavlů), Prague, Matfyzpress, 81–85, 2006.
  6. I. Picková, V. Jirásek, J. Schmiedberger, Discharge generation of atomic iodine, *WDS'07 Proceedings of Contributed Papers: Part II - Physics of Plasmas and Ionized Media* (eds. J. Šafránková and J. Pavlů), Prague, Matfyzpress, 194–197, 2007.
  7. I. Picková, J. Schmiedberger, V. Jirásek, M. Čenský, Generation of atomic iodine in RF discharge, *WDS'08 Proceedings of Contributed Papers: Part II - Physics of Plasmas and Ionized Media* (eds. J. Šafránková and J. Pavlů), Prague, Matfyzpress, 37–41, 2008.

8. I. Picková, P. Kudrna, M. Tichý, New experimental device for investigation of RF discharge plasma in Ar + $I_2$ mixture, *WDS'09 Proceedings of Contributed Papers: Part II - Physics of Plasmas and Ionized Media* (eds. J. Šafránková and J. Pavlů), Prague, Matfyzpress, 223–227, 2009.
9. I. Picková, P. Kudrna, M. Tichý, Langmuir probe measurements in the hollow cathode plasma jet system, *WDS'11 Proceedings of Contributed Papers: Part II - Physics of Plasmas and Ionized Media* (eds. J. Šafránková and J. Pavlů), Prague, Matfyzpress, 131–135, 2011.
10. I. Picková, M. Tichý, P. Kudrna, Langmuir probe measurements in electronegative RF plasma, *WDS'13 Proceedings of Contributed Papers: Part II - Physics of Plasmas and Ionized Media* (eds. J. Šafránková and J. Pavlů), Prague, Matfyzpress, 134–138, 2013.